University of Trento

Center for Mind/Brain sciences (CIMeC)

Doctoral School in Cognitive and Brain Sciences (XXXII cycle)

Brain Functional Connectivity and Alcohol Use Disorder: a graph theoretical approach

Advisor:

Angelo Bifone

PhD Candidate:

Giulia Forcellini

Submitted in partial fulfillment of the requirements for the degree of Doctor of Philosophy in Cognitive and Brain Sciences.

A.A. 2016-2019

CONTENTS

ABSTRACT

Resting-state functional MRI (rs-fMRI) represents a powerful means to assess brain functional connectivity in healthy subjects and in neuropsychiatric patients. Aberrant functional connectivity has been observed in subjects affected by Alcohol Use Disorders (AUD) and other forms of substance dependence, a major health issue worldwide with limited treatment options. Despite intense investigation, the specific neuronal substrates involved and the functional implications of aberrant connectivity in these patients remain unknown. Moreover, it is unclear whether treatment can reverse these alterations, and normalize functional connectivity.

Several methodological and conceptual questions in the analysis of functional connectivity are still open, and contribute to this uncertainty. Functional connectivity is defined in terms of correlated MR-signal fluctuations, and in-scanner patient motion and other nuisance signals can introduce spurious correlations, thus representing substantial confounding factors. At a more general level, understanding the effects of complex conditions, like AUD, on brain connectivity and their functional implications requires a deep comprehension of the brain organizational principles at multiple scales, a tremendous challenge that is at the heart of modern neuroscience.

In this PhD dissertation I address some of the outstanding questions in the analysis and interpretation of aberrant functional connectivity in AUD. To this end, I have embraced the formalism of graph-theory, a powerful framework to assess the effects of alcohol abuse on the local and global topological organization of resting state connectivity. On the methodological side, I have investigated the effects of subject's motion on the structure of resting state networks, and compared efficacy of different approaches to remove motion-related confounds. Moreover, I demonstrate the importance of network sparsification to remove spurious connections from the graph while maximizing the structural information that can be extracted from the system.

Leveraging these methodological developments, I have evaluated functional alterations in different samples of AUD patients. In two independent studies, I demonstrated specific alterations in the topological organization of the insular cortex and subcortical basal structures in recently detoxified alcoholics. Interestingly, protracted abstinence appears to partially normalize functional connectivity, thus suggesting that alcohol-induced alterations in connectivity may be amenable to treatment. Based on these findings, I have studied the effects on brain functional networks of a putative novel treatment based on deep Transcranial Magnetic Stimulation (TMS). Specifically, I analyzed resting state connectivity in AUD patients subjected to repetitive TMS of the bilateral insula and of the anterior cingulate cortex (ACC), and demonstrated treatment-induced changes that may underlie the efficacy of this potential treatment in surrogate clinical read-outs.

Keywords: Functional Connectivity; Network Neuroscience; Graph theory; Modularity; Alcohol Addiction; TMS

PREFACE

This PhD thesis will mostly focus on the exploration of functional brain alterations in Alcohol Use Disorder (AUD). The alcoholic brain has been observed to present structural and functional changes that may be implicated in the inception and maintenance of addictive behaviors. Yet, the specific functional substrates involved remain unclear and highly complex. In recent years, increasing attention has been put on the study of brain *functional connectivity*, the network of interactions that determine the complex interplay between functional segregation and integration in the brain. Identification of altered neural connectivity in neuropsychiatric disorders may be of importance for the development of more targeted treatment that may reverse the observed aberrancies. Main goals of my PhD work are the study of brain functional connectivity in different samples of AUD patients, and the evaluation of the effects of novel and promising treatment option based on deep Transcranial Magnetic Stimulation (deepTMS).

For the evaluation of functional connectivity changes involved in AUD I decided to resort to an advanced and complex methodological analysis based on a graph theoretical approach. Graph theory represents the foundation of network neuroscience, a powerful framework enabling the exploration of the topological organization of brain functional network at different scales. Specifically, I focused on the modular structure of functional connectivity, a descriptor of the embedding of different functional units within the system and a means to identify the topological role that specific brain structures can play within the entire network. Yet, despite the promises and advances that graph theory contributes to the neuroscience community, this approach still presents several aspects that need to be addressed. Thus, before the application of complex network neuroscience analysis to the clinical and intervention studies evaluated in this thesis, I approached some of the limitations present in the field. In detail, I examined the effects of the application of a threshold to functional weighted brain graph, a crucial step in data processing that is much debated due to a lack of agreement upon its use in

the scientific community. A further critical point that I explored relates to the understanding of the effects that head movements and motion correction techniques can have on the topological structure of the functional network.

This PhD Thesis is organized in 5 chapters.

In the **first chapter** I will explore the definition of addiction, a severe brain disorder which represents a major health issue in our modern society. Moreover, I will delve into the details of Alcohol Use Disorders, one of the most prevalent mental disorders worldwide. I will introduce methods to study and analyze brain functional connectivity, and I will extensively review the state-of-the-art of the scientific literature in the field. The **second chapter** will describe methodological developments that will be subsequently applied to the analysis of clinical data. In the first section of the chapter I will review the most salient aspects of the debate upon the thresholding process in functional connectivity and I will explore the definition of commonly applied thresholding techniques. Aim of this chapter is the identification of the impacts that this particular step employed to reduce the density of functional graphs can have on the topology of the network. To achieve this, I will leverage two novel random graph models and the world of spectral entropies extended to complex networks, which enables the comparison of an empirical network to its randomized counterpart at all scales. Following this investigation, I will present an example of the application of an optimal threshold to a case-control study, thus proving its benefits in a real-world example. The second section of this methodological chapter will explore the definition of the effects of head movements over brain functional connectivity. To this end, I will employ the same methods based on first principles described in the previous section of the chapter. Importantly, this methodological chapter describes innovative and advanced tools that I will subsequently apply to the study of functional connectivity alterations in clinical studies. Leveraging these findings, I will evaluate functional connectivity alterations in different samples of AUD in the **third chapter** of this thesis. Specifically, in the first half of this chapter I will report the investigation of brain functional alterations in recently detoxified alcohol dependent patients as compared to a matched sample of healthy controls. The focus of this study is on the modular structure of the functional networks and the altered topological role of key regions involved in AUD and reward processes. In the second part of

this chapter I pursued replication of these findings in an independent sample of AUD patients, with strikingly similar results. Importantly, the validation of these novel findings in a separate cohort of patients strengthened the hypothesis of the central role played by specific neural regions, such as the insular cortex, to maintain addictive behaviors. A natural development of these study will be reported in the **fourth chapter**. Here, I will explore the efficacy of a novel treatment for AUD patients, based on the application of deep TMS. Two studies with the same experimental design will be addressed in this chapter. The first study will test the efficacy of deep stimulation of the bilateral insula, the second will target the anterior cingulate cortex. Besides testing the clinical efficacy of this novel treatment, this chapter will also try to evaluate the functional neural changes induced by a perturbation of the network by means of deep magnetic stimulations. The **fifth chapter**, the last one of this thesis, will extend this approach to pharmacological studies. Indeed, in the central and main part of this thesis, I tested the effects of a chronic exposure to a substance of abuse – alcohol – upon the functional brain network. Conversely, in the last part, I will test the effects of an acute injection of a drug of abuse, namely ketamine. Importantly, I will evaluate the functional connectivity organization in a complex study design, where, besides addressing ketamine-induced alterations, I will further assess the modulatory effects that two different pharmacological agents, risperidone and lamotrigine, can have on ketamine-evoked changes.

1 INTRODUCTION

This first introductory chapter will describe Alcohol Use Disorder, together with a short review of the identified alterations in the structural and functional alcoholic brain. The neuroimaging of the addicted brain will be extensively described after a closer evaluation of the most recently developed methodological approaches for the evaluation of functional connectivity organization.

1.1 ADDICTION AS A BRAIN DISORDER

Addiction is a severe and complex brain disorder. It is characterized by compulsive substance seeking and intake, even despite severe consequences affecting patients' social, economic, and working lives. It is a relapsing disorder, related to an inability to reduce or inhibit drug intake, together with motivational and physical withdrawal syndromes when the access to the drug is prevented (American Psychiatric Association). The concept of addiction evolved in the past years. Indeed, it is now applied also for the description of "behavioral addictions", where a progressive loss of control over a specific behavior (gambling, internet, food, etc.) can lead to a very similar symptomatology as the one induced by substances addiction [Grant and Chamberlain, 2016]. In the 5th version of the Diagnostic and Statistical Manual of Mental Disorders (DSM-5, [American Psychiatric Association, 2013]) an important advancement has been made in the classification of this disorder, which now falls under the chapter of "Substance-Related and Addictive Disorders".

Specifically, substance-related disorders refer to recurrent drugs use causing clinically and functionally significant impairments, such as health problems, disabilities, and failure to meet responsibility. The advancement in its definition, including its view as a brain disorder, comes from the rapid growth of the knowledge in the field, its increasing prevalence worldwide, as well as a strong need to

decrease social stigma related to addiction. The DSM-5 identifies nine classes of substance addiction: alcohol, caffeine, cannabis, hallucinogens, inhalants, opioids, sedatives, hypnotics and anxiolytics, stimulants and tobacco.

Among all the addictive substances, alcohol is the most abused. Despite being highly socially accepted and legal in most of the countries, this addictive substance presents severe deleterious effects related to its excessive use. Alcoholic beverages contain ethanol, a psychoactive substance with strongly addictive properties. Alcohol Use Disorder (AUD) represents a major public concern worldwide, with a high health and societal cost. In the worldwide population over 15 years of age, total alcohol consumption is at the level of 6.4 liters per capita, with the highest amounts observed in European countries [World Health Organization (WHO), 2018]. In Europe, the 1-year prevalence of AUD is estimated to be at 3.4%, with men drinking more than women, resulting in nearly 11 million people affected [Rehm et al., 2015]. AUD is among the most prevalent mental disorders worldwide, contributing to global comorbidities and mortality. Indeed, according to the World Health Organization, in 2012, 5.3% of all global deaths were attributed to alcohol consumption [World Health Organization (WHO), 2018].

As every form of addiction, AUD is a chronic brain disease, with several functional and structural brain systems implicated, besides strong genetic, pharmacological, and sociocultural components [Volkow and Morales, 2015]. The interaction between these different components is making it an extremely complex disorder. The chronic abuse of alcohol, as well as any other drug of abuse, induces long-lasting neuroadaptations, with a subsequent alteration and unbalance of neuronal circuits. The severity and high prevalence of this chronic brain disorder emphasize the need for an effective treatment, which is now lacking. The identification of clinical endophenotypes, such as alterations and malfunctioning of underpinning brain circuits, is crucial to seek therapeutic options, with the chance to improve clinical outcomes and avoid relapse, a critical aspect of this complex and devastating disorder.

Box 1 DSM-5 criteria

DSM-5 criteria for AUD are as follow:
"A maladaptive pattern of substance use leading to clinically significant impairment or distress, as manifested by 2 or more of the following, occurring at any time in the same 12-month period:

- Alcohol is often taken in larger amounts or over a longer period than was intended.
- There is a persistent desire or unsuccessful efforts to cut down or control alcohol use.
- A great deal of time is spent in activities necessary to obtain alcohol, use alcohol, or recover from its effects.
- Craving, or a strong desire or urge to use alcohol.
- Recurrent alcohol use resulting in a failure to fulfill major role obligations at work, school, or home.
- Continued alcohol use despite having persistent or recurrent social or interpersonal problems caused or exacerbated by the effects of alcohol.
- Important social, occupational, or recreational activities are given up or reduced because of alcohol use.
- Recurrent alcohol use in situations in which it is physically hazardous.
- Alcohol use is continued despite knowledge of having a persistent or recurrent physical or psychological problem that is likely to have been caused or exacerbated by alcohol.
- Tolerance, as defined by either of the following:
  1. A need for markedly increased amounts of alcohol to achieve intoxication or desired effect.
  2. A markedly diminished effect with continued use of the same amount of alcohol.
- Withdrawal, as manifested by either of the following:
  1. The characteristic withdrawal syndrome for alcohol
  2. Alcohol (or a closely related substance, such as a benzodiazepine) is taken to relieve or avoid withdrawal symptoms."

1.1.1 The addiction cycle

Social drinkers, limited to an occasional use of alcohol, are clinically highly different from patients indulging in an escalating alcohol use with loss of control. In European regions, representing countries with the highest drinker rates, 59.9% of people aged 15 or older are current drinkers, however, only the 8.8% of this population developed AUD during their lifetime (Center for Behavioral Health Statistics). As with most drugs of abuse, alcohol consumption starts with an initial recreational use, shifting into a severe addiction only in few users. However,

the long-term exposure to alcohol, despite being a necessary condition, is not sufficient to fall into the development of the disorder [Volkow et al., 2016], individuals' vulnerability is a crucial key for the instauration of addiction. The transition from the occasional use to the compulsive alcohol seeking that characterizes addiction is involving genetic, environmental, cellular, and molecular mechanisms, which are the focus of current neurobiological drug abuse research. Different stages characterize the disorder, all with specific behavioral and neural critical aspects, mostly comprising an interplay of impulsive control behaviors and compulsions. From the voluntary to the chronic relapsing stage, the combination of these two elements leads to an addiction cycle, comprising three stages, from an initial binge/intoxication, to withdrawal and negative affects, until preoccupation/anticipation [Koob and Volkow, 2010]. Generally, the impulsivity domain dominates the early stages, when individuals are predisposed towards unconsidered actions, regardless of the consequences. Compulsivity, on the opposite, dominates the final stages, leading to loss of control and perseveration over maladaptive behaviors (Figure 1.1).

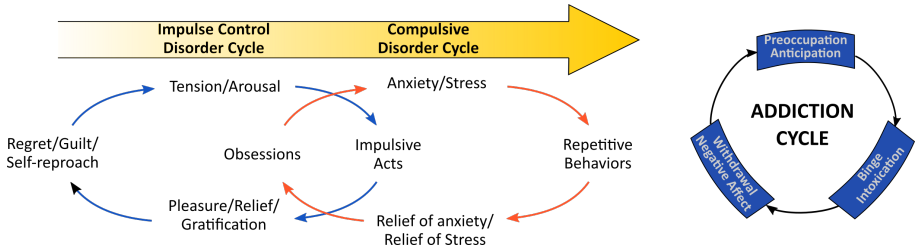

Figure 1.1: The addiction cycle, adapted from [Koob, 2011]. On the left, stages of impulsive and compulsive disorders related to reinforcement. On the right, cycle of impulsivity and compulsivity in addiction

The combination of these processes, leading to the shift from positive to negative reinforcements induced by alcohol, makes this cycle more and more intense, driving the patient to develop severe pathological forms of addiction. The most impacting aspects of the disorder consist on the inability of patients to break this cycle, keeping on falling into relapse, followed by new stages of intoxication, binge, and withdrawal. All these mechanisms and transitions are related to long-lasting changes in several neural systems, altering the communication and interactions between different brain regions. Neural areas with a central role in addiction are mostly related to the mesocorticolimbic system [Volkow et al., 2013]. This neural circuit is characterized by dopamine projections, crucial in the processing

of reward-related stimuli and motivated behaviors. Indeed, as all other drugs, alcohol activates these brain regions related to reward circuits, causing an immediate release of dopamine, a central brain neurotransmitter. When the exposure to the substance is protracted in time, our brain develops higher levels of tolerance towards the drug, reducing its spontaneous release of dopamine [Volkow et al., 2016]. This is finally leading to crucial neuroadaptations, which are playing a key role in the shift towards maladaptive behaviors. Such pathological behaviors give rise to subsequent inabilities to suppress impulsive and compulsive urges towards drugs intake [Goldstein et al., 2009].

Given the strong impact that drugs of abuse have on the brain, the study of these alterations, both at a structural and functional level, is now one of the centers of attention of clinical research, thanks to the growing and fast development of a precious tool: **neuroimaging**.

1.2 MAGNETIC RESONANCE IMAGING: A KEY TO STUDY BRAIN DISORDERS

In the past decades, neuroscience has benefited from the fast development of non-invasive technologies that give us the possibility to explore the details of brain structures and functions *in vivo*. These include advanced neuroimaging techniques, like Magnetic Resonance Imaging (MRI), magnetoencephalography (MEG), or electroencephalography (EEG), all with different spatial or temporal resolutions. EEG and MEG, for example, are both techniques that enables the study of brain function with high temporal resolutions, in order of milliseconds, lacking, however, in spatial details. These techniques are respectively based on the detection of spontaneous electrical or magnetic fluctuations induced by neuronal activity, and measured through sensors on the scalp. In contrast, MRI has emerged as a dominant imaging method with high spatial resolutions, in the order of millimeters, but lower temporal resolution that is however adequate to capture the hemodynamic fluctuations that are thought to reflect changes in the underlying neuronal activity. Importantly, the mix of these two aspects give us a key element

for the study of brain functional and anatomical mechanisms in pathological and healthy conditions.

MRI was first developed in the 1970s, and has undergone tremendous growth since then. This technique exploits strong magnetic fields and radiofrequencies to generate three-dimensional images, able to separate different tissues (e.g. white matter, gray matter, cerebrospinal fluid) according to their intrinsic magnetic properties. Through the use of different magnetic gradients and electromagnetic fields (i.e. pulse sequence), MRI can, indeed, detect tissue properties, thus distinguishing different tissue types. Through this, it is now possible to map brain structures details, such as gray matter thickness, or white matter fibers integrity. From a functional perspective, fMRI represents a powerful means to evaluate the metabolic correlates of neural activity, through the measurement of blood oxygen level-dependent (BOLD) signal. Indeed, blood oxygenation levels change rapidly in relation to the activity of groups of neurons, the localization of brain activity.

The world of functional neuroimaging provided neuroscientists with an essential tool to elucidate the relationship between brain function and anatomy, a topic that previously had been explored mostly through the study of the effects of brain lesions. The use of this novel technology led to incredible advancements in brain understanding, from the idea of the specific specializations of brain regions, to the concept of strong distributed networks underlying cognitive processes.

This technique has a long tradition of task-based measurements, where volunteers, while laying in the MR scanner, are asked to perform specific behavioral tasks with the purpose to evaluate the activation of brain regions engaged by that particular condition. This is extremely valuable for the identification of brain structures responsible for specific complex processing functions, and a key to evaluate the basis of cognitive dysfunctions in brain disorders. Adding to this, in the 1990s, a breakthrough finding revealed the presence of spontaneous slow fluctuations related to brain activity even at rest, in a task-free condition, signal that was previously identified as noise [Biswal et al., 1995]. This result opened the way for the study of brain functional connectivity, namely the identification of brain regions whose spontaneous oscillations at rest are consistently correlated, or statistically dependent, giving rise to underlying brain networks (Figure 1.2). Specifically, these baseline fluctuations are related to cortico-cortical connections

with a specific spatial structure [Lowe et al., 2000], and are consistent across subjects, identifying patterns of functionally related regions [Damoiseaux et al., 2006]. These spontaneous fluctuations are distinctly observed in brain regions involved in visual, motor, language, auditory, and higher-order processes. These correlated fluctuations, forming resting state networks, are thought to reflect the spontaneous communication between spatially distinct brain regions, indexing the strength of their functional coupling. The complex and efficient continuous communication between brain regions is crucial for a correct integration of information in the whole brain. This is making the study of functional neural networks at rest of central importance in brain disorders, to understand how anomalies in the flow of information in the brain can result in pathological conditions.

In this work I will mostly review and dwell into the details of the study of brain functional connectivity measured at rest. A number of different analysis techniques have been developed for the study of this spontaneous intrinsic activity of the brain. One of the first and most applied approaches lays on the selection of a targeted brain region, *seed*, to determine the temporal correlations between this extracted area and other separated anatomical structures in the brain [Lowe et al., 1998]. Another promising approach relies on an Independent Component Analysis (ICA), a data-driven approach with no need of *a priori* selection of specific brain regions. The power of this technique comes from the use of algorithms that, through the analysis of the whole temporal activity originated from all the voxels in the brain, can decompose the BOLD signal into statistically maximally independent components [Beckmann et al., 2005]. This decomposition reveals components with specific spatial maps. From these spatial maps, it is possible to identify components related to physiological fluctuations (e.g. heart beats, respiration, head movements) or to neuro-functional systems. Given the strength of ICA, this method is now also widely applied to regress out noise components from functional images, preparing the data for subsequent analysis [Pruim et al., 2015, Salimi-Khorshidi et al., 2014]. Moreover, the application of ICA reveals resting brain patterns with high spatial consistency across subjects. These patterns encompass functionally related regions, e.g. structures implicated in motor functions, visual processing, auditory processing, attention functions, and many more [Damoiseaux et al., 2006]. It is now well-established that brain regions with simi-

lar functional properties often show coherent spontaneous fluctuations also in the absence of the functional task they sub-serve. All these components constitute so-called resting-state networks, and are key elements in the fast development of the field of resting-state functional connectivity (RSFC). Altogether, the analysis of RSFC constitutes a precious tools in clinical settings, where we can map abnormalities and alterations in these spontaneous activation patterns in populations with neurological or psychiatric disorders.

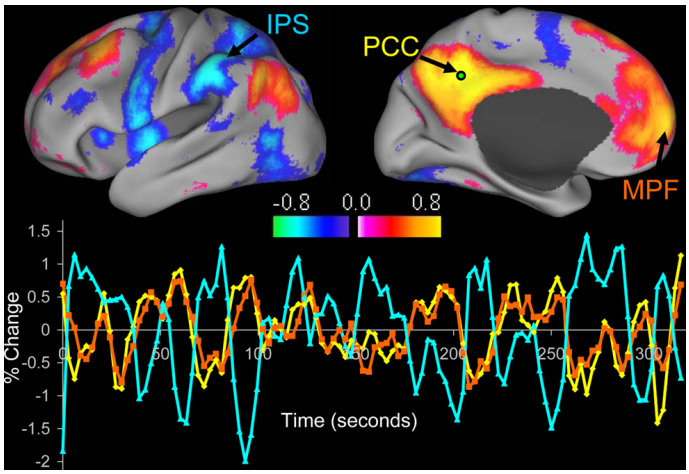

Figure 1.2: Intrinsic correlations at rest identified through a seed region within the posterior cingulate (PCC) reveal regions positively correlated within the medial prefrontal cortex (MPF), reflecting the so-called Default-Mode Network (DMN), and a set of negatively correlated regions in the Inferior Parietal Sulcus (IPS), from [Fox et al., 2005]

The study of brain functionality is an extremely complex endeavor; we are still at the beginning of the understanding of all the facets of brain function, but the exploitment of these technological and methodological developments gives us precious advancements to finally grab its finer details. Altogether, the analysis of RSFC constitutes a precious tool in clinical settings, where we can map abnormalities and alterations related to these spontaneous activation patterns in populations with both neurological or psychiatric disorders. Moreover, RSFC studies allows us to investigate clinical populations that might not be able to perform specific tasks while laying still in an MR scanner.

1.3 FROM FUNCTIONAL BRAINS TO FUNCTIONAL NETWORKS.

The study of brain functional connectivity has led to the emergence of a new promising field: the world of connectomics. **Connectome** is a term coined a bit more than ten years ago [Sporns et al., 2005], referring to a comprehensive map of neural connections. The field recently experienced a rapid growth, and it owes its increasing popularity to the simultaneous fast development of advanced neuroimaging techniques and the growing confidence in handling complex systems, grounded in the physics world of network science [Fornito et al., 2016]. The merger of these two worlds, neuroscience and network science may help understand the topological organization of one of the most complex systems ever studied, our brain. Despite being a relatively young field, we can now count more than 2k scientific articles *per year* published in peer-reviewed journals.(Figure 1.3).

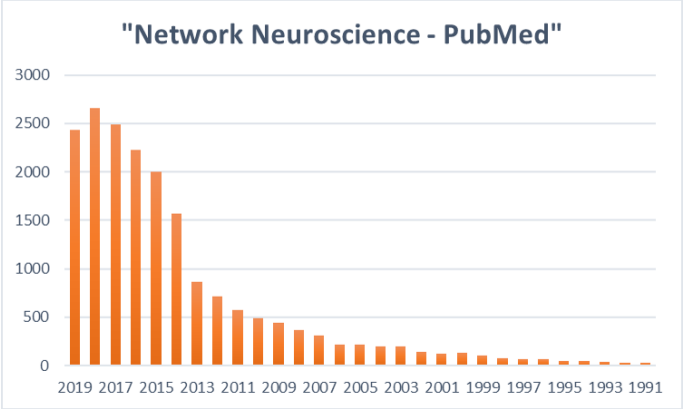

Figure 1.3: Number of publication in Network Neuroscience from 1990. Data from PubMed, updated the 21st September, 2019.

A *graph*, or network, is a mathematical structure used to model the relations between all the different components of a system. In a graph, these components are represented as *nodes* connected by *edges* (or links; figure 1.4).

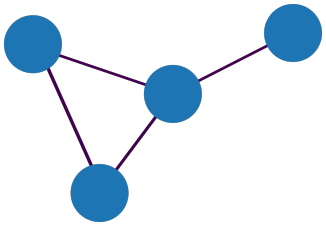

Figure 1.4: Example of a graph with four nodes and four edges

The study of the connectivity patterns of these edges in a system provides information on the topological organization of the interactions among its components.

These mathematical tools are exploited in many scientific fields, from biology, to informatics, finance, or social sciences. The brain can be naturally represented as a graph, where anatomical regions can be mapped as nodes, and the relations between them (structural or functional) constitute the edges. Through this framework, we have the opportunity to investigate the topological organization of functional and structural brain connectivity.

The first step in the representation of neuroimaging data in the form of a graph is the definition, of nodes; this is normally achieved by a procedure dubbed *parcellation*, whereby anatomically or functionally defined regions are identified as sufficiently homogeneous to represent a unit of the graph [Zalesky et al., 2010b]. The second step requires the adoption of a measure of similarity between nodes to define the edges of the graph. Magnetic Resonance Imaging makes it possible to model both structural and functional neural information as a graph. Structural networks, for example, can be defined starting from imaging data of white matter axonal bundles, as measured with Diffusion Tensor Imaging techniques. With white matter fibers it is therefore possible to characterize network's edges, whose strength can be defined by different structural measures, such as, for example, the estimated number of streamlines between anatomical regions, or fibers integrity, as defined by Fractional Anisotropy, a measure of water diffusion within the axonal bundles [Jones et al., 2013]. A different perspective can be explored through functional connectivity networks, central focus of this thesis work. As already revised, through fMRI we can quantify spontaneous fluctuations of brain regions while at rest. In this case the interconnecting links between brain nodes are defined based on a measure of temporal correlation among time-series extracted from parceled cortical and subcortical regions. In both cases, the definition of nodes and edges within our network result in a final graph represented by an **adjacency matrix** – also defined as connectivity matrix - where each element reflects the presence and strength of connections between pairs of nodes. The connectivity matrix offers a simpler and more comprehensive means to deal with complex networks. Each row and column of such matrix represent a specific node N, whereas all the entries reflect the pairwise connectivity between nodes, with the final construction of an NxN matrix, as described in figure 1.5. Another strong advantage offered by graph theory lays in the possibility to work with a number of different graphs.

In network neuroscience, we can mostly address *undirected graphs*, represented by symmetrical connectivity matrices, where the directionality of the influence exerted from one node on another cannot be mapped.

When we deal with functional connectivity networks, we represent functional relations between nodes through temporal correlations, as measured by **Pearson correlations**. This approach gives rise to fully connected *weighted graphs*, indicated as $\mathbf{W} = \{\omega_{ij}\}$, where the defined edges reflect the strength of the interaction between specific nodes, and the links represent different weights, ω. In some cases, the binarization of the graph can be applied, resulting in simple *binary graphs*, $\mathbf{A} = \{A_{ij}\}$, where the entries of the matrix equal 1 if a connection between nodes is present, or 0, if no connection is present. In the functional connectivity domain, however, binarization may discard important structural information. Given the difficulty in dealing with fully connected graphs, it is common practice to sparsify the matrix, namely applying a specific *threshold* and set to 0 all the matrix entries below this given value [van den Heuvel et al., 2017b]. Afterwards, it is choice of the experimenter, to subsequently work with sparse weighted networks, or with binary networks, setting to 1 all the connections surviving the thresholding procedure. This aspect, together with other methodological issues now present in the network neuroscientific field, will be extensively reviewed and discussed in the chapter 2 of this thesis.

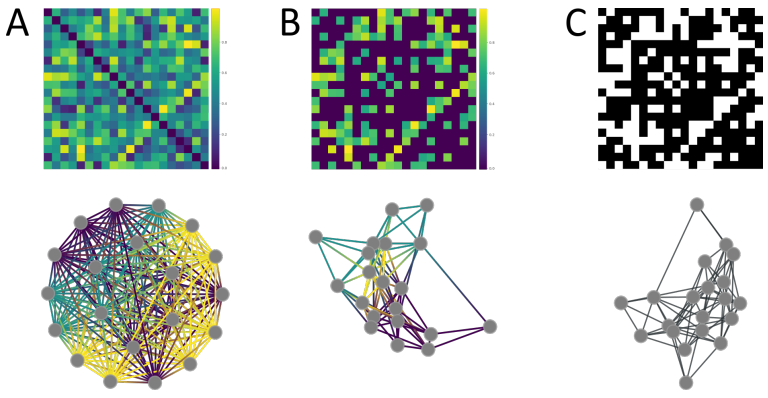

Figure 1.5: Examples of graph matrices and networks. In Panel A, we show an undirected full weighted graph. Panel B represents the same undirected graph after the application of a given threshold. Panel C shows the same graph after binarization, where all the entries surviving the thresholding procedure are set to 1, all the others to 0.

1.3.1 Graph topological metrics and the brain

Network science contributes concepts and tools that enable the study of the brain functional organization, such as the interplay between integration and segregation in healthy and pathological conditions [Bullmore and Sporns, 2009]. Indeed, by representing the brain as a graph, we can evaluate the topological properties at global and local scales of the whole system, by means of the numerous metrics that this theoretical approach offers (figure 1.6).

At the local scales, namely the topological organization at the node level, the most straightforward and basic metric is represented by the **degree**. The degree of a node in a graph – denoted as k_i -, is defined as the number of edges connected to it. It can also be defined as *degree centrality*, assuming that nodes with higher numbers of connections will play a more central role within the whole system, whereas regions with lower degree might subserve a more peripheral role. This basic topological metric is mostly used with binary networks, given that it simply quantifies the total number of links attached to a given node. In weighted graphs, this measure can be equivalent to the node **strength**, computed as the sum of the weights of all the edges connected to that node. These topological measures are crucial to identify the so-called **hubs**, namely specific nodes in a network with higher degree or strength compared to the others. The study of hubs is of central importance in the evaluation of the organization of brain disorders, as it was proved that when these core regions start losing their centrality the overall network appears pathological [Fornito et al., 2015].

At the global scale, **density** of a network, a key aspect that will be addressed in chapter 2, is defined as the proportion of the actual links present over the number of all possible edges within the network, represented as:

$$\rho = \frac{2E}{N(N-1)}, \tag{1.1}$$

where N are all nodes in the network and E all the edges. Another core graph metric defines the topological distance, or **path length**, that is the number of links necessary to "travel" from one node to another. The characteristic path length, L, reflecting a global measure, is the average shortest path length between all pairs of nodes, and indicates how the graph is well integrated.

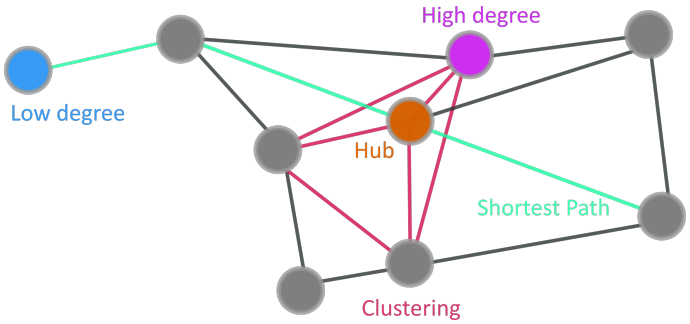

Figure 1.6: Examples of common topological graph metrics

Based on this core metric, we can evaluate the so called **global efficiency**, another measure of integration of the network, defined as the inverse of the average path length of the network. Efficiency can moreover be measured at the local level. **Local efficiency** reflects the extent to which a node is integrated within its neighbor nodes, measured as the inverse of the average path length within a subgraph comprising all its neighbors. These path based measures are indicative of the *integration* properties of the network, frequently addressed in neural networks as means to evaluate how rapidly the functional – or structural – information can be combined between anatomically separated brain regions. In lay terms, they can estimate how information flows efficiently between one brain region and another.

Additionally to topological measures of integration, graph theory offers tools to assess the segregation features of the system. In section 1.2, we have seen how our functional brain presents anatomically separated groups of brain regions subserving specific cognitive or processing functions. Measures of **segregation** allow the identification and quantification of these interconnected groups of neural regions [Rubinov and Sporns, 2010]. At a local scale, the segregation level of a single node is quantified through its **clustering coefficient**, which is the proportion at which a node's neighbors are also neighbors of each other [Watts and Strogatz, 1998]. This reflects the presence of triangles in a network; the more triangles are present, the more a graph shows segregation properties. Conversely, at a global scale we can assess the brain modular organization.

1.3.2 The Modular Brain

With a more complex framework, graph theory has also been extensively employed to study the presence, at a global scale of the network, of a modular architecture. This is characterized by the presence of nodes more tightly connected within themselves and loosely connected with the rest of the graph, forming so called *modules*, supporting a balance of integration and segregation. These subcomponents in a network are also dubbed "communities", a term borrowed from social sciences, used for the description of a natural trend in people to form groups (i.e.circles of friends, families, etc...) within society. The degree to which the whole system can be subdivided into separately interconnected modules, reflects the **modularity** of the network [Newman, 2004]. The study of modular organization is focus of attention in the study of most of real-world networks. Modularity, indeed, is a feature that can be observed in most complex systems, and provides strong advantages also from an evolutionary perspective, conferring more robustness and adaptability [Sporns and Betzel, 2016]. From this perspective it has been shown that modular organizations emerge spontaneous in biological systems, comprising brain networks, promoting a crucial flexibility, essential in ever-changing environments [Kashtan and Alon, 2005]. In the details of brain functional networks, it is proven that a modular system allows a more flexible organization of neural functioning, together with a faster rate of transformation of information within the network. With the organization of different nodes into segregated communities, the brain is more adaptable both to external perturbations and to continuous changes in loads of cognitive demand and environmental conditions [Meunier et al., 2010]. The robustness conferred by this topological architecture favors, indeed, the possibility to re-arrange only specific clusters of nodes - and not the whole system - when the network is forced to face external challenges. This notion comes from the idea firstly introduced in the early 60s by Simon [Simon, 1962], who elegantly discussed the complexity of hierarchical systems and coined the concept of "nearly-decomposable systems". According to his view, complex systems evolve into a hierarchical structure, composed by subelements that more strictly interact with a subset of other elements closer to them, and less with elements outside this subset. Interestingly, this definition appears

strongly analogous to the concept of modularity previously discussed. In his elegant essay, Simon observed that this feature is indeed shared by most complex systems, from social, to physics, chemistry and so on. As a matter of fact, this property allows simplification of a system, it provides increasing stability among compartments (i.e. modules) and would subsequently grant the adaptation of one module without affecting the others, conferring important evolutionary and adaptive advantage. With a number of clear and effective examples, Simon efficiently explains the crucial benefits that this feature handles to most real-world network. Among these, the robustness gained by the system is neatly discussed thanks to the intuitive watchmakers' example. This short example sees two watchmakers, Hora and Tempus, who differently assembled their products:

"The watches the men made consisted of about 1,000 parts each. Tempus had so constructed his that if he had one partly assembled and had to put it down-to answer the phone say-it immediately fell to pieces and had to be reassembled from the elements. The better the customers liked his watches, the more they phoned him, the more difficult it became for him to find enough uninterrupted time to finish a watch. The watches that Hora made were no less complex than those of Tempus. But he had designed them so that he could put together subassemblies of about ten elements each. Ten of these subassemblies, again, could be put together into a larger subassembly; and a system of ten of the latter subassemblies constituted the whole watch. Hence, when Hora had to put down a partly assembled watch in order to answer the phone, he lost only a small part of his work, and he assembled his watches in only a fraction of the man-hours it took Tempus."

In this very short but compelling anecdote, the strong advantages that a modular organization confers to the whole network is clear. First of all, modular structures allow the evolution or modification of one module at a time without affecting the rest of the system, which is already well-adapted. For example, in neural networks, thanks to this feature, if one brain region is damaged, only a sub-element of the whole network is affected, leaving the rest of the system unaltered. Furthermore, after damage of one single community, its re-arrangement will be more rapid and efficient [Meunier et al., 2010]. Overall, such compartmentalization does not, of course, prevent communication between separated modules, yet, allows an optimal trade-off between the segregation and integration of the information flow. This further translates into another crucial feature essential for functional

brain networks: the time-scale separation. Indeed, this hierarchical decomposition grants a faster intra-modular processing of the information, coupled with a slower inter-modular processing, a key characteristics of complex cognitive and behavioral functioning [Meunier et al., 2009]. In the details of neural networks, our brain is continuously subject of developmental changes, and the presence of well-segregated neural structures is a key element to limit the impact that these external perturbations can exert over the system. Such compartmentalization can prevent global functional disruptions, as it allow the system to rewire, in case of perturbations, only specific modules, leaving unaffected the global architecture.

Given the strong benefits that modular structures handle to the functional brain, it is of no surprise the popularity that this approach gained to study these underlying organizations in both healthy and pathological conditions [Meunier et al., 2010, Sporns and Betzel, 2016, Alexander-Bloch et al., 2010, Bordier et al., 2018, de Haan et al., 2012]. Such attractiveness consequently led to the development of complex community detection methods, employed to unravel the underlying organization of cortical and subcortical neural nodes. The most implemented methodological technique for community detection lays on the *modularity maximization* [Newman, 2004].

Modularity maximization is, indeed, the most commonly applied method in network neuroscience. It consists in the maximization of a modularity quality function, resulting in a partitioning of all nodes into non-overlapping communities. A specific formulation of a multiresolution maximized modularity commonly evaluated is defined as $Q_{\text{˛}}$ and represented as:

$$Q = \sum_{i,j} \left[A_{ij} - \gamma P_{ij} \right] \delta(C_i, C_j), \tag{1.2}$$

where $\mathbf{A}_{ij}$ is the studied adjacency matrix, with i being a node assigned to the community C_i, and j a node assigned to the community C_j. The function $\delta(C_i, C_j)$ is here set to 1 if the two nodes, i and j, are assigned to the same communities, and to 0 otherwise. The parameter γ represents a resolution parameter, set by the experimenter, with values ranging from 0 to 1. The smaller the values, the more the maximization function will tend to identify smaller communities. To conclude, the element P_{ij} represents the expected weight of the edge connecting the two

nodes, under a specific network null model, typically the configuration model [Garcia et al., 2018]. The resulting Q value will range from 0 to 1, the stronger the modular architecture detected at the large scale of the network, the more this value will be close to unity. In a random network, for example, lacking of a well-structured organization at large scales, Q will be close to 0. The simplicity of this algorithm made it the most employed technique for the study of brain functional and structural architecture. However, despite being simple to use and computationally tractable, this algorithm comes with different shortcomings. Among these, the present algorithm may generate degenerate solutions. Indeed, the output of the partitions identified with such approach can be highly different in terms of their similarity, but present a nearly identical maximal modularity value [Good et al., 2010]. This *degeneracy* phenomenon stands in the identification of these sub-optimal partitions, which can be, however, misinterpreted as optimal. Because of this intrinsic characteristic of modularity, it is clearly not optimal to choose a partition based on the identified maximum value of Q. One common solution requires the computation of a large number of different partitions, thus selecting a median of all the solutions. This requires, after the computation of several partitions, the creation of an association matrix $\mathcal{A}$, whose edges are proportional to the probability that two nodes fall into the same community. Following, the community detection algorithm is applied to this consensus matrix. However, modularity maximization suffers another important shortcoming, the *resolution limit*. Modularity, indeed, is not able to correctly identify communities smaller than a certain scale, determined by the square root of the total number of edges in the network. Specifically, it is not able to detect modules with a total number of links lower than the square root of all the links present in the graph. Trying to overcome this limitation, it is common to test the algorithm several times setting different values of the γ parameter [Garcia et al., 2018]. Examples of functional modules commonly revealed with modularity maximization are depicted in figure 1.7.

Another methodological approach employed for community detection comes from the world of information theory, and exploits random walkers to detect the optimal graph partition. Considering a network, we can imagine a random walker going from one node to another, using edges as "paths" to traverse the whole network. In this case, the random walker is used as a proxy for information diffusion

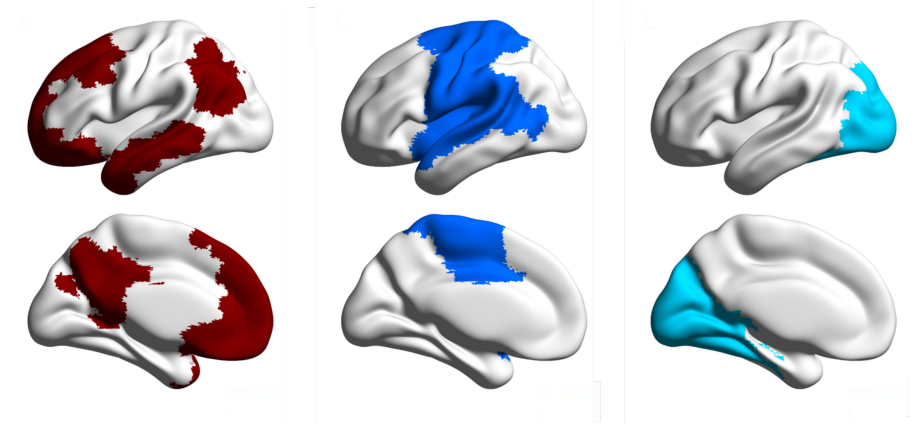

Figure 1.7: Examples of modules commonly identified in resting-state functional networks, comprising the DMN, the somatosensory network, and the visual system.

within the graph. If a graph presents a strong community structure, with modules containing more internal links – thus, more paths for the walker – it is highly plausible that the walker will remain trapped within such structure for more time, highlighting the presence of a module. The most commonly applied strategy implementing this approach is *InfoMap* [Rosvall and Bergstrom, 2008]. The idea behind this technique is to maximally compress the information diffusion that can be decoded within the graph. From this, the optimal partition is identified as the one yielding the minimum description length of an infinite random walk. InfoMap is considered as one of the best-performing algorithms for community detection, and is therefore now often applied also within the framework of network neuroscience [Power et al., 2011, Avena-Koenigsberger et al., 2018, Gordon et al., 2018]. Compared to Q maximization, this method suffers from degeneracy and resolution limit to a smaller extent [Nicolini et al., 2017]. The resolution limit of InfoMap, indeed, does not depend on the size of the whole network such as in Modularity, but depends on the number of inter-cluster edges [Kawamoto and Rosvall, 2015]. This algorithm can also detect much smaller communities than those revealed by the maximization of the Q function [Yang et al., 2016b], a crucial aspect when we need to address functional brain systems. Similarly, its degeneracy landscape is much less critical compared to the one observed with Modularity [Nicolini et al., 2017].

Given the advantages of this latter method, in the present thesis work I will most implement the InfoMap algorithm, with a consensus approach, when addressing the modular organization of RSFC in healthy and clinical populations.

So far, I have thoroughly discussed the importance of the evaluation of a modular structure in real-world brain networks, representing a key strength for the evolution and survival of the system. Importantly, the detection of the modular structure in a network allows the identification of key regions playing specific roles within the overall organization in terms of network integration and segregation. Two topological metrics give us an index of the role of a given node, according to the modular architecture: the participation coefficient and the module degree. **Participation coefficient**, indicated by P_i, is an inter-modular connectivity measure, related to the proportion of links of a given node towards nodes belonging to external modules. It is defined as:

$$P_i = 1 - \sum_c \left(\frac{k_{ic}}{k_i} \right)^2, \tag{1.3}$$

where k_{ic} is the number of links of node i to nodes in module c and k_i is the total degree of node i.

On the opposite, the **within-module degree**, indicated by z_i, relates to the proportion of links of a node towards other nodes within its own module, and is defined as:

$$z_i = \frac{k_i - \langle k_{c_i} \rangle}{\sigma_{k_{c_i}}}, \tag{1.4}$$

where $\langle k_{c_i} \rangle$ is the average degree of nodes in the same module c of node i and $\sigma_{k_{c_i}}$ is the standard deviation of degrees of nodes in module c.

With the combination of these two metrics it is possible to classify nodes on the basis of the role they play within the network. For example, if a node presents high values in its participation coefficient, we could conclude that this specific region has a central role in connecting one module to others, i.e. in the integration of the modules into a cohesive structure. Hubs with high participation coefficient are therefore dubbed **connector hubs**. Conversely, nodes with high within-module degree and low participation coefficient i.e. strongly embedded within their own module, determine the presence of segregated subnetworks, and

are dubbed **provincial hub** ([Guimera and Amaral, 2005]; figure 1.8). It is critical, when addressing the modular organization of brain networks, to be able to interpret and classify the role that different brain regions play within the global architecture [Sporns et al., 2007]. All these special nodes are crucial for a correct flow of information within the network; with the disruption or alteration in the segregation or integration of central hubs, the system can develop pathological conditions [Fornito et al., 2016].

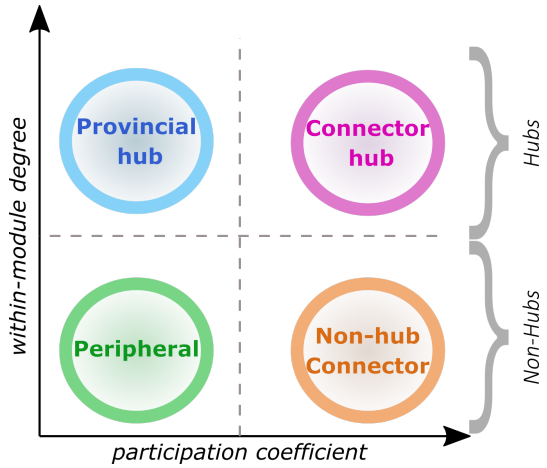

Figure 1.8: Role of nodes classified by means of participation coefficient and module-degree, reflecting their function withi the global brain architecture [Guimera and Amaral, 2005].

Overall, network neuroscience can elucidate the specific role of different regions within the system, clarifying as well the way the network would be affected in the case of local or global topological alterations.

1.4 NEUROIMAGING OF THE ADDICTED BRAIN

So far, I reviewed the most recent technologies and techniques that have been implemented in the study of brain functioning. One of the most important keys that these methods provide is the chance to also grasp how structural and functional brain systems are misshaped by neurological and psychiatric disorders.

In this section, I will review the recent and breakthrough findings that neuroimaging brought to the understanding of brain alterations induced by long-lasting and chronic alcohol intake. In details, the understanding of how specific neural regions are altered in their structures and functioning in addiction

is hopefully leading to the development of new possible treatments. Finding target regions for effective treatments is, indeed, center of attention in functional neuroimaging studies. Ideally, we could evaluate how to manipulate functional aberrancies detected in brain disorders, such as addiction, bringing the neural activity of specific regions back to their baseline "healthy" functioning.

Related to addiction, the prolonged intake of drugs, such as alcohol, can eventually alter the transmission of specific neurotransmitters in the brain, leading to subsequent aberrancies in overall brain function and structure. The first impact that substances have on the brain is the sudden and sharp increase in dopamine release. Dopamine is an important neurotransmitter in the human brain, whose function is mostly related to the so called "brain reward system". The brain reward pathway comprises specific neural regions, from the basal ganglia (striatum, globus pallidus, thalamus), to the nucleus accumbens, amygdala, and prefrontal cortex area. This neural circuit is responsible for the response to pleasurable and motivating behaviors, evolved for the motivational learning. When any kind of reward – from behaviors to substances – activates this system, dopamine is released, producing a feeling of pleasure, and we learn the association between that trigger and pleasure. Drugs can, indeed, activate the brain reward system, eliciting a reward signal subsequently learned and associated to pleasurable effects of these substances [Volkow et al., 2016]. Addiction works exactly as a learning process: repeated intakes of a specific drug of abuse cause a subsequent association with the environmental stimuli related to the experienced pleasure. However, with more and more exposures to the same rewarding stimuli and effects, our brain gets desensitized, and dopamine neurons stop firing when the substance is taken, but start firing, instead, in response to stimuli related to the drug (i.e. conditioned stimulus). These events lead to compulsive drug-seeking behaviors, typical in addiction, increasing strong cravings for the drug, and incentive salience mechanisms. The motivational learning phase of addiction, comprising crucial neuroadaptations, underlies the first stage of the addiction cycle previously reviewed, namely the "binge-intoxication" stage.

Overall, addiction strongly affects the brain reward system. This pathway loses its natural orientation towards ordinary pleasurable rewards, reorienting to the more powerful release of dopamine that drugs and their environmental cues ex-

ert. This results in a severe change in motivation and behavior [Volkow et al., 2016]. With prolonged and chronic intakes, the reward circuitry experiences an important reduction in the release of dopamine, as well as in dopamine D2 receptors [Volkow et al., 2002]. This reduction in the functioning of the dopamine system seems to be directly related to a subsequent increase in the reward threshold [Koob, 2013]. As a consequence, the motivation naturally experienced towards non-drug-related stimuli is severely affected, falling into an increased sensitivity to the abused drug [Volkow and Fowler, 2000]. Addicted people will thus stop feeling the strong euphoria and positive feelings associated to the drug intake, and will start, instead, to feel increasing urges to take the drug as to reduce the negative affects experienced. During the withdrawal stage, indeed, negative affects, such as anxiety, dysphoria, stress, irritability, dominate the addicted person. All these neurochemical adaptations drive towards severe negative reinforcements, becoming a core aspect in addiction. The addicted behavior is no longer driven by voluntary actions seeking rewards, but by strong and negative compulsions. In this phase, drug intake becomes purely a means to counteract the negative emotional state associated to withdrawal. At this stage, compulsivity becomes an important negative reinforcement that perpetuates addiction, leading to relapses. Relapse is one of the most crucial keys in alcohol addiction. Despite repeated therapeutic interventions, most patients experience relapse, falling back into the addiction cycle.

1.4.1 Structural and functional alterations in alcohol addiction

All the internal and external processes underlying addiction may affect the brain at a structural and functional level. Imaging techniques open a view over these alterations. Over the years, thanks to the use of structural and functional MRI, different findings increased the knowledge regarding brain aberrancies induced by chronic alcohol intake. At a structural level, acute and chronic effects induced by alcohol consumption have been consistently revealed to involve both white matter and gray matter volume changes [Fritz et al., 2019]. One of the most common analysis techniques aiming at the evaluation of regional WM and GM partitions, without the necessity to predefine a region of interest, is Voxel-Based Morphometry (VBM).

This methodological analysis allows a voxel-wise comparison of the whole brain. Related to the study of addiction, several studies reported neurotoxicity effects induced by a long-lasting alcohol intake which led to important brain atrophy in different regions [Gazdzinski et al., 2005, Chanraud et al., 2007, Mechtcheriakov et al., 2007, Wrase et al., 2008, Rando et al., 2011, Fritz et al., 2019]. Important reductions in GM volumes have been shown to involve focal regions such as frontal and prefrontal cortices, temporal cortex, insular cortices, hippocampus, thalamus, and cerebellum (figure 1.9, [Dupuy and Chanraud, 2016, Chanraud et al., 2007, Mechtcheriakov et al., 2007]). Significant WM loss is also reported in alcohol addiction, mostly comprising the corpus callosum [Chanraud et al., 2007], the largest white matter structure in the human brain connecting the two hemispheres. Interestingly, some of these damages also seem to be related to the symptomatology underlying alcohol addiction. For example, correlations of volumes reductions have been reported between corpus callosum changes and executive functions impairments. In addition, brain regions volumes appears to be sensitive also to drinking related measures. A correlation between GM decreased volumes in temporal cortices and age at first drinking is, indeed, reported by the same authors [Chanraud et al., 2007]. Neuroimaging-based measures may also give insights over future drinking behaviors, such as GM volumes reductions in frontal and prefrontal cortices predicting earlier relapse [Rando et al., 2011]. More severe brain atrophies is, indeed, present in patients that later relapse, compared to abstainers [Gazdzinski et al., 2005], with a particular involvement of the amygdala, which appears smaller in relapsers [Wrase et al., 2008]. This knowledge might be crucial for therapeutic options, reinforcing personalized treatments. Overall, some of the volume changes mostly reported involve the basal ganglia. As previously mentioned, the basal ganglia are a core ensemble of brain regions crucial within the reward system. Structural alterations in alcohol addiction include the caudate, putamen, amygdala, and nucleus accumbens [Dupuy and Chanraud, 2016, Fritz et al., 2019]. The progression of alcohol addiction, shaping rewarding behaviors as extensively reviewed, may be the key contribution to the changes experienced in these central regions, which are, indeed, related to motivational learning, reward evaluation, and cue-induced relapse [Fritz et al., 2019].

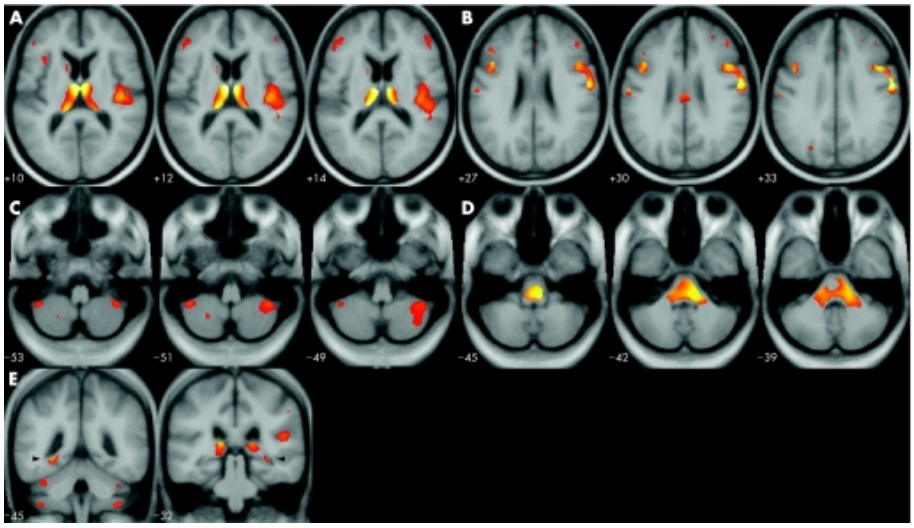

Figure 1.9: Areas of significant GM and WM reductions in alcohol addiction, from [Mechtcheriakov et al., 2007]

Functional alterations in alcohol addiction, measured by fMRI, are found both during task performance and at rest. Measuring BOLD activity changes in response to specific tasks is often applied to evaluate functional brain alterations related to cue-reactivity, craving, impulsivity, or self-control [Fritz et al., 2019]. This approach is crucial to understand functional brain alterations that might lead to subsequent behavioral deficits, possibly driving patients to the inability to evaluate risks and dangers related to alcohol consumption, maladaptive decision-making, and to the incapacity to quit drinking. It has been proven, for example, that alcohol dependent patients show a strong alcohol cue-induced attentional bias. Moreover, this attentional bias to alcohol cues was related to an activation of visual and attention brain areas, such as the occipital cortex, anterior cingulate cortex, amygdala, insula, and thalamus [Vollstädt-Klein et al., 2012, Wrase et al., 2008]. In line with this, AUD patients seem to more strongly recruit several networks in response to alcohol cues, such as the default mode network (DMN), the salience network, and the executive control network [Myrick et al., 2004].

The study of functional connectivity has also proven increasingly helpful in the evaluation of brain alterations involved in alcohol addiction. The first network that was proven to be disrupted in alcoholic patients was the DMN [Chanraud et al., 2011]. The DMN is considered as the most representative network found in resting conditions, it comprises a set of brain regions that appear to be more highly synchronized when the brain is not performing specific tasks. This includes the

posterior cingulate cortex, inferior parietal cortex, medial prefrontal, medial temporal cortices, and the precuneus. Alongside, disconnectivity patterns in alcohol addiction involve specifically also the executive, salience, basal ganglia, and visual networks [Chanraud et al., 2011, Müller-Oehring et al., 2014, Weiland et al., 2014, Vergara et al., 2017]. The reduction in functional connectivity in specific brain regions such as the precuneus, insula, and visual cortex could be a hint related to the dysfunctional interoceptive awareness typical of alcoholic patients [Vergara et al., 2017]. What seems more striking is that AUD patients specifically show an increase in between network connectivity, but, at the same time, a weaker pattern of within network connectivity. Altogether, these functional alterations raised insights towards the hypothesis of a "disconnection syndrome" in alcohol addiction [Dupuy and Chanraud, 2016]. A related striking finding, in addition, linked this altered pattern of between and within networks connectivity to the severity of the disorder [Fede et al., 2019]. It was, indeed, possible to predict the severity of the Alcohol Use Disorders Identification Test (AUDIT) scores, a common self-report questionnaire used in clinical settings to assess alcohol dependence, through the disrupted resting-state functional connectivity identified in patients. These findings are critical for clinical settings. The ability to predict the severity of the disorder by means of fMRI, without the necessity to rely on self-reports, is of crucial relevance and may provide insights regarding target structures for treatments.

In recent years, however, a distinct region, key in the control of conscious emotional experience, gained increasing attention: the insula, a central station for interoceptive signals, processing bodily sensations [Naqvi and Bechara, 2009].

1.4.2 Insular cortex and its role in interoception

The insular cortex is a core region of the brain responsible for interoception, the sense of physiological condition of the body (1.10; [Craig, 2009]). This collection of processes is key in the set of awareness we daily experience, such as hunger, thirst, pain, or even, for example, the need for alcohol. Given the strong impact that alcoholic beverages, as well as other set of drugs, have on the body, it is not surprising that interoceptive processes might play such a central role in the onset and maintenance of addiction. The interest in the involvement of the insula in

addiction took more hold from the observation that smokers with damages in this region were able to quit smoking much easily than smokers with damages in other areas of the brain. These patients even reported that "their body forgot the urge to smoke" [Naqvi et al., 2007].

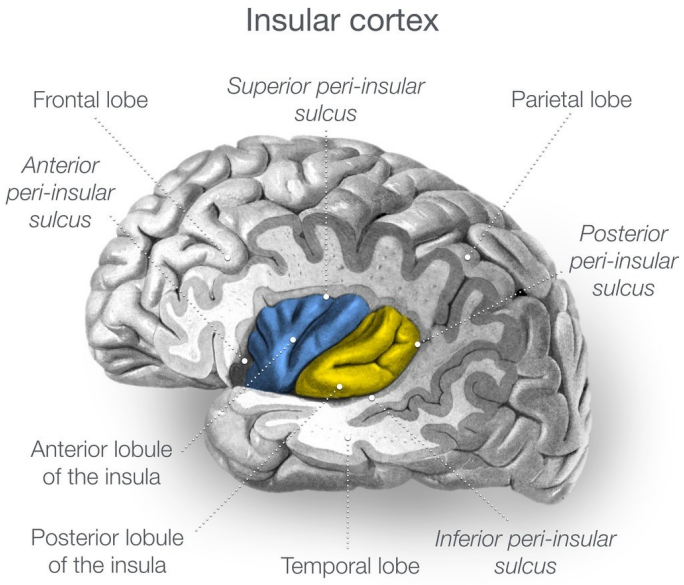

Figure 1.10: Neuroanatomy of the insular cortex. Case courtesy of A.Prof Frank Gaillard, Radiopaedia.org, rID: 46846

The insula is a complex brain structure, anatomically divided into various subregions (figure 1.10) . From a cytoarchitectonic point of view, it can be split into granular and agranular insular cortex [Chikama et al., 1997]. The former comprehends the posterior portion, mostly responsible for somatosensory, vestibular and motor integration. More interest for addiction lays, instead, in the latter subdivision, comprising the anterior portion of the insula. This portion receives input from limbic regions, both cortical and subcortical, processing autonomic and visceral information into emotional functions [Naqvi and Bechara, 2009]. The bodily representation of visceral needs directly influences feeling states, with the subsequent formation of emotional cues, guiding our behavior and needs. The central role played by the insula is, indeed, to translate interoceptive signals generated by substances intake into conscious bodily appreciations of these effects (1.11). Each drug of abuse has a specific bodily effect, which sometimes becomes more addictive than the drug itself. The feeling of smoke flowing into the upper airways, plays, for example, a crucial role in the establishment of nicotine addiction. The

more substance users fall into addiction, the more these stimuli, both physical and environmental, gain an emotional valence, mediated by interoceptive centers with their base in the insular cortex. The insula would encode these interoceptive effects of drugs, leading to the formation of conscious cue-induced urges, through its connection towards frontal regions. Such process would consequently increase drug craving, defined as a "pathological desire" of the substance of abuse. The growing evidence coming from neuroimaging studies now corroborates the involvement of this central region in addiction, consistent with this interoception-centered model of addiction [Verdejo-Garcia et al., 2012].

1.4.3 Insular alterations evidence from clinical neuroimaging

From neuroimaging, insular anomalies have been consistently identified in alcohol dependent patients, both from a structural and a functional perspective. From a structural perspective, neuroimaging techniques have been applied to the evaluation of cortical thickness as well as differences in structures volume. Morphometric methods have identified brain tissue shrinkage and changes related to alcohol consumptions. Mechtcheriakov and colleagues [Mechtcheriakov et al., 2007] were the first to identify gray matter alterations in the insula, together with other cortical regions, providing one of the first evidence associating alcohol addiction to abnormal neural density. Shortly after this study, Jung et al. [Jung et al., 2007] focused their attention on the evaluation of specific anatomical alterations in the insular cortex. This work led to the identification of shape abnormality in the insula, with a consistent reduction of left-right asymmetry. Interestingly, these anomalies correlated to the duration of the illness, suggesting an association of insular deformities with chronic alcohol consumption. Neuropsychological scores, related to executive functions disrupted in alcoholic patients, were also found to correlate with reduced insular volume [Chanraud et al., 2007]. Furthermore, corroborating insula role in compulsive alcohol intake, its volume was found to be related to abstinence length, with a recovery of its tissue in patients abstaining from drinking alcohol (figure 1.12, [Cardenas et al., 2007, Demirakca et al., 2011, Durazzo et al., 2011, Makris et al., 2008, van Eijk et al., 2013]. Both abstinence and binge drinking affect insular volume, with more severe shrinkage associated with high frequency

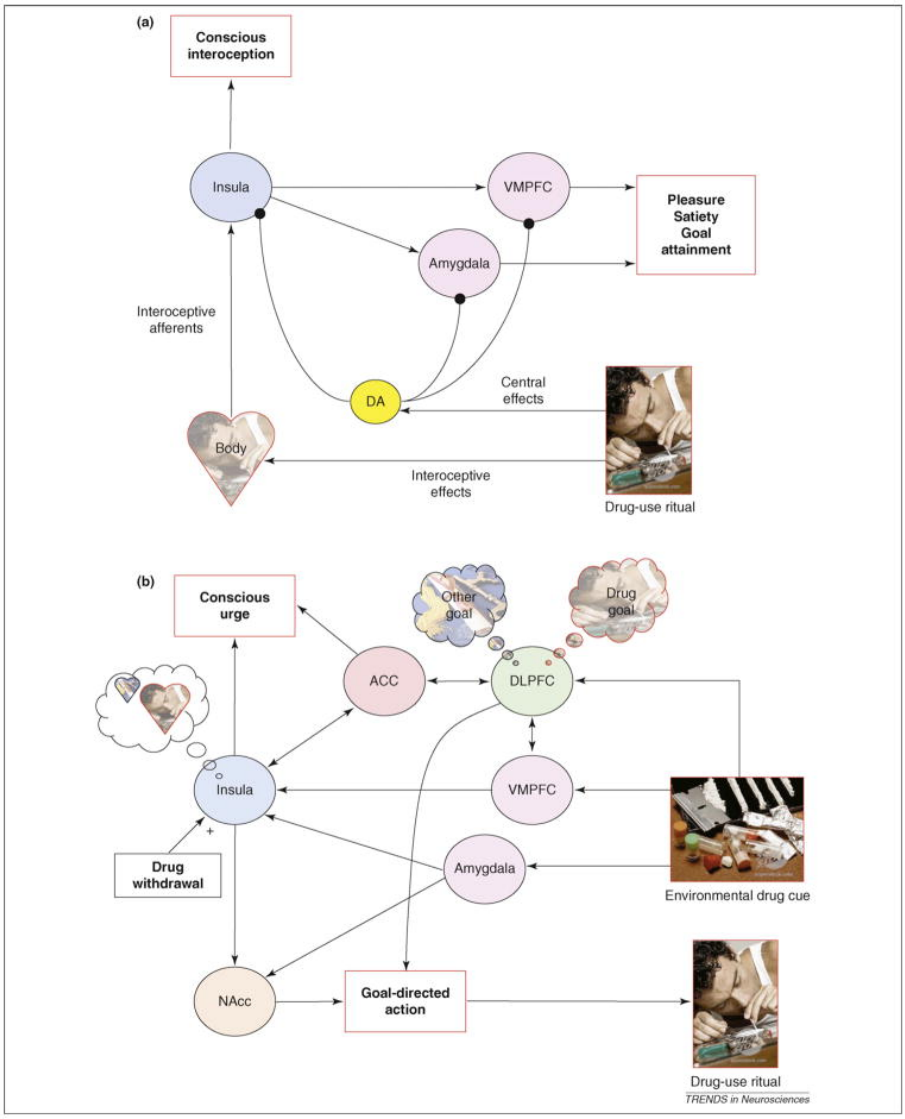

Figure 1.11: From [Naqvi and Bechara, 2009]. Schematic model of the interoceptive functions of the insula. The insula is necessary for the formation of drug-use rituals, representing the interoceptive effects of drugs. Once the subject is exposed to environmental drug cues, the system reactivates the representations of these interoceptive effects, involving higher-order processes driving decision-making (ACC and DLPFC) and conscious feelings.

drinking [Chung and Clark, 2014]. Moreover, among all the regions of the brain reward system, the insula shows the most pronounced structural alterations, further suggesting its central role in the overall addiction system [Makris et al., 2008]. Altogether, an increasing number of studies identified gray matter reductions in the insular cortex of alcohol dependent patients [Yang et al., 2016a, van Holst et al., 2012, Senatorov et al., 2014].

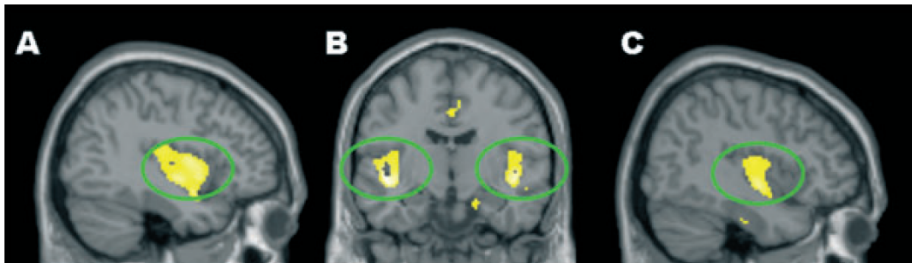

Figure 1.12: Voxel-based morphometry of gray matter loss in the insular cortex for alcohol dependent patients, from [Demirakca et al., 2011]

Similarly, also functional alterations seem to be prominent in the insular cortex of alcohol dependent patients. Several tasks designed to evaluate changes in the functioning of specific brain regions involved in addiction-related behaviors reported altered insular activity in alcoholic patients. The functional responses in this region in alcohol use disorder patients is, however, not as clear as its anatomical shrinkage. During social exclusion tasks, for example, alcoholics revealed higher insular activation compared to healthy volunteers, reflecting difficulties in negative emotional regulation [Maurage et al., 2012]. An increased activation is also present in heavy drinkers compared to light-drinkers when exposed to alcohol-related cues, related to higher compulsivity, establishing a likely neural correlate of compulsive alcohol seeking [Grodin et al., 2018]. Abnormal higher activity of the bilateral insula was shown also in binge drinkers in a well-established decision-making task, with its activation correlating with urgency scores [Xiao et al., 2013]. Impulsiveness was also found to be related to a higher activity of the insula during reward anticipation in patients compared to control, emphasizing again the role of this structure in conscious urges [Villafuerte et al., 2012]. Moreover, alcoholic cue presentation was found to increase insular activation with this altered activity being related to the severity of the disease [Claus et al., 2011]. Conversely, decreased activation is reported during risk-taking decisions [Li et al., 2009], similar to a trend in decreased activity recently found in alcoholic patients in an Ultimatum Game task, which evaluates rational decision making [Cortes et al., 2018]. Reductions in the connectivity between putamen and insular cortex has been reported in patients during tasks of response inhibition [Courtney et al., 2013]. Conversely, meta-analyses addressing neural basis related to cue-reactivity [Chase et al., 2011] and craving [Kühn and Gallinat, 2011] in drug addict did not find any specific activation of the insula. Altogether, these findings show some

inconsistencies, with a general trend towards abnormal activation of the insular cortex when patients are exposed to alcohol-related cues or emotional decision-making. Interestingly, insular anomalies in alcohol addiction seem to be mostly associated to compulsions and urges [Grodin et al., 2018, Xiao et al., 2013]. These evidence would confirm an altered interoceptive role played by the insula, unable to adjust external environmental cues and internal needs. From task-based functional neuroimaging, however, findings regarding alcohol addiction remain controversial, probably due to the heterogeneity of tasks. These contrasts pose the need for further research investigating what abnormal insular functionality can be related to.

1.4.4 Evidence from the emerging field of functional connectivity

I already highlighted some of the main disruptions reported in the resting-state functional connectivity in alcohol addiction, which led to the definition of a "disconnection syndrome" hypothesis. Among these alterations, one of the functional resting state networks of greatest interest in the field of addiction is the so-called salience network (figure 1.13, [Seeley et al., 2007]). This specific functional network is composed by insular regions coupled with the anterior cingulate cortex. It has been suggested that this resting-state system sub-serves the capacity of the brain to integrate sensory information with visceral, autonomic and hedonic stimuli. This network shows aberrant connectivity in a number of different studies addressing resting state functionality in alcohol dependent patients, leading to further evidence of insular alterations related to alcohol drinking [Camchong et al., 2013, Müller-Oehring et al., 2014, Sullivan et al., 2013, Vergara et al., 2017, Zhu et al., 2015]. However, even for functional connectivity related studies, it is possible to observe some discrepancies and controversial findings concerning the role of the insula. A very interesting result relates to the evidence of reduced resting state synchrony within the insular network. This reduction was found to be present in detoxified patients that later relapsed, compared to patients that, in the opposite, remained abstinent [Camchong et al., 2013]. This suggests a critical role of resting state functional synchrony in maintaining abstinence during detoxification. Specifically, in this case, the role of the insular network seems predominant. Strong re-

ductions in synchrony were identified also with the dorsolateral prefrontal cortex network, a central system in the brain, sub-serving executive control processes regulating emotions. Further reductions in between regions synchrony in relapsers were present in the connectivity within the visual and the insular networks.

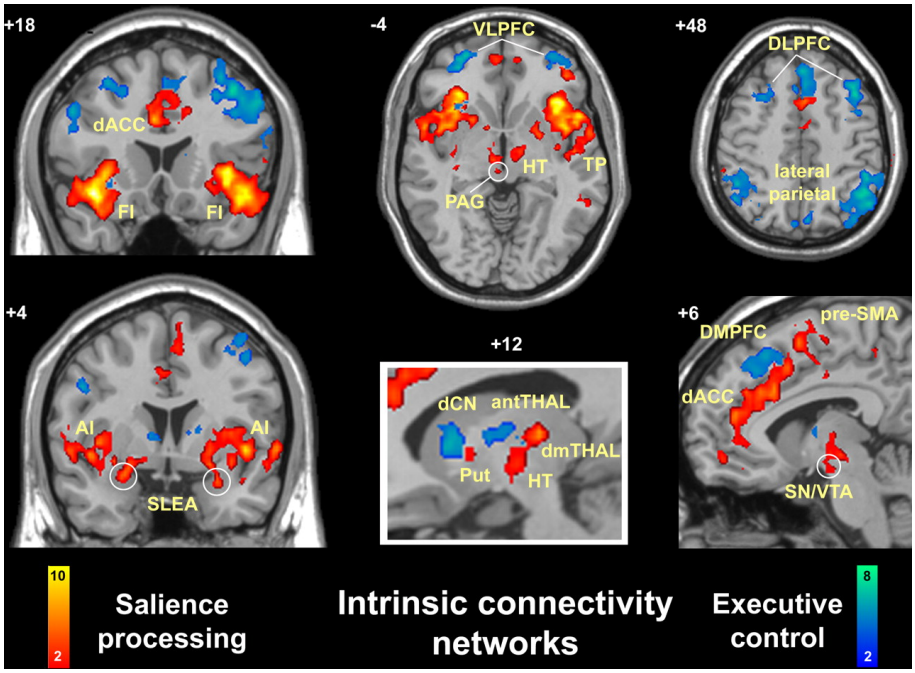

Figure 1.13: Salience network identfied by means of Independent Component Analysis

Altogether, this suggests faulty processing in sensory awareness and attention, most likely leading to aberrant decision-making, which can later evolve into relapse. Such findings can be crucial for further investigation of effective treatments for this chronic brain disorder, having highlighted the important role that the insula can play in remaining abstinent. In line with this evidence, a lack of synchrony between the insular regions and the DMN was later found in early abstinent patients [Sullivan et al., 2013]. Decreased synchrony between the insula and parietal or frontal cortices was similarly reported in this last study, confirming previous evidence of an altered communication within this core region and many other brain networks. In addition, a study by Müller-Oehring and colleagues [Müller-Oehring et al., 2014] reported a reduction in the within-network connectivity of the salience system. However, opposite to previous findings, this functional connectivity investigation revealed excessive outside-network connectivity, in turn related to poorer performance. Here, results revealed a likely inability to confine brain activation to specific functional areas in AUD, with the necessity to involve

external regions, differently from healthy individuals; this aberrant involvement of functionally different brain areas may probably be in line with the excessive activation of brain regions observed through task-based fMRI studies. As mentioned previously, hypo-connectivity within the salience network was specifically identified in alcohol drinkers when compared to smokers, suggesting a possible specificity driving underlying mechanisms of alcohol and nicotine [Vergara et al., 2017]. Here, drinking, as well as cigarette smoking, also reduced the connectivity among the insula and different cortical areas. Contrasting results show, instead, an increase in within-network connectivity for different resting state systems, including the salience network [Zhu et al., 2015]. In line with previous investigations, this study revealed an increase in between-network connectivity, among the salience and executive control systems. Being the insular cortex a central area for reward processing, interoception, and, among many other functions, emotional decision-making, all these growing evidence addressing its aberrant connectivity corroborate its central role in the development and maintenance of alcohol addiction. Good integration between different brain regions is necessary for the stability and functioning of the network. Alterations in these systems may cause aberrant behaviors, such as an excessive craving of alcoholic beverages leading to the inability of patients to avoid relapse. Specifically, this observed hypo-connectivity within the insular system can underlie a reduction in substance use awareness. It is interesting to observe, however, some discrepancies present in functional connectivity investigations. Functional brain activity can be easily influenced by external factors. Even a subtle difference in the number of abstinent days from alcohol can alter systems of hypo- or hyper-connectivity. Müller-Oehring and colleagues [Müller-Oehring et al., 2014] , for example, identified increased between-networks connectivity, opposed to a decreased within-network reduction in connectivity strength, by evaluating long-term abstinent patients, similar findings as those reported by Sullivan group [Sullivan et al., 2013] in abstainers. Patients from the group of Zhu [Zhu et al., 2015] were, instead, short-term abstainers (less than two weeks), and showed both between and within networks increase in connectivity. Hypo-between network connectivity is also reported in the investigation carried out by Vergara and colleagues [Vergara et al., 2017], which was, on the contrary, assessing functional activity in drinking patients. It might be possible to hypothe-

size that an increase in between-region connectivity appears during a withdrawal state, opposite to a reduced functional synchrony likely induced by the presence of ethanol.

1.4.5 New promises from network neuroscience: a graph theoretical approach

In the previous sections, I introduced the fast development of a novel emerging field, grounded in the physics world of network science, and which has proven to be incredibly precious for the identification of subtle topological organizations in the network of the human brain.

However, so far, very few studies investigated alterations in the network organization of alcohol dependent patients [Morris et al., 2017, Sjoerds et al., 2015, Zorlu et al., 2017]. Even though only few studies are present in the literature, a clear trend has now emerged. Specifically, decreased functional connectivity strength and efficiency of the overall network have been reported in alcohol dependent patients in all these studies. In network science, the efficiency of a network indexes how efficiently the information flows between different nodes and part of the system. Interestingly, the reduction in the global system efficiency has been reported to correlate with the duration of alcohol dependence [Sjoerds et al., 2015], reflecting the disruption of network integrity with continuous alcohol drinking. Alcohol dependence seems to be associated with a lower efficiency of local subcortical brain regions of the reward system, such as the thalamus, pallidum, and caudate [Sjoerds et al., 2015, Zorlu et al., 2017]. Conflicting findings report an increase in local efficiency in alcohol dependent patients compared to poli-drug users, reflecting stronger segregation of neural systems induced specifically by alcohol consumption [Morris et al., 2017]. Interestingly, this alteration in local efficiency was normalized by a single dose of naltrexone, a common drug used for the treatment of alcohol addiction [Morris et al., 2017]. This same study, in line with previous investigations, revealed a reduction in global functional connectivity in alcoholic patients compared to both poli-drug users and healthy volunteers. Decreased global efficiency was also observed in a different sample of poli-drug users (comprising patients with an AUD diagnosis) coupled, however, with an increase in the local degree of different regions, comprising the insula [Wang et al.,

2015]. The imbalance between overall functional connectivity reduction and the increase in local degree or local efficiency reported may reflect alterations of the flow of information in specific functional areas. The presence of regions with a higher efficiency may underlie an exaggerated role of these regions, such as the insula, which might unbalance the system normal functioning.

Taken together, these few investigations show a trend towards a reduction in the overall efficiency of the network, with an unbalanced integration of specific regions involved in addiction in the whole system. This new and advancing graph theoretical approach promises to identify finer alterations underpinning brain pathologies, revealing the specific topological organization through which different brain regions communicate with each other. Hence, more studies in this growing field are necessary to shed light over the network functioning of alcohol addiction, with a focus on the integration and segregation of the insula within this complex brain system.

1.4.6 A new target for alcohol addiction?

Understanding brain functional alterations involved in addiction is of tremendous importance for the development of new treatment options, improving the clinical outcome of this chronic relapsing disorder. The research of a successful pharmacological or behavioral therapy in alcohol addiction is, however, extremely complex. As I reviewed, different studies seeking neurological biomarkers of addiction report discrepant results. Addiction is a highly heterogeneous disorder, and an efficient treatment might depend on a number of distinct factors [Heilig et al., 2011], comprising genetic variability, duration of the disorder, abstinence days when starting the treatment, and many other factors. Few pharmacological treatments are now available, and they do not show efficacy in all patients. The first medication approved for alcohol addiction was naltrexone, an opioid antagonist, found to reduce craving as well as the experienced reward when drinking alcohol. Unfortunately, not all patients respond to treatments with naltrexone, with a rate of response found to be highly related to a genetic variance. Alcoholics with a positive family history of addiction better responded to treatment [Monterosso et al., 2001]. Another line of pharmacological treatment for alcohol dependence com-

prises, instead, the use of a glutamate antagonist, acamprosate. The use of such drug is related to evidence suggesting the development of a hypergluatametrgic state in the brain with the progression of alcohol dependence [Heilig and Egli, 2006]. Similar to naltrexone, the use of acamprosate decreases craving, however, its efficacy in the whole AUD population remains modest. Chronic exposures to alcohol induce long-term and long-lasting neural changes, which can be challenging to reverse and avoid relapse for a good clinical outcome.

A new promising treatment option rely on techniques of neural stimulation (figure 1.14). Transcranial Magnetic Stimulation (TMS) is a non-invasive method, with both neurostimulatory and neuromodulatory characteristics. By delivering magnetic pulses over the scalp, TMS generates electrical activity in targeted brain regions, altering neuronal excitability [Spagnolo and Goldman, 2016]. This new treatment approach has already been approved for treatment resistant depression, through a stimulation of prefrontal cortices [Lam et al., 2008], and for obsessive compulsive disorders. The most common approach, investigated as a possible therapy for addiction with TMS, exploited the delivery of repetitive pulses over the scalp, targeting the dorsolateral prefrontal cortex (DLPFC), a region easily reachable by TMS and demonstrated to reduce craving [Johann et al., 2003]. However, studies exploiting this specific approach report contrasting findings, likely due to small sample sizes, or by the lack of follow-up controls on alcohol consumption [Del Felice et al., 2016, Herremans et al., 2012, Mishra et al., 2015]. The strongest limitation of this specific stimulation protocol lies in the depth of the targeted regions. As extensively reviewed, the insula plays a critical role in the maintenance of addictive behaviors, with morphological and functional alterations. However, this cortical region is embedded deeper in the brain. The development of a specific magnetic stimulation coil, the H-coil, represented a tremendous development in the field, as it allows targeting deeper brain regions, delivering a simultaneous bilateral stimulation [Roth et al., 2007]. Having the chance to artificially manipulate the activity of the insular cortex could represent a critical treatment option, as it could give us the possibility to reverse the unbalanced and altered activity that this region presents in addiction. Insular gray matter volume, as well as its functional activity, is found to be correlated to the severity of alcohol addiction, meaning that if we could act on its functioning we might be able to finally improve the clinical

outcome of many addicted patients [Jung et al., 2007, Chanraud et al., 2007, Sjoerds et al., 2015, Grodin et al., 2018]. Moreover, immediate smoking cessation induced by lesions in the insular cortex seems to confirm the view that manipulation of the activity of this central region may help control addictive behaviors [Naqvi et al., 2007]. Unfortunately, H-coils are not widely diffuse, being a new and expensive technique, not extensively corroborated, yet; hence, not many studies addressing its functionality are present in the literature. An impressive study, however, tested this specific coil stimulating the insula and prefrontal cortices on smoking addicts, with very promising results in the reduction of cigarettes craving [Dinur-Klein et al., 2014]. Clinical trials in alcohol-addicted patients, testing the efficacy of this encouraging treatment option, are now ongoing, hopefully leading to a final and efficient therapeutic mechanism.

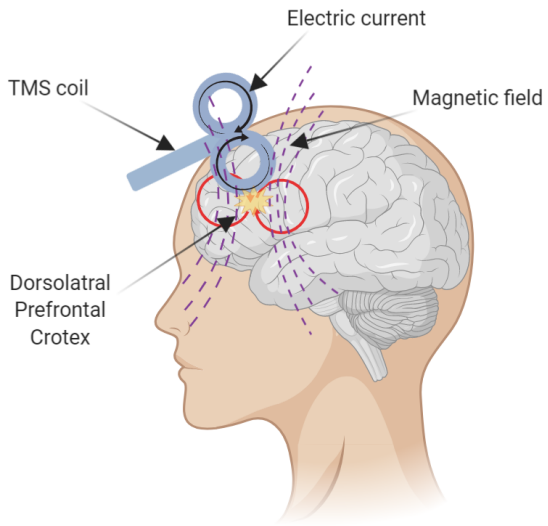

Figure 1.14: Schematic representation of TMS functioning

Specifically, the evaluation of changes, both at a behavioral and at a brain functional level, after the application of a treatment exploiting deep TMS is under investigation (`http://sybil-aa.eu/`). By scanning treatment-seeking patients with MR technologies before and after several sessions of TMS, it will be possible to look at changes in brain activity patterns induced by magnetic perturbations. Exploiting the emerging field of network science, extensively reviewed, it is possible to specifically evaluate how the brain network organization can be altered. As the insular cortex has been found to play an excessive role in the overall func-

tional network of AUD (Bordier et al., in prep), it would be possible to address how its embedding within the system may change after repetitive stimulations. Indeed, we could consider a deep TMS treatment as a focal perturbation of connectivity networks. This approach can help in a finer understanding of how the flow of information through the insular cortex can be altered and manipulated. If coupled with a successful behavioral outcome, such as a reduction in alcohol craving, the evaluation of network characteristics before and after treatment could highlight possible predictors of response as well as biomarkers of alcohol addiction. This novel treatment approach is now promising, but in need of thorough investigations and clinical assessment. Altogether, alterations in the role played by the insular cortex in AUD are now well established, from brain morphology to abnormal functional activity patterns. Alcohol addiction is a severe and chronic disorder; it is not only affecting patients' lives, but also their families, with social, economic, and health consequences. The identification of biomarkers and possible predictors of response to treatment for this disorder has a crucial importance. Merging novel neuroimaging techniques, with advanced methodological and analytical approaches, together with the use of new treatment options, can have an important impact over the understanding of the biological basis for alcoholism. Still, more work is needed to shed light over the specific malfunctioning mechanisms of the insula in alcohol addiction, being the present literature rich of controversial results. This direction, however, is now promising, given the growing evidence of the exaggerated and altered role played by this interoceptive region in alcohol addiction, likely being the final target of this chronic brain disease.

In the present work, I will try to go into the details of the altered functional mechanisms in alcohol dependent patients, through the evaluation of a cross-sectional study assessing differences between a cohort of patients and a sample of healthy volunteers. I will explore these characteristics by means of a graph theoretical approach, with a specific emphasis over the modular architecture identified in these samples. Following, I will test the efficacy of the novel proposed treatment based on a deep brain stimulation of the insular cortex. However, before dwelling into the details of these clinical study, I will have to address several methodological issues now present in the world of network science, such as how

to deal with head movements and their correction during preprocessing steps, and how to properly threshold the resulting functional connectivity matrices.

2 EVALUATION OF METHODOLOGICAL ISSUES

As disclosed in the introductory chapter, before dwelling into the clinical aspects of this work I will explore some open questions present in the methodological façade of the functional connectivity world.

Indeed, despite the growing confidence in handling complex network systems, a number of critical methodological issues remains open. Despite the strengths of this approach, several critical questions need to be considered for the sake of populations' comparability. Among these, the sparsification procedure is one of the most debated aspects now present in the scientific literature. This controversy is particularly crucial for the evaluation of functional brain networks, which, as previously mentioned, are by definition complete networks. However, complete networks are intractable and spurious correlations might affect the majority of links. For this reason, thresholding seems an essential step. Nevertheless, it is argued that the application of a specific threshold might substantially impact the topological organization of the final extracted network, and this uncertainty has now led to a trend in the community to completely avoid this procedure and directly work with full systems. Yet, the lack of a sparsification procedure might be misleading and hinder the real organization of the network. Deeper investigation of this aspect is thus crucial to subsequently carry out accurate network analysis.

Another crucial aspect that might hinder the topological organization of the network, by injecting spurious correlations within the system, stands in the presence of motion artifacts in functional brain data. In the following chapter, I will thus face another critical debate present in the resting-state functional connectivity field, related to the correction of small head movements that the participant can make while laying in the MRI scanner. The finding of the dramatic effects that motion can have on resting-state functional connectivity data resulted in an explosion of novel strategies aiming at the removal of such artifacts. Unfortunately, the lack of a ground-truth functional architecture of the human brain make it extremely

hard to evaluate the effects of a thresholding procedure and the efficacy of the introduced pre-processing techniques, which might "clean-up too much". Both operations might, indeed, risk to remove genuine neural correlates together with artifactual signals.

These issues are particularly relevant when we compare clinical populations, where we need to maximize comparability across different samples. Given these strong impacts, I dug into more details, and developed a brief methodological study with the aim to evaluate specific effects of the thresholding procedure, questioning the existence of an optimal threshold point, as well as effects of head movements over functional connectivity data and their modulation by different motion-correction techniques.

Specifically, I will introduce procedures to generate null models of a functional connectivity network, i.e. a randomized version of the graph, and tools grounded in information theory to measure the distance between the empirical network and its corresponding random counterpart. This approach enables assessing the effects of sparsification or motion correction on the structure of the network at various scales by measuring the gain in structural information with respect to the null model, thus circumventing the lack of a ground-truth structure. Following a description of the methods, I will apply this approach in an exemplary patient-control study, to demonstrate its use, and will extend it to the demonstration of the existence of an optimal threshold for network sparsification, and to the evaluation of various pipelines for the removal of the effects of in-scanner head motion.

2.1 THRESHOLDING FUNCTIONAL CONNECTIVITY NETWORKS

As I thoroughly reviewed, the study of the brain as a complex network experienced a tremendous growth in the past decade. Yet, it still faces major debates.

Indeed, given the promises of handling complex networks, a growing number of studies resorted to the application of graph theoretical methods to characterize both the healthy and the diseased brain [Fornito et al., 2015, van den Heuvel and Hulshoff Pol, 2010]. This is mostly achieved by means of resting-state functional connectivity (RSFC) measurements, where inter-regional correlations in

spontaneous low-frequency oscillations (0.01 Hz – 0.1 Hz) of brain activity can be extracted, mapped as a graph, and thus reflect the underlying brain functional architecture.

Despite its increased popularity, this approach still experiences a lack of agreement on several methodological aspects related to network construction [Hallquist and Hillary, 2019], possibly hindering replicability and study reliability. One of the most contentious methodological issue lays in network sparsification. Specifically, functional connectivity networks are generally derived from pairwise correlations of spontaneous fluctuations extracted from each pair of brain regions, resulting, by definition, in a fully connected weighted matrix. However, dense networks are computationally demanding. In addition, weak links, which represent the overwhelming majority of edges, might contain spurious correlations, and the interpretation of the biological meaning of negative links is somewhat dubious [Saad et al., 2012, Murphy and Fox, 2017]. For these reasons, it is common to artificially remove such links from the system, thus working with sparse networks, where all the entries below a given value (the threshold) are set to 0. Ideally, this approach would ensure the removal of spurious links, and maximize the identification of the underlying functional architecture. To achieve this, the application of a global threshold to weighted dense matrices is the most popular approach, thus reducing the density of the graph. Given the importance of this procedure, a growing number of thresholding techniques are reported in the literature [Hallquist and Hillary, 2019, van den Heuvel et al., 2017a, Bordier et al., 2017, Santarnecchi et al., 2014, Lohse et al., 2014, Schwarz and McGonigle, 2011]. The two most common approaches rely on the application of an "absolute threshold" or a "proportional threshold" [van den Heuvel et al., 2017a]. Yet, both suffer from several shortcomings, resulting in an arbitrary choice of the final threshold applied. The former approach requires the choice, *a priori*, of an absolute threshold t, where all the links below this given value are excluded from the network and set to 0. An issue associated to this method lays in the risk to obtain networks with different levels of density (defined as the proportion of all possible connections in the network) which might be significantly problematic when addressing case-control studies, as patient groups may have a different edge-weight distribution compared to controls. Given that many graph topological metrics are sensitive to the number of

edges in the network, the latter approach –proportional thresholding- tries to overcome this aspect [Achard and Bullmore, 2007]. Here, the density of the network is fixed, only retaining a proportion of the strongest edges in the network. To rule out the possibility that subsequent results may be driven by the choice of this proportional threshold, many studies evaluate a range of different densities (e.g. from 5% to 25% of density) [Hallquist and Hillary, 2019]. Again, also this approach suffers from a similar drawback as the application of an absolute threshold: in case-control studies, patients often present a lower functional connectivity strength, and fixing a specific density may include weaker and spurious links in the patient group, while possibly discarding valuable information in the control group. It is therefore suggested to give closer attention to the choice of the threshold, controlling either for individual density or functional connectivity strength, when possible [van den Heuvel et al., 2017a].

Still, the choice of the threshold in this framework remains arbitrary. Many other solutions have been proposed, such as "soft thresholding" [Schwarz and McGonigle, 2011] or "windowed thresholding" [Santarnecchi et al., 2014]. Both methods stress the importance of negative and weaker connections, which might not be related to experimental noise, but contain valuable information. For example, Santernecchi and colleagues [Santarnecchi et al., 2014] reported a high correlation between weakest links and subject-specific features, thus proposing the application of "windowed thresholds", where the average edge weight of connections is fixed within a certain range. Others, instead, revealed the randomness of these weaker and negative connections [van den Heuvel et al., 2017a, Zalesky et al., 2016]. Other methods introduced for the analysis of brain networks comprise, for example, the minimum spanning tree (MST; [Tewarie et al., 2015], or efficiency cost optimization (ECO; [de Vico Fallani et al., 2017]. The former interestingly defines a fully connected sub-network minimizing the link weight while capturing essential properties of complex networks. Conversely, the latter approach aims to remove weakest connections while ensuring an optimal trade-off between the efficiency and the economy of the network. Overall, an increasing number of thresholding techniques has been introduced, yet, the topic is still center of a heated and opened debate, concerning the significance of negative links, the "correct" density retained, or the "correct" significance level of a specific edge.

All these methods, however, do not consider a crucial aspect that should be the center of attention when sparsifying a matrix: the underlying topology of the network. Indeed, it is possible that the removal or the inclusion of key edges can alter both the mesoscopic and microscopic topology of a network [Esfahlani and Sayama, 2018, van Wijk et al., 2010]. Under this framework, a percolation-based procedure has been proposed [Gallos et al., 2012, Bordier et al., 2017, Esfahlani and Sayama, 2018]. A percolation analysis [Gallos et al., 2012] is a data-driven approach, which identifies a sparsification threshold proved to maximize the modular information that can be extracted from the network [Bordier et al., 2017]. This procedure iteratively removes all the weakest edges, to the point where the network starts breaking apart. This ensures the connectedness of all nodes in the network, and maintains its topological integrity [Esfahlani and Sayama, 2018] (figure 2.1).

In principle, the search for an optimal trade-off between discarded spurious correlations and retained structural information from the network should be the main goal in the sparsification process. However, there is no ground truth for real-world networks, and the identification of a correct approach, as extensively reviewed, is not straightforward and is often considered an arbitrary choice. Adding to this, it is now argued whether the sparsification procedure itself might actually inject artifacts within the network of interest. In line with this idea, a recent study revealed the introduction of some complex features in the network as a pure effect of thresholding [Cantwell et al., 2019]. Considering the lack of agreement and this arbitrariness, together with an uncertain significance of the weakest and negative links, there is now a trend in the literature to completely avoid the application of a threshold, directly working with fully connected networks [Schlesinger et al., 2017, Goulas et al., 2015, Bassett et al., 2011, Rubinov and Sporns, 2011].

In the present work, we try to overcome some of these methodological aspects, and tested the effects of global thresholding on structural information by resorting to a novel tool grounded in information theory. Specifically, we embrace the framework of maximum entropy random graph models in its classical and spectral perspective, based on the pioneering work by De Domenico and Biamonte who enabled the extension of Von Neumann entropy to complex networks [De Domenico and Biamonte, 2016]. Specifically, this approach provides an information-based

measure that takes into account the entire network structure [Squartini and Garlaschelli, 2017]. In lay terms, we can use spectral entropies as a tool to assess the structural information contained in a network as function of a scale factor, β [Nicolini et al., 2018, De Domenico and Biamonte, 2016]. The strength of this formalism lays in the dynamical description of a diffusion process taking place over the network. Hence, spectral entropies provide a scale-resolved, information-based metric to define and optimize network models. The same framework enables the measure of distance between networks which can be rigorously defined in terms of quantum relative entropy, or information divergence [Wilde, 2013]. This quantifies the information gain when a model is used to explain an empirical observation, and gives us a measure of how much two networks are distant in terms of entropy, at all scales. Through the implementation of models of maximally random networks with specific local or global properties, we can evaluate the deviation of these random systems from their empirical counterpart at different scales. Specifically, in our case we fit classical maximum entropy network models to RSFC empirical networks, and compare them with their maximally random counterparts. A strong advantage of spectral entropies is the possibility to explore differences between real and random networks, at all possible thresholds and scales. For this reason, we seek the existence of an optimal point where the empirical network is maximally distant, at all scales, from its random counterpart. By revealing a threshold maximizing the divergence of a network from a null model, we can prove the existence of an optimal balance between the removal of spurious links and precious structural information. Hence, we can provide a means for the choice of the threshold and its identification, in a completely data-driven and theoretically sound procedure.

In the present thesis I will not dwell into all the mathematical details of spectral and relative entropies and the aforementioned random models, which can be found in Nicolini et al. [Nicolini et al., 2019], yet, I will try to disseminate in lay terms the power of these methods.

First, I will show the effects of the thresholding procedure over a functional connectivity network from a healthy populations, identifying an optimal threshold points which maintains the network fully connected. Afterwards, I will report an example of an application of this procedure on a case-control study with

schizophrenia patients. Indeed, the application of this specific threshold maximizes the structural information that can be extracted, and we could, thus, reveal modular alterations that were never identified before [Bordier et al., 2018].

2.2 MATERIALS AND METHODS

In this methodological section I will briefly introduce the novel methods that we employed to evaluate the thresholding effects over functional networks. First, I resorted to two random network models used to fit the empirical systems. The technical details of these models can be found in Nicolini et al. [Nicolini et al., 2019]. To address the distance between the generated random networks and the empirical resting-state network, I applied the spectral entropy formalism, and defined a measure of network distance based on relative entropy.

2.2.1 Data and preprocessing

To evaluate the effects of different thresholding on the network structure, we have chosen a standard available resting-state network computed as a group average of 27 healthy volunteers as in Crossley [Crossley et al., 2013]. Functional data was acquired with a Siemens Tim Trio 3T scanner, with a TR=2s, TE=31ms, recorded for 5 minutes. Regional timeseries were extracted for 638 nodes, head rotations and translations together with their derivatives and mean cerebrospinal fluid time series were regressed and band-passed (0.01 – 0.1 Hz). The functional connectivity matrix was derived by means of pairwise Pearson correlations, normalized by the Fisher transform, and finally averaged over each subject. The network corresponds to the unthresholded version made publicly available through the Brain Connectivity Toolbox (BCT, [Rubinov and Sporns, 2010]). We leverage this network to evaluate the effects of thresholding on the system. For this purpose, we apply a range of different absolute threshold, from $w = 0.1$ till the point when the network starts breaking apart. Here, absolute thresholding corresponds to the removal of all edges with weight $w_{ij} < t$, where t is a real positive number. With the term percolation threshold we mean the highest value of absolute threshold such that

the undirected network remains connected, hence with one connected component. The percolation analysis of the Crossley network is shown in Figure 2.1.

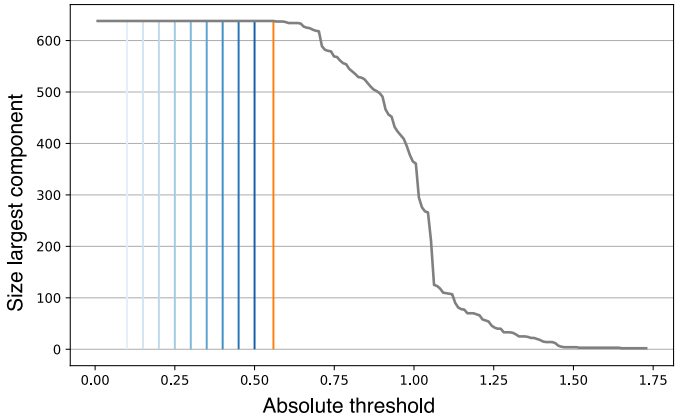

Figure 2.1: Percolation analysis for the group average matrix. The blue lines The blue lines corresponds to threshold values from 0.1 to 0.5, the orange line is the percolation threshold, where the largest connected component starts breaks apart.

2.2.2 Random Graph Models

In network neuroscience null models have been extensively used for the statistical testing of hypothesis, namely, to determine whether specific topological metrics are informative or not for a given system when compared to a random network [Fornito et al., 2016]. An example of a straightforward method used to generate random networks relies on rewiring algorithms [Maslov and Sneppen, 2002]. Such systems iteratively reshuffle graph links, while maintaining constrained topological features. However, due to the high number of rewirings needed, this approach has a very large cost and results to be biased [Cimini et al., 2019]. For these reasons, to build maximally random counterparts of the empirical networks, we resort to a more theoretically sound method based on first principles, grounded in information theory and statistical mechanics. This is based on the Maximum Entropy method [Park and Newman, 2004]. This framework lays its basis in the connection between information theory and the physics of many interacting elements [Cimini et al., 2019]. The main concept of this method is the notion of Entropy, which can be defined as a measure of uncertainty. In lay terms, we have zero entropy when observed events only have one possible state. Contrary, if we are completely igno-

rant with respect to all the possible states of a system (i.e. maximum uncertainty), the entropy is maximum. From the principle of maximum entropy we can build null models by means of the Exponential Random Graph (ERG) model. Here, null models are defined as objects matching some properties of an empirical network, while remaining maximally non-committal with regard to all other properties not explicitly specified. Null models are thus used to describe maximally random networks with specific features. Importantly, within the Maximum Entropy formalism a model is not simply defined as a single network, but as a probability distribution over many possible networks. Indeed, from a set of given constraints observed in an empirical system, an ensemble of networks is constructed, resulting in a probability distribution over all the possible allowed configurations [Squartini and Garlaschelli, 2017]. The model is hence defined by the probability distribution that maximizes entropy (i.e. gives the maximally uncertain solution). This results in the construction of networks that have the same properties enforced from the empirical system, but are otherwise maximally random. This is crucial to detect statistically significant patterns in real-world networks. A schematic representation for the creation of null models is depicted in figure 2.2. For example, we could create a network simply by fixing the number of nodes and edges, where the pattern of connectivity links is drawn randomly (defined as **Erdos-Renyi** graph). From this we can compute some topological metrics, if such metrics match those evaluated from a neural graph, we could conclude that these features of the brain network are completely random.

Overall, null models should not be either too complex or too simple. Indeed, by building random networks with too few parameters we would risk to oversimplify our system. On the contrary, if we impose too many constraints on our model, we might over-fit it, and the random system would perfectly match the empirical data, describing all its features [Betzel and Bassett, 2017].

The application of the ERG models formalism to the study of brain connectivity networks allows a better evaluation of the complexity of the system and can be crucial to assess complex brain properties [Azondekon et al., 2018]. Yet, very few studies explored the strong potential of this approach as applied to the neuroimaging field [Simpson et al., 2011, Sinke et al., 2016, Obando and De Vico Fallani, 2017, Azondekon et al., 2018]. First application of this methodology to the

study of brain networks comes from the study of Simpson and colleagues [Simpson et al., 2011], where they systematically assessed the advantages in using ERG models to model, analyze, and simulate whole-brain networks. Importantly, they underlie their utility as means to assess simultaneously a number of complex network properties. As an important contribution, this study suggests the powerful insights that this family of models can contribute to the investigation of the brain architecture, from its local to global properties, by simulating single subjects' original networks. Furthermore, ERG models appeared particularly promising for the construction of group-based resting-state functional networks [Simpson et al., 2012]. Application of this formalism has proven successful also to reproduce EEG brain networks [Obando and De Vico Fallani, 2017], where ERG models could capture both integration and segregation topological properties. Such findings were further confirmed by the application of this family of models to combined MEG and fMRI data [Azondekon et al., 2018], where it was possible to statistically reproduce main properties of brain networks. Overall, these few studies importantly revealed the power of this formalism as applied to the study of the brain topological architecture. Importantly, one of the main contributions of this approach comes from the possibility to explore simultaneously several local properties and subsequently evaluate how they can give rise to global topology [Sinke et al., 2016]. Through this approach we can, indeed, create families of model networks sharing similar properties of the empirical data, and provide a more robust network-based diagnostic [Azondekon et al., 2018].

Given the unbiased result and more analytically tractable features of this model, here, we embraced the Maximum Entropy formalism. Specifically, we generated random models for RSFC networks that are complex enough to match simple local features of the network, but remains uninformative over higher order patterns. Importantly, these models have to take into account the continuous nature of link weights, the density and weighted structural patterns. From these, we analytically build the maximally random counterpart of empirical networks, where only specific properties are maintained, on average.

The first model employed, the simpler, constrains the number of links and total weight of our thresholded resting-state network, together with an external threshold parameter t. This model is dubbed *Continuous Weighted Thresholded Enhanced*

Random Graph Model, CWTERG. This simple model describes an ensemble of networks whose total weight and number of links are constrained, thus it can be considered an extension of the Erdos-Renyi random graph to thresholded weighted networks. The second model we used is more complex in nature, as both the degree and strength sequences of the random network are constrained to match the empirical ones. Importantly, this model also considers the inhomogeneity of the degrees and strengths present in the empirical network. We refer to this model as the *Continuous Weighted Thresholded Enhanced Configuration Model* (CWTECM). The technical and mathematical details of these models can be found in [Nicolini et al., 2019] and in appendix A of this thesis.

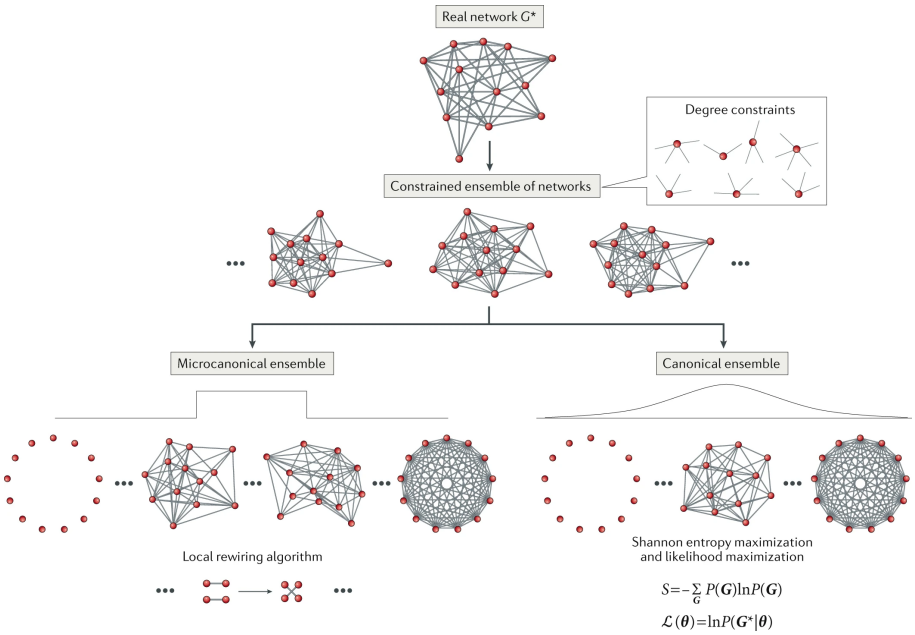

Figure 2.2: The real network $\mathbf{G}^\star$ is the source of constraints on the ensemble. In this case, the constraints are the degrees k^* of $\mathbf{G}^\star$. The microcanonical approach relies on the link rewiring method to numerically generate several network configurations, each with exactly the same degree sequence of $\mathbf{G}^\star$. The probability $P(\mathbf{G})$ of a network $\mathbf{G}$ in the ensemble is non-zero only for the subset of graphs that realize the enforced constraints exactly, as indicated by the schematic probability distribution. Provided the sampling is unbiased, $P(\mathbf{G})$ is uniform for these graphs. The canonical approach obtains $P(\mathbf{G})$ by maximizing the Shannon entropy S while constraining the expected degree values within the ensemble and then maximizing the likelihood LL of $P(\mathbf{G}^\star)$ to find the ensemble parameters $\theta^\star$, such that the expectation values of the degrees match the observations in $\mathbf{G}^\star$. Thus, $P(\mathbf{G})$ is non-zero for any graph, ranging from the empty to the complete one, as indicated by the schematic probability distribution. From [Cimini et al., 2019].

Thanks to these models, we finally get two different random counterparts for the resting-state empirical network, and we can evaluate how distant the brain

system is from its random at all scales. We achieve this by means of spectral and relative entropies.

An appendix is present at the end of this thesis to clarify the mathematical formulations underlying the classical formalism of the maximum entropy random graph models and the two null models introduced in this work.

2.2.3 Spectral and relative entropies

To address how far from random a brain network can be, we embraced Maximum Entropy random graphs models. However, the simple definition of these models is not enough to disentangle the significance of the information contained in the network at all scales. Hence, to quantify the similarity between a network and its randomized counterpart, we resort to the Von Neumann relative entropy. This measure of spectral entropy is crucial to capture the intrinsic multiscale structure of brain networks. It represents a natural generalization of classic Shannon entropy, which, thanks to the work of [De Domenico and Biamonte, 2016] can be extended as a means to define distances between pairs of complex networks. In contrast to Shannon entropy, here the classical probability distribution is replaced by a density matrix $\boldsymbol{\rho}$ that describes the result of constraining the diffusion properties on the network. In details, the Shannon entropy replaced within the Von Neumann Entropy can be represented as:

$$S(\boldsymbol{\rho}) = -\operatorname{Tr}[\boldsymbol{\rho}\log\boldsymbol{\rho}], \tag{2.1}$$

where, the density matrix $\boldsymbol{\rho}$ is defined as follows:

$$\boldsymbol{\rho} = \frac{e^{-\beta \mathbf{L}}}{\operatorname{Tr}[e^{-\beta \mathbf{L}}]}. \tag{2.2}$$

Similarly to its classical form, Von Neumann entropy is a mathematical function that corresponds to the amount of information contained in a system. Indeed, this measure can quantify the information contained at all scales of a network, as a function of a scale factor β [Nicolini et al., 2018]. The role of the β parameter is crucial, and provides an important means to assess the network structural information at different scales. An intuitive description of this formalism is based on

the diffusion of a random walker over the network. β represents a normalized diffusion time of the diffusion process. We can imagine a random walker diffusing over the network, it will first diffuse over local nodes, to finally reach diffusion at the larger component scale when we tune the scaling factor. Specifically, in the $\beta \to 0$ limit, the Von Neumann entropy carries information related to local connectivity patterns. If we move to the limit of $\beta \to \infty$ it will describe the large scale structure of the graph. If the network comprises modules of densely interconnected nodes that are more loosely connected with the rest of the network, the random walker will spend more time within the module, generating a plateau in distribution of spectral entropy as a function of β. The cartoon depicted in figure 2.3 shows a clearer explanation of the behavior of spectral entropies. Comparing the spectral entropy of an empirical network with that of a null model, e.g. obtained by randomization of the edges of the original network, enables the analysis of the structural information at different scales. For small value of β, the spectral entropy reflects node-wise structure, and differences between the empirical network and a null model obtained by constraining local features is small. For larger β, the spectral entropy reflects structure at larger scales, e.g. the presence of modules that cannot be captured by the random model, and differences are larger. Thanks to its intrinsic properties spectral entropy can disentangle a large number of properties of the network, aggregated in a single quantity.

Of critical relevance, Von Neumann entropy allows the definition of a metric for the comparison of two different networks, which are represented by their respective density matrices ($\boldsymbol{\rho}$ and $\boldsymbol{\sigma}$). Through this, we can measure network similarity, by means of **relative entropy** $S(\boldsymbol{\rho}\|\boldsymbol{\sigma})$, a positive quantity which results zero if and only if $\boldsymbol{\rho} = \boldsymbol{\sigma}$. This powerful approach allows the crucial quantification of similarity between an empirical network and its random counterpart. Namely, we can assess, from local to large scales, how much a brain system is distant from random.

Here, we compared real-world networks with their randomized counterparts defined from both maximum entropy models CWTERG and CWTECM. As mentioned, the two models preserve different degrees of complexity. The CWTERG model constrains local features. As a result, the randomized network, when compared to the empirical, will show very similar spectral entropy in the $\beta \to 0$

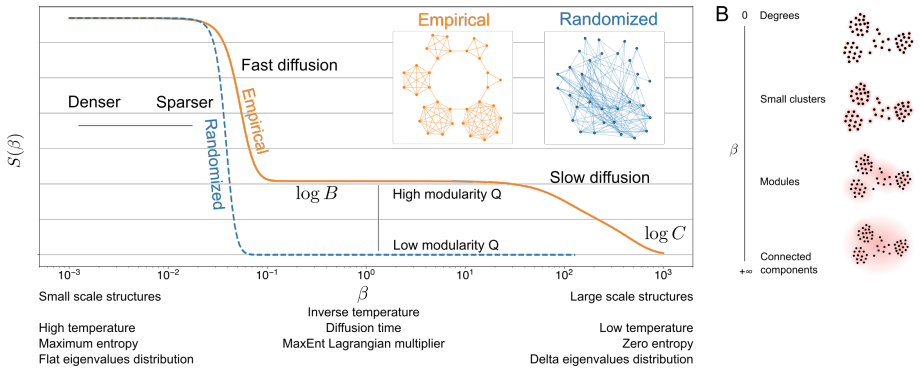

Figure 2.3: Von Neumann spectral entropy of a highly ordered network (orange), and its randomized counterpart (blue). For small values of β the spectral entropy reaches its maximum value $S = \ln n$, while in the large β limit it tends to the logarithm of the number of connected components (ln C) (zero for weakly connected graphs). Intermediate values of β highlight mesoscopic structures. The height of the plateau is related to the overall modularity of the network, while its positioning on the x-axis depends on network link density. Differently from the highly regular ring of cliques (orange), the randomized network (blue) shows no structure at all scales, hence its Von Neumann entropy decreases rapidly. Panel B shows that low β correspond to local features while large β describes large scale features.

but will strongly differ at larger β where the local properties imposed cannot model the mesoscopic structures. The outcome should differ when considering the CWTECM, which forces the model to maintain degree and strength sequences, two global features that might model more complex features of the network. Therefore, we would expect similar values of relative entropy not only at very small β, but also at a larger domain.

2.3 RESULTS AND DISCUSSION

As mentioned previously, one potential issue in the rsFC field lays in the choice of the thresholding level, which might affect to a great extent the subsequent graph theoretical analysis [Bordier et al., 2017]. Here we use our theoretical framework to explore the effects of thresholding in functional connectivity networks, and to evaluate the existence of an optimal thresholding point.

To address this issue, we considered an empirical network of resting-state functional connectivity from a cohort of healthy participants, and we applied different levels of absolute thresholds (from 0.10 till the point where the network breaks

apart). Hence, we first computed the spectral entropies of thresholded networks and corresponding null models, at all scales. We then used relative entropy to quantify the information theoretic distance as a function of threshold.

Figure 2.4 shows spectral and relative entropies for the empirical network and both models, at all the investigated threshold points. First, we observe that at lower threshold levels (depicted in light blue) the diffusion time of the empirical network is much faster, reflecting the effect of network density. As expected, diffusion time at all scales decreases with increasing sparsity, as shown by the right-shift of the resting-state network spectral entropy curves in panels A and D. This same thresholding effect is clear also when observing the spectral entropy curves of both null models (dashed lines in panels A, D) which, in turn, reveal a right-shift dependent on network density. However, these shifts in the random networks do not reach the same larger β domain as their empirical counterpart.

Another relevant effect of thresholding is the revelation of a clear-cut mesoscopic diffusion pattern for increasingly sparser networks. Indeed, large scale structures of the empirical network are emerging only for higher thresholds (darker blue), as reflected in figure 2.4A by the presence of "information shoulders", i.e., parts of the spectral entropy curve where the slope changes relatively fast . Yet, this phenomenon is not equally present in the two null models. Should the thresholding procedure highlight mesoscopic structures only accounted by local constraints, we would expect similar high values of S on both the thresholded random counterparts of the empirical graph. However, the CWTERG shows no indications of a high-level organization at any threshold, as seen by the sharply falling entropy within a very small range of β (Figure 2.4C). Indeed, as previously demonstrated, the CWTERG destroys the local structure by completely shuffling nodes' neighborhoods. As a result, diffusion rapidly covers the whole network, as every node forms connections to any other node with uniform probability.

On the other hand, the spectral entropy of the CWTECM closely corresponds to the one of the empirical network over a broad range of β values. This result is clear once interpreted in terms of the preservation of the local structure described by the degree and strength sequence that is enforced by the CWTECM. Noticeable differences only appear at large scales for increasing thresholds. In accordance with the results of reference [Cantwell et al., 2019], we observed that as a function

of the threshold, the community structure is the only feature that is not accounted for by local properties.

This is even more evident from the observation of their respective relative entropies, in panels B and C. The resulting relative entropy from the CWTERG is very high, and attains its maximum at slightly lower values of β than for the CWTECM: it takes less time for a random walker to explore a random network than a complex network where modules and local structures may hamper the diffusion process. Moreover, for both cases, relative entropies accentuate the effects of thresholding, as they present higher values with higher levels of threshold, and reach their maximum peak around the percolation point, just before the network starts breaking apart.

Importantly, the results in Figure 2.4 demonstrate that in both cases the maximal distance in spectral entropy of the empirical network from the null model is obtained at percolation level. This is an indication that the community structure is highlighted around the percolation point. Indeed, the rapidly falling entropy of the CWTECM for this specific sparsity indicates uniformity at large scales.

The importance of the thresholding procedure revealed by this approach, is also reflected by the very small relative entropies of the CWTECM at lower thresholds. Indeed, at lower thresholds ($0.1 \leqslant t \leqslant 0.4$) the empirical network follows its random counterpart even at large scales, confirming how the correct threshold is crucial for the identification of clear-cut structures.

Taken together, these results show that complete, unthresholded network is close to its null model and presents a high level of randomness. This is due to the presence of spurious correlations that affect particularly the weaker edges. Removal of weak edges by thresholding is beneficial, and the distance between the empirical network and its random version is maximal at percolation point, just before the network starts breaking apart. After this point, the network is not fully connected, with single nodes separated from the rest, a condition which would not ensure, for example, optimal detection of the underlying community structures. For this reason, we did not subsequently evaluate thresholding approaches that would not ensure full connectedness of the system (e.g. ECO, [de Vico Fallani et al., 2017].

This is the sparsification threshold that strikes the optimal balance between removal of spurious correlations and undesirable suppression of structural information that may be contained in the weaker edges. Importantly, this result is independent of the particular choice of null model.

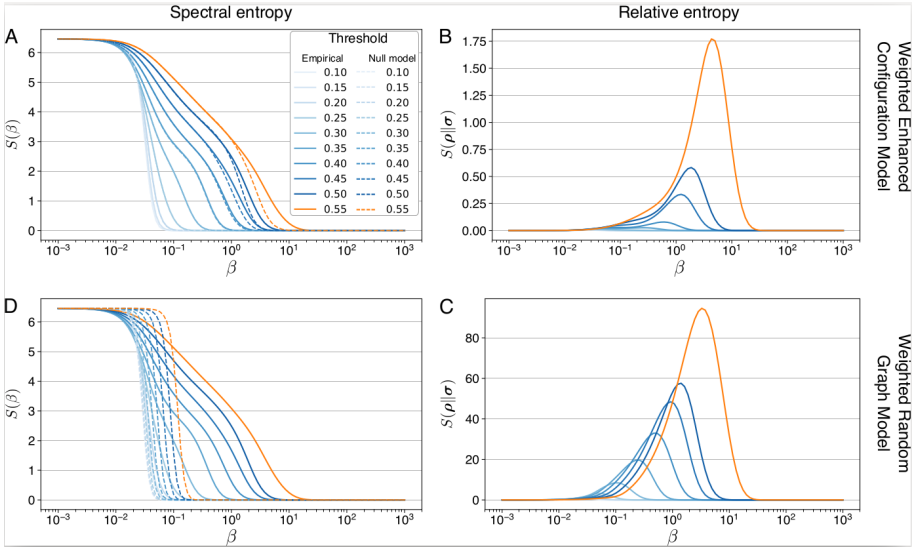

Figure 2.4: Spectral entropies and relative entropies of the group average brain functional network compared to its randomized counterparts. Blue shaded lines represent networks thresholded at absolute values from 0.1 to 0.5. Orange lines denote the network at percolation threshold. Solid lines are the curves relative to the empirical network. Dashed lines are the curves relative to the randomized networks.Panels A,B show the results with respect to the CWTECM model. Panels C,D show the results with respect to the CWTERG model.

2.4 THE APPLICATION OF A PERCOLATION THRESHOLD TO CASE-CONTROL STUDIES

Here, we could prove by means of first principles methods the critical importance of the application of a sparsification procedure to complex systems. More importantly, we revealed the existence of an optimal thresholding point, which crucially allows the identification of higher-order level structures. A number of suboptimal approaches have been applied in network neuroscience, ranging from proportional thresholding, i.e. the imposition of a predetermined network density, to the avoidance of any sparsification at all. Hence, we hypothesize that previous studies might have failed to reveal a clear-cut high level structure in functional

brain networks by applying the same absolute or proportional threshold to different populations.

For this purpose, I will briefly present here an example of a case-control study where we investigated differences in the modular architecture after the application of a percolation thresholding. Complete dissemination of this study can be found in [Bordier et al., 2018]. In details, we assessed differences in the modular organization in a sample of patients affected by schizophrenia (SCZ) compared to a sample of healthy controls (HC). Schizophrenia is a complex and devastating psychiatric disorder, it severely affects patients and relatives' lives. For these reasons, it is one of the most studied psychiatric disorders in the neuroscientific community. Specifically, aberrant functional connectivity has been thoroughly reported in a variety of studies [Friston and Frith, 1995, Liu et al., 2008, Calhoun et al., 2009, Fornito et al., 2012, Anderson and Cohen, 2013]. In addition, with the use of a graph theoretical approach, functional connectivity strength as well as Modularity were found aberrant in SCZ patients, , related to an imbalance between functional integration and segregation [Bassett et al., 2008, Yu et al., 2011, Alexander-Bloch et al., 2012, Yu et al., 2012, Lerman-Sinkoff and Barch, 2016].

Here, we specifically investigate the modular organization, resorting to a community detection function that we previously proved to be resolution-limit free. This method relies on Asymptotical Surprise, a fitness function rooted in probability theory [Nicolini and Bifone, 2016]. Interestingly, the application of this specific algorithm revealed a heterogeneous modular organization of the human brain, with a distribution of communities spanning multiple scales [Nicolini et al., 2017]. Thanks to this approach, it is possible to identify even more subtle alterations in the structural architecture of the functional brain, allowing to appreciate differences across groups that might not be detected by more common resolution limited methods.

Through the application of both a percolation threshold and a Surprise algorithm, we proved the presence of specific local fragmentations within the patient group that were not previously identified but that might be key for the understanding of schizophrenia functional aberrancies.

This section does not specifically aim to unravel the functional alterations underlying schizophrenia, but intends to highlight the benefits of a percolation thresh-

olding as applied to a case-control study. For this reason, I will not dwell into all the details of the study, which can be found in [Bordier et al., 2018].

2.4.1 Matherials and Methods

We selected MRI data from the open COBRE database (`http://fcon_1000.projects.nitrc.org/indi/retro/cobre.html`, [Ambite et al., 2015]). This specific dataset involves one group of 91 healthy controls (64 males, 14 females) and one group of 78 patients diagnosed with schizophrenia according to the DSM-IV (65 males, 26 females). Age ranged from 18 to 65 years in both groups.

EPI images at rest were acquired with a Siemens MIND TRIO 3T Scanner, with a TR=2s and TE=29ms. More details can be found in [Çetin et al., 2014]. A total of 150 volumes were acquired for each subject. Standard preprocessing was done as in [Bordier et al., 2018], based on the regression of 6 standard movement parameters extracted with SPM8.

Following, BOLD time series were extracted for each participant from 638 brain regions, by averaging the voxel timeseries within each ares, defined by a template [Crossley et al., 2013], and band-passed (0.01–0.1Hz). Functional connectivity was defined in terms of pairwise Pearson correlations at a subject's level. Finally, a group-level functional connectivity matrix was calculated by averaging individuals' matrices after Fisher-transform.

As already introduced, we applied a percolation threshold to both groups in order the reduce link density and maximize the structural organization that can be extracted from the network. Following this sparsification procedure we applied the Asymptotical Surprise quality function, as means to detect modular architecture.

Furthermore, by means of the two null models introduced in the previous section, I describe the relative entropies for both groups; first with the application of a common proportional thresholding, then at percolation.

2.4.2 Results and discussion

To evaluate differences in overall functional connectivity at the group level, we examined the edge-weight distribution for both full networks, depicted in figure 2.5. From this, we observed a significant left-shift in the average z-score distribution of the SCZ patients matrix ($p<10^16$). This is line with previous findings of a substantially reduced global functional connectivity in schizophrenia [Lynall et al., 2010]. Similarly, the SCZ group presented a significant reduction in global efficiency (HC: 0.32; SCZ: 0.23), further demonstration of altered network integration in patients.

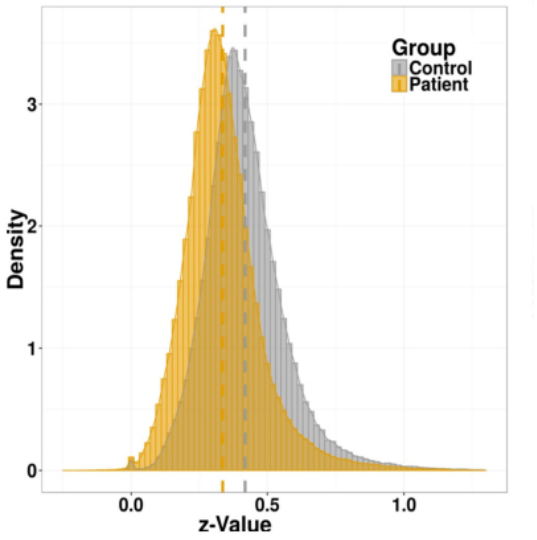

Figure 2.5: Edge-weight distribution of the adjacency matrix for the two experimental groups.

Relative entropies

To better appreciate the advantage of the proposed percolation thresholding we show here the relative entropies for two conditions. In the first we evaluate the application of one of the most common thresholding techniques in network neuroscience, i.e. proportional thresholding (figure 2.6). In the latter we show, in contrast, spectral and relative entropies of both groups at percolation figure 2.7 . For the former example, we fixed a link density of 10%. Considered the relation of most graph topological metrics to the network density, this is one of the most common approaches employed in brain network studies [Hallquist and Hillary, 2019, van den Heuvel et al., 2017a]. Following, we generated for both groups two maximally random counterparts: the first by means of the CWTECM, where both the strength and degree sequences are constrained, and the second by means

of the CWTERG, which only preserves the number of links and the total weight. In the panels A and B of figure 2.6, we plot the spectral and relative entropies for both groups of healthy controls and patients, compared to their null models. Again, we first observe, that, in contrast to the simpler CWTERG, the CWTECM, with its large number of parameters, can better reproduce the features of the empirical networks over a larger intervals of β. Indeed, the local properties of the empirical network, which are described in the small β range, are closely matching the model.

Importantly, healthy controls consistently display higher Von Neumann entropy at medium-large scales, a typical fingerprint of community structure. Moreover, the shoulder in the large β domain, which are associated to reduced inter-modular density, are lacking in the patient group. In addition, for both null models, the spectral entropies for healthy controls deviate more from their random counterparts, than for the patients, as reflected by their respective relative entropies. Here, the maximum peak for healthy controls is both higher and towards the right hand of the interval. From a direct inspection of the relative entropy curves of patients, in the domain of mesoscopic structures ($1 \leqslant \beta \leqslant 10^2$), the randomized network is much closer to the empirical, strong indication of a lack of clear-cut modular architecture. Interestingly, the reduction in relative entropies for the patients' network is observed in both models. To sum-up, from this observation we could conclude that the network derived from patients groups is closer to random compared to the one of healthy controls. However, if we examine the same networks thresholded at percolation, we can observe a very different pattern (figure 2.7).

In panel A of figure 2.7, we can observe the spectral entropy curves for both controls and patients at percolation, together with their respective null models obtained by means of CWTECM. From this plot we can clearly appreciate an opposite trend as the one previously examined in figure 2.6. Notably, the curve from schizophrenia patients (in blue) now shows higher spectral entropies at all scales as compared to controls. This effect can be explained in terms of density of the final sparse matrices at percolation. Indeed, the network of patients shows lower density (density: 0.04, at t=0.62) in contrast to healthy controls (density: 0.08, at t=0.61). Yet, we still cannot appreciate any shoulder at larger beta domains, opposite to controls, possibly reflecting a global structure with similar intra-modular

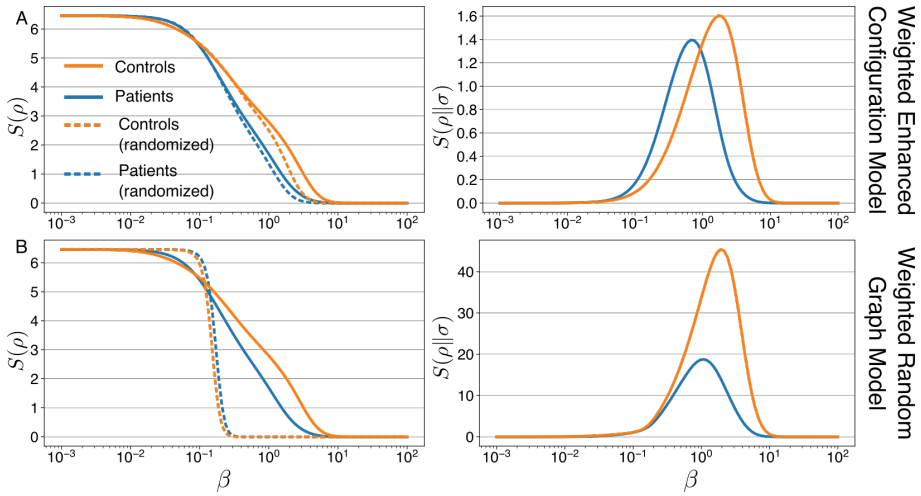

Figure 2.6: Spectral entropies of group average fMRI matrices from control and schizophrenic patients. Panels A,B show the entropy and relative entropy of controls and patients networks, thresholded at a 10% fixed density, with respect to their randomized counterpart with the CWTECM and CWTERG.

density across different communities. An interesting observation comes from the inspection of the relative entropies presented in panel B of figure 2.7. Unexpectedly, we see a strong increase in the relative entropy of SCZ patients, reflecting a higher detachment of this network from its randomized counterpart at percolation, computed by means of the CWTECM.

In the case of this patients-control study, we could thus demonstrate that the application of a specific threshold, which ensures fully connectedness of all nodes, can maximize the distance of a given network from its random counterpart. This observation is of critical importance. Indeed, when taken at a fixed proportional density, as commonly applied in many network studies, we could conclude that the network extracted from patients would appear much closer to random as compared to healthy controls. In contrast, thanks to the application of a percolation approach we demonstrated larger distance for SCZ patients, a finding that would not be otherwise appreciated.

Modular structure in SCZ patients

To determine modular partitions for both groups, we applied maximization of Asymptotical Surprise by PACO, a resolution-limit free method. Further details in [Nicolini et al., 2017].

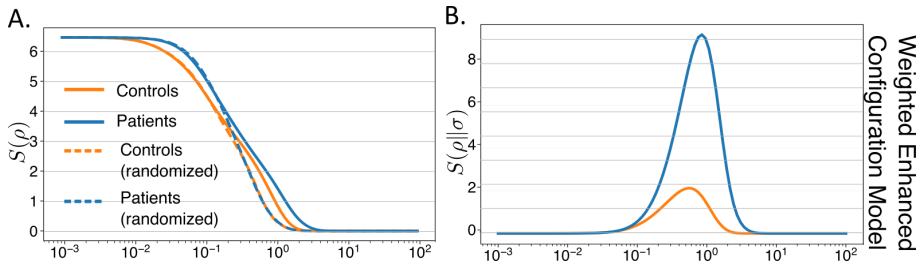

Figure 2.7: Spectral entropies of group average fMRI matrices from control and schizophrenic patients. Panels A, B show respectively the entropy and relative entropy of controls and patients networks, thresholded at percolation (Controls: t=0.61; Patients: t=0.62.) with respect to their randomized counterpart with the CWTECM.

Interestingly, we found 44 communities in the control group (module size range: 144-1 nodes) and 39 communities in the patient group (module size range: 73-1 nodes). Despite the reduced number of modules found for SCZ, we observed an overall modular fragmentation and reorganization. Namely, larger communities in controls appeared broken-up into smaller modules in patients. These specific fragmentations are particularly evident in sensorimotor, visual, and auditory cortices (Figure 2.8). Considering the visual module (first biggest community in HC), we found this region to be split in the patients' group, with primary visual cortex standing as an independent community together with the caudal part of the inferior temporal gyrus. A similar pattern can be observed in the second largest community of HC, the sensorimotor cortex. Indeed, in the healthy group this module comprises the somatosensory, sensorimotor, and temporal auditory cortices. Opposite, the modular organization of SCZ patients revealed a substantial fragmentation of this module, which breaks-up dorsoventrally intro four different clusters. Further fragmentations and reorganizations are present also in temporal and language regions, whereas superior frontal cortices appeared intact.

Overall, we identified substantial alterations in the modular structure of functional connectivity in schizophrenia patients. This major reorganization predominantly affects primary sensory regions, while leaving unaffected higher-order cortices. Interestingly, this is in line with previous documentations related to altered sensory experience and processing in SCZ [Bleuler, 1950, McGhie and Chapman, 1961, Chang and Lenzenweger, 2005]. The aberrancies localized here in primary sensory brain regions might indeed drive the impairments in basic perceptual processing, suggesting that disorders in SCZ may occur already at the level of

early sensory processing. The inefficiency in sensory systems in this population of patients is also consistent with the hypothesis of aberrant "efference-copy" processing which might underlie the occurrence of positive symptoms [Pynn and DeSouza, 2013]. It is argued that altered sensory processing can lead to a failure in disentangling internal from external stimuli, thus giving rise to auditory hallucinations and delusions often experienced by SCZ patents. The sensory fragmentation in motor and primary sensory regions identified in this study might suggest the altered role that different sensory modalities play in this devastating disorder. A promising follow-up to this investigation could evaluate the relation at a single-subject level between the severity of positive symptoms in these patients and the underlying break-up of motor and primary sensory regions into separated smaller modules. Unfortunately, this could not be explored in the present study. Indeed, the main goal of this study was to evaluate the performance of a novel partition algorithm (i.e. Asymptotical Surprise; [Nicolini et al., 2017] in the detection of the brain modular architecture. To ensure an optimal performance, this resolution-limit free method requires a big sample size. For this reason, we specifically selected a publicly available dataset which could comprise a sufficient number of patients (78 SCZ) and controls (91). Unfortunately, the selected database did not provide clinical data sufficiently complete for all participants, thus preventing single-subject analysis and the investigation of the relation between individual brain network measures and symptomatology.

In conclusion, with this study we successfully replicated some of the most commonly observed functional connectivity alterations in SCZ, comprising a reduction in functional strength, overall disconnectivity, and reduced network efficiency at a global level. Notably, a similar modular fragmentation has never been reported in these patients. A study from [Lerman-Sinkoff and Barch, 2016] revealed similar partitions between patients and controls at the group level, yet, specific local alterations in nodal membership were identified at the single subject level in somatosensory, auditory, and subcortical regions. This is strongly in line with the alterations we identified here. It is likely that our use of a more sophisticated partition algorithm, together with the application of a percolation threshold, which maximizes the structure that can be extracted from the network, helped us in revealing specific local fragmentations that could not be identified otherwise.

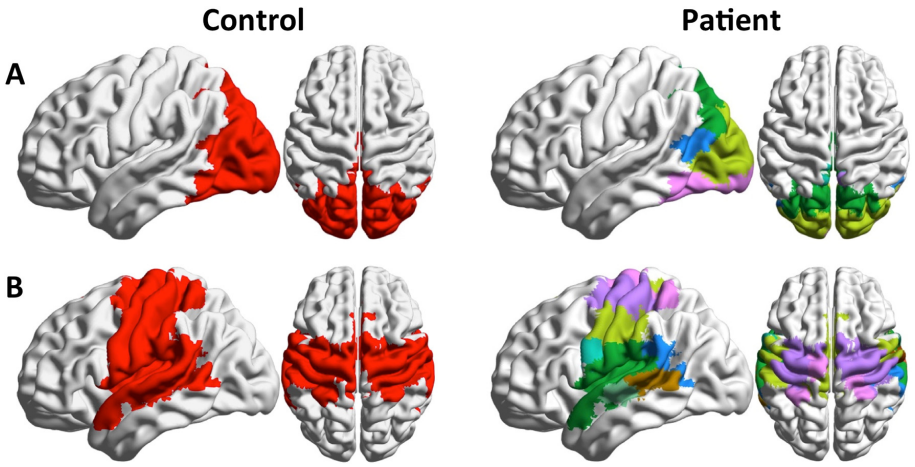

Figure 2.8: Specific modular fragmentations in SCZ compared to the HC group. Panel A: Community 1 of control group and overlapping communities in the patients' group. We can observe a prominent fragmentation of the visual cortex in SCZ. Panel B: Community 2 of control group and overlapping communities in the patients' group.

Altogether, we have demonstrated with theoretically sound methods based on first principles, the existence of an optimal thresholding point, which can maximize the structural information that can be extracted from a complex network. In addition, we showed the benefits of its application to a case-control study, where we could identify specific structural alterations in the functional network that were never previously reported.

2.5 THE IMPACT OF MOTION ON RESTING-STATE FUNCTIONAL CONNECTIVITY

At the beginning of this chapter I already introduced another contentious debate in the brain functional connectivity community: the impact of motion and its correction. The investigation of functional connectivity patterns been thoroughly used to explore neural differences among clinical populations, across lifespan, or personality traits. The popularity of this approach also comes from the simplicity of data acquisition, which simply requires the participant to lay still in the MR scanner for periods ranging from 5 to 15 minutes. The acquired timecourses are then used to extract correlation patterns between segregated brain areas, reflecting

the underlying organization of our brain when it is not engaged in any task-based activity.

Unfortunately, the measurements of resting-state functional connectivity is extremely sensitive to even very small head movements (<0.2mm) that the participants can do while in the scanner. The knowledge of the introduction of spurious changes in signal intensity caused by these movements has been clear since the initial applications of this approach [Biswal et al., 1995, Friston et al., 1996]. However the real dramatic effects of these confounds have started to emerge only recently, as revealed by [Van Dijk et al., 2012, Power et al., 2012, Satterthwaite et al., 2012]. These three studies, independently published in *NeuroImage* just a few months apart, revealed the critical effects that even very subtle head movements can have over resting-state functional data. Specifically, they highlighted the necessity to re-evaluate findings from previous published data related to clinical populations that might move more in the scanner, such as children, patients, or elderly cohorts, and further stressed the importance to more strictly control the presence of motion in functional data. The occurrence of motion might, indeed, hinder the robustness and reliability of functional connectivity measures, possibly leading to misinterpretation of subsequent findings. This happens because of sudden changes in the signal intensity of all voxels in the brain in relation to the movement.

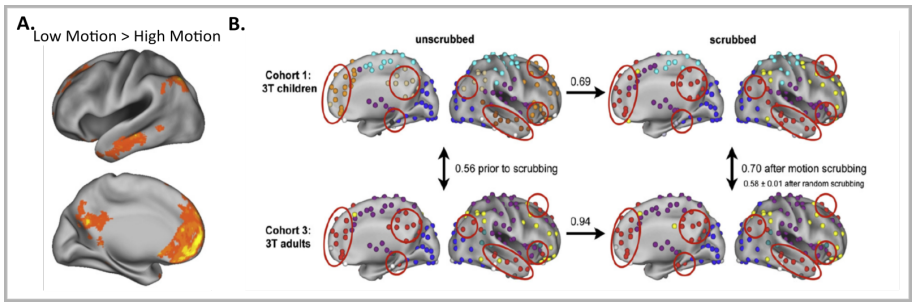

Figure 2.9: Examples of effects that motion can have over functional connectivity. Panel A shows differences in activation map between groups with different degrees of motion. Specifically, shows an artefactual lower functional connectivity in the DMN in a group of participants with higher degrees of motion (from [Van Dijk et al., 2012]. Panel B shows alterations in the topological organization in a sample of children moving more in the scanner as compared to adults, and an example of how specific techniques of data cleaning (i.e. scrubbing) could partially restore the functional brain architecture (from [Power et al., 2012].

Importantly, a single head movement can induce changes in BOLD signal spreading to the whole brain in a regionally specific manner. In this case, it is likely

that in one specific brain regions we would assist to an increase in the signal, whereas another portion of the brain can simultaneously show decreased signal intensity, artefactually injecting anticorrelations. Even more striking, Van Dijk and colleagues [Van Dijk et al., 2012] revealed that groups with different degrees of head movements yielded different activation maps (figure 2.9). In details, motion was associated with decreased functional coupling in the DMN and frontoparietal networks. This is induced by an increased local coupling related to these subtle movements, together with a reduction in the long-range correlations strength [Power et al., 2012]. The dramatic finding is furthermore emphasized by the revelation that these substantial changes are present in the timecourses despite the compensatory spatial realignment and regression of the six head motion parameter that has always been applied to functional data. Indeed, it appeared that the spatial realignment of the data could only correct the spatial shifts induced by head movements, but the changes in signal intensity cannot be corrected from this procedure [Power et al., 2012]. For these reasons, the evaluation of head motion within resting-state functional connectivity data is of critical importance, as it might result in different activation patterns across groups that could be mistakenly interpreted as neuronal effects.

Unfortunately, the description of motion by means of realignment estimates, described as three translational and three rotational displacements, are only a simplification of head movements, being a representation of absolute displacements related to a fixed position. Conversely, relative movements, measured from one volume to the next, better represent the overall signal disruptions. Relative displacement measures, such as Framewise Displacement (FD; [Power et al., 2012]), have thus been introduced to track head movements. Importantly, FD highly correlates to rapid signal changes, measured by means of DVARS, a metric indexing the rate of change of BOLD signal across the brain [Power et al., 2012]. An effective approach to assess the impact of motion over the functional timecourse simply consists in plotting signal intensity of all voxels in the brain throughout time. Such representations are dubbed *grayplots*, as depicted in figure 2.10. Here, we can clearly see the sudden signal disruptions induced by even very small head movements (0.35mm). Critically, from these graphics it is evident how these motion-

induced alterations are broadly shared across all voxels and can further spread also to the following time points.

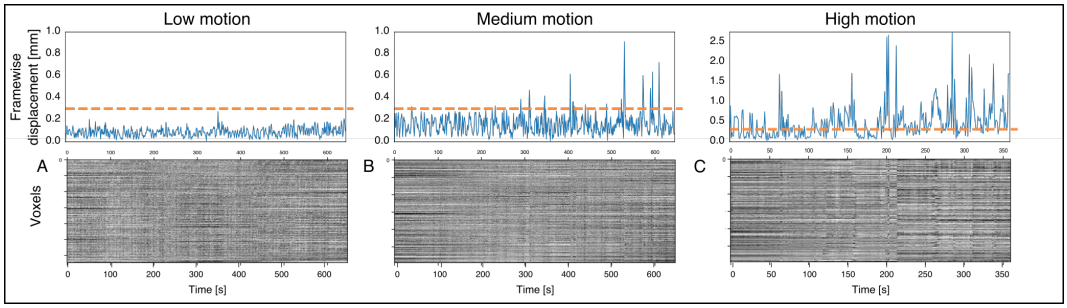

Figure 2.10: Grayplots showing the effects of head movements of resting functional signal

Given the difficulties in detecting neurophysiological events if the data is contaminated with movement artifacts, methods to recover signal of interest are crucially important [Siegel et al., 2014]. From this insight, the RSFC world experienced a proliferation of denoising strategies aiming to mitigate the influence of movement artefacts on functional connectivity timeseries [Power et al., 2012, Pruim et al., 2015, Salimi-Khorshidi et al., 2014, Muschelli et al., 2014, Satterthwaite et al., 2013]. However, not all pipelines exhibit equal efficacy and efficiency in removing spurious signal, and this ambiguity introduced high uncertainty among investigators as to which approach to use. First attempts for the removal of head movements effects from functional MRI data dates back to the early investigations in the field, and relied on rigid body transforms for images' realignment [Friston et al., 1996]. This approach has now become a mandatory step in the preprocessing of MR functional data, where the head position at each time point, with respect to a reference scan, is described by six standard movement parameters. Following, these motion estimates have been introduced as optional steps employed to correct motion-related disruptions, by including them as nuisance variables regressed out from the BOLD signal by means of GLM estimations. Unfortunately, the correction of motion artefacts simply based on these head movements parameters are now proven to fail in disentangling spurious effects from the signal of interest [Ciric et al., 2017], even if their first derivatives and squared terms are included as regressors in the model [Friston et al., 1996]. Adding to this strategy, one of the now most common approaches also further requires the inclusion of regressors extracted from signal originated in noise-related tissues, such as ventri-

cles and white matter, regions mostly susceptible to physiological artefacts (heart beats, respiration, etc.) which may interfere with the resting BOLD signal [Cole et al., 2010]. These are just some of the increasing number of denoising strategies now employed in the field. For example, some other popular approaches rely on models that remove from the data timeseries obtained from signal decompositions, such as Principal Component Analysis (PCA) or Independent Component Analysis (ICA), which display improved performance compared to the more simple regression of noise-related time courses. PCA based methods, dubbed CompCor [Behzadi et al., 2007, Muschelli et al., 2014], aim at removing principal components within high-noise areas, which can be defined in anatomical terms (aCompCor), thus extracting the first principal components from white matter or ventricles timeseries, or in terms of temporal variance (tCompCor), through the identification of high-variance voxels. Even more popular are the approaches based on ICA. By means of decomposition of the signal generated from all voxels in the brain, it is possible to specifically separate neural-related signal from different sources of noise, both motion-related and physiological. Here, noise components are characterized as time-series associated to specific spatial maps that define motion or physiological artefact effects. In details, noise components can be identified through some of their most relevant characteristics, such as their spatial maps (localized in white-matter, ventricles, or the edges of the brain), their time course (i.e. characterized by irregular oscillation patterns), and the distribution of their power in frequency domain (i.e. very high or very low frequencies; [Griffanti et al., 2017]). The increasing popularity of this approach comes from the development of specific algorithms that help in the selection of such components, either with a trained classifier (ICA-FIX; [Salimi-Khorshidi et al., 2014], or by means of a priori heuristics (ICA-AROMA, [Pruim et al., 2015]). Another mostly controversial denoising strategy, seemingly highly effective for the removal of widespread artifacts, resorts to the removal of the so called Global Signal (GSR; [Fox et al., 2009]). This consists in the regression from functional data of the time course of the mean signal computed across all voxels in the brain. This particular approach presents important controversies. Despite appearing effective for the removal of artifactual signal [Power et al., 2015], its application is still under debate, given the increased number of anticorrelations following its application, together with the uncertainty

related to the risk of also removing genuine signal [Saad et al., 2012]. Interestingly, all these techniques appear to markedly benefit from the further application of censoring operations [Power et al., 2012, Satterthwaite et al., 2012, Ciric et al., 2017]. Precisely, temporal censoring requires the identification of specific volumes affected by artifacts, generally flagged as outliers by means of FD and DVARS, which are subsequently discarded and removed (or interpolated) from the time course. Most common procedures include scrubbing [Power et al., 2012], spike regression [Satterthwaite et al., 2012], or despiking [Patel et al., 2014].

It is now clear that the introduction of all these different denoising pipelines also installed uncertainty in neuroscientists, who are thus facing the dramatic effects of motion while not having a real agreement as to which operation, among all the possible cleaning strategies, can be a better fit for resting-state functional data. Several studies tried to address this issue the efficacy and efficiency of all these pipelines against different benchmarks. For example, a brilliant work from Ciric and colleagues [Ciric et al., 2017] revealed better efficacy of the application of GSR together with censoring operations as means to more effectively reduce noise. However, at the same time, they also stressed the importance of the evaluation of the specific final goal of functional connectivity analysis, given the heterogeneity of the investigated methods. Indeed, different strategies may be differently appropriated according to the specific analysis design. Similarly, the combination of both FIX and GSR was reported to be the most effective approach for the removal of motion-related effects in a similar study conducted by Burgess and colleagues [Burgess et al., 2016]. However, it is important to notice that the application of GSR, which introduces an important number of anticorrelations within the functional timeseries, can affect network based studies, by altering the degree-distribution. Furthermore, it is not clear whether some of the aforementioned approaches might also remove genuine functional signals.

Here, we decided to evaluate how motion and motion correction strategies can influence the topological structure of functional connectivity networks, by means of the previously introduced novel methods based on first principles. These effects are of critical importance, mostly when addressing studies with clinical populations that might move differently, as we must ensure maximal comparability across groups. Thus, our goal here is not to evaluate which pipeline can most ef-

fectively remove the spurious effects injected by movement artifacts, but to study and identify an optimal trade-off between motion artifact removal and loss of structural information at all scales. To do this, we resorted to a publicly available dataset, and the evaluation of both spectral and relative entropies on groups of participants with different degrees of motion after the application of the most popular denoising strategies. Specifically, we evaluate three different groups of healthy participants, perfectly balanced for age and gender, with exactly same acquisition procedures, but different for in-scanner motion. Thus, at the group level, we would expect these participants to share same global functional connectivity characteristics. If we spot differences, they should be driven by the presence of motion, altering the time series. From an entropy point of view, if motion is injecting spurious structures within the network, we would expect higher degrees of relative entropies. Opposite, if the injection of motion within the time course simply adds random noise, we expect lower relative entropies, namely we would expect that the network mostly affected by motion would be closer to randomness. Furthermore, we apply a set of different motion-correction strategies, based on different principles. First of all, we hypothesize that an effective pipeline would reduce the differences induced by head movements across the three groups. Nevertheless, an effective pipeline which also does not remove genuine signal from the network should further maximize the relative entropies, thus making the network as far away from its random counterpart as possible.

2.5.1 Materials and Methods

Aim of this brief side-project is the evaluation of the effects of head movements over the structural organization of functional resting-state data analyzed by means of a network theoretical approach. Specifically, I applied 3 different motion correction techniques to three different groups of healthy volunteers extracted from a publicly available dataset, and differing only in the amount of motion artifacts within the functional time course. To assess these impacts over functional data at all scales, we resorted to the previously introduced random graph models, together with the evaluation of both spectral and relative entropies, as means to compare resting-state networks to their random counterparts.

Data and preprocessing

We selected neuroimaging functional data from the MPI - Leipzig Study for Mind-Body-Emotion Interactions project (LEMON, [Mendes et al., 2019]), obtained from the OpenfMRI database, accession number ds000221.

From this dataset, participants were selected according to the age range; only subjects ranging from 20 to 30 y.o. were included in our study, to avoid age effects in subsequent analyses. All MRI data were acquired with a 3T scanner (Magnetom Verio, Siemens Healthcare, Erlangen, Germany). A total of 117 subjects were selected. Structural and functional images were preprocessed with FSL (v 5.0, [Jenkinson et al., 2012]). High-resolution structural images were registered to the MNI template and segmented (fast segmentation), separating white matter and ventricles masks. Functional preprocessing included motion correction and realignment (mcflirt), coregistration to the structural image using boundary based registration (BBR) and then normalized to the MNI template.

Motion groups

For the purpose of the study, all participants were divided into three different groups according to their degree of motion (Low, Medium, and High motion), measured as the proportion of outlier volumes present within the time series. To evaluate the motion level of each subject, Framewise Displacement was computed according to Power [Power et al., 2012]. Timepoints were flagged as outliers affected by motion when FD > 0.3mm. Criteria for group subdivision were the following:

- Low motion (N 39) = <1% data affected
- Medium motion (N 39) = 1-5%data affected
- High motion (N 39) = >5% data affected

We finally included 39 subjects per group, balanced for age and gender (X=0.571, p=0.752), but different for in-scanner motion (ANOVA: F=152.136; p<0.0001). Summary of the groups is further presented in table 2.1. Given the otherwise homogeneous characteristics of these three evaluated groups, we hypothesized that

Table 2.1: Summary demographics and motion estimates employed for the distinction into three different motion groups.

	Motion Groups			Stats
	Low	**Medium**	**High**	
N	39	39	39	
Gender				
Men	28	26	27	X=0.571, p=0.752
Women	11	13	12	
Proportion outliers				
Mean	0.0018	0.0255	0.1649	
SD	0.0023	0.0113	0.0931	
Min	0.0000	0.0108	0.0618	
Max	0.0077	0.0495	0.3771	
FD				
Mean	0.1152	0.1449	0.2084	F=152.136, p<0.0001**
SD	0.0184	0.0185	0.0325	
Min	0.0711	0.0968	0.1549	
Max	0.1423	0.1716	0.3114	

potential between-group in functional organization should be driven by motion effects.

Motion-correction pipelines

Based on the growing debate related to the correct noise-correction technique to apply on resting-state data, we tested two different and popular pipelines, plus one pipeline where no de-noising strategy was applied. We selected and analyzed the results on the following pipelines:

Po: no motion-correction technique applied beside image realignment with carried out with mcflirt (FSL; [Jenkinson et al., 2002];

FIX: based on the FMRIB trained classifier of Independent Component Analysis, components related to noise (FIX, [Salimi-Khorshidi et al., 2014], extracted from single-subjects timeseries;

9P: regression of different factors, including 6 movement parameters, the average signal extracted from white matter and ventricles, plus the regression of the

global signal (GSR), measured as the average of all the voxels of the brain extracted from subject-specific brain masks;

Altogether, I specifically selected pipelines based on different principles. One strategy relies on independent components classification (FIX), the second includes the regression of the global signal (P9), a controversial practice. As reference, for the simple evaluation of pure effects of motion over the architecture of the functional network, I consider a pipeline where only the mandatory image preprocessing steps (realignment, normalization, coregistration, filtering) have been applied (P0).

Before the regression of all the confound parameters from subjects' time series, a butterworth bandpass filter of 0.01 and 0.1 Hz was applied to all the regressors, avoiding reintroduction of signal related to nuisance covariates [Lindquist et al., 2019].

From an effective pipeline we would expect a reduction in the differences induced by motion in the three groups. At the same time, we would expect that the attenuation of these differences would not alter the topological structure of the functional networks.

Functional Connectivity Networks

For each participant, we extracted regional mean time series from 638 parceled areas, based on the same functional template employed for the datasets analyzed in the previous sections [Crossley et al., 2013]. A Butterworth bandpass filter of 0.01 and 0.1 Hz was applied to all the time series. Following, we generated functional connectivity adjacency matrices by means of Pearsons correlations. All individual matrices were z-Fisher transformed as to ensure comparability. Finally, we built group matrices by averaging all individual networks.

Overall functional connectivity strength in every network is addressed as the mean of all positive links [van den Heuvel et al., 2017a]. Differences among groups in terms of connectivity strength are measured by means of simple t-tests. Following, spectral entropy is evaluated on networks thresholded at percolation, whereas to address relative entropies we investigated a similar range of thresholds as the one assessed in the previous example (absolute thresholds from 0.1 till the point when the network breaks apart).

First, we evaluate the effects of motion and denoising strategies over functional connectivity strength. An increase in the overall functional strength induced by motion has already been reported in the literature [Ciric et al., 2017]. Yet, we specifically want to replicate this effect, together with the evaluation of the effects of different pipelines over our three motion groups. The assessment of spectral and relative entropies of all groups will follow.

2.5.2 Results and Discussion

Here, I will briefly report and discuss the main results revealed by this methodological side-project. First, I will simply introduce the effects of motion on the overall functional network by means of functional connectivity strength. Second, I will investigate whether these motion-induced effects can be related to a reduction or increase of entropy in the system. As an important remark of this section, I will address how different denoising strategies can mitigate or exacerbate these effects. Specifically, we considered the three pipelines described before: P0 with no motion correction, a second pipeline based on FIX, and 9P a pipeline that includes global signal regression. We applied these pipelines on three motion groups: low, medium, and high motion (see data and preprocessing section). These three groups are defined on the framewise displacement (FD), a metric commonly used to evaluate the amount of head motion in rsFC [Power et al., 2012], which is computed as the sum of the absolute values of the derivatives of the six motion parameters.

First of all, we leveraged these three groups with different degrees of motion without the application of any kind of denoising strategy (P0) as means to evaluate the pure effects of motion.

In line with previous reports, we first observed a substantial increase in functional connectivity induced by motion in P0. As we can observe from panel A of figure 2.11, the distribution of link weights for the medium and high motion groups is right-shifted compared to the low groups, reflecting higher functional strength. At the subject level this shift is highly significant across all groups (medium>low: $p<0.00001$; high>low: $p<0.0001$). Through the application of specific denoising strategies we sought to investigate at what degree they could re-

duce this spurious difference in functional strength between groups. As we can observe from the histograms depicted in panels B and C of figure 2.11, both pipelines appear to significantly decrease the differences in the edge-weight distribution at the group level across different motion conditions. Specifically, the pipeline based on independent components classification (FIX) substantially reduces the right shift of the medium and high motion groups that was previously revealed in Po. Importantly, in this condition the edge-weight distribution of the medium group now almost completely overlaps with the low motion curve. Yet, at the individual level the functional connectivity strength, measured as the mean of all positive edges in the graph, shows statistical difference (medium>low: $p=0.007$). In contrast, the histogram representing the edge-weight distribution extracted from the high motion group still presents a highly significant right shift reflecting higher functional strength (high>low: $p<0.001$). A different pattern is revealed in the strength distribution after the application of GSR. In this case, all curves are highly overlapping, indicating similar functional connectivity across the three groups. This is furthermore revealed by the lack of significant differences at the individual level in edge strength (high>low: $p=0.8$; medium>low: $p=0.48$). Yet, the distribution of these curves presents a concerning issue, related to their centering around zero. After GSR the number of negative correlations dramatically increases, involving half of the edges within the network. These observations are in line with previous reports and concerns related to the controversial application of this denoising approach [Ciric et al., 2017].

As stated previously, the aim of this brief methodological study does not involve the simple evaluation of the effects of motion and motion correction techniques over the functional connectivity distribution, which was already extensively explored in previous investigations [Ciric et al., 2017]. In addition to the replication of previous findings, we resorted to the application of our null models as to assess whether these techniques could render the overall network closer or more distant from its random counterpart, by means of relative entropies.

In figure 2.12 we show the spectral entropy curves and relative entropies for the three pipelines considered. In light of the previous findings, we present here only the results related to the CWTERG, given the constraints present also at large scales from the CWTECM. Panels A, B, and C show the Von Neumann entropy

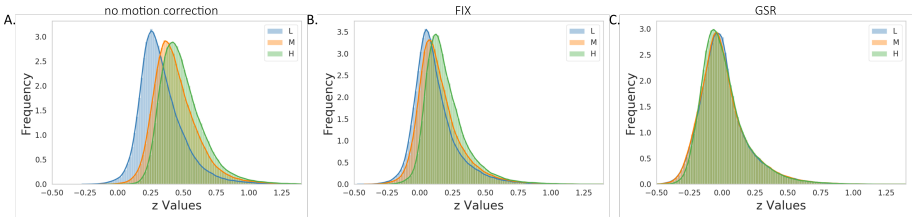

Figure 2.11: Effects of motion and commonly applied motion-correction techniques over the distribution of functional connectivity strength. Panel A depicts effects of motion as assessed by means of a pipeline where no motion correction strategies has been applied (P0). As a consequence of motion, we observe strong changes in the functional connectivity strength across the three groups (medium>low: p<0.0001; high>low: p<0.00001). Panel B represents the effects of the application of FIX over edge-weight distribution. Differences among groups are still present but attenuated (medium>low: p=0.007; high>low=p<0.001). Panel C shows the effects of application of GSR. Differences among groups are not present (medium>low: p=0.48; high>low: p=0.8).

curves of the differently pre-processed resting-state networks across three degrees of motion. In this specific case, we applied one single thresholding procedure, namely the lower absolute threshold that would ensure connectedness in all three motion groups within the same pipeline (t=0.44 for P0, t=0.29 for GSR, t=0.25 for FIX). We can observe that, when considered at the same absolute threshold, the low motion group always shows higher spectral entropy across the entire β range. This is especially evident in the P0 pipeline. It appears, indeed, that movement artifacts significantly affect the mesoscopic patterns within the empirical network. This trend is confirmed by the smaller entropy values of the high motion group compared to the medium, which is observed across all analysis pipelines. In the details of the P0 pipeline (Fig. 2.12A), this point is further highlighted by the lack of a clear-cut modular structure in both the medium and high motion groups, whereas a small shoulder present at medium scales for the low motion group highlights a different degree of inter-modular density. A similar trend suggests that head movements tend to make the network closer to its null model, i.e. more random. Popular correction techniques mitigate this confounding effect, decoupling functional connectivity and motion.

Panels B and C of Figure 2.12 show spectral entropy curves for the pipelines FIX and GSR, respectively. As already discussed, both pipelines importantly reduce the difference in spectral entropy between the three groups.

It is noteworthy that the application of the FIX pipeline, in panel B, highlights the presence of more prominent shoulders in all groups, again a signature of mesoscopic organization. From this view, the cleanup of resting-state data through independent component analysis would help in emphasizing the global structure of the network, despite the presence of head movements. The same cannot be appreciated in the groups pre-processed with a GSR pipeline, where the differences in spectral entropies are reduced, but no clear large-scale structure seems to emerge from these curves.

Notably, these effects are observed when the same absolute threshold is applied to the three motion groups. Indeed, we should remark that the difference observed across the three motion groups in terms of their spectral entropy curves, despite the application of robust motion-correction strategies (panels B and C, figure 2.12), strongly depends on the different densities resulting from the application of the same absolute threshold. It is important to notice that, although FIX and GSR strongly reduced the difference in functional connectivity strength across conditions, the medium and high motion groups still present higher overall strength, induced by the introduction of spurious correlations by motion. This results in denser networks when the same absolute threshold is applied, subsequently reducing entropy. Yet, from the relative entropies generated over several different absolute thresholds, we can appreciate a strong effect related to the sparsification procedure. In Panels D, E, F of figure 2.12, the relative entropies of the high motion groups for all pipelines and their respective null models are presented. In the interest of space, we report only the high motion group, which is more affected by head movements and shows more evidently the beneficial effects of the application of different preprocessing pipelines and thresholds. Here, we observe a very similar pattern to the one already studied in the thresholding effect example. Indeed, with the application of increasing thresholds, the distance of the empirical network from its random counterpart with same density gets higher, and it reaches maximum at percolation, despite the presence of motion and independently from the pipeline applied. Specifically, we can observe a higher relative entropy at percolation for the pipeline based on GSR (panel F). This pre-processing technique notably benefits from the thresholding procedure, considering the substantial difference between the maximum relative entropy attained at percolation and its val-

ues for denser networks. In line with previous studies [Ciric et al., 2017], the main effect of GSR is an increase in network modularity, mirrored by greater values of relative entropies at large scales, suggesting a well-organized high-order architecture. Yet, the lack of an "information shoulder" in the spectral entropy curve suggests the presence of a more uniform structure, with similar intra-modular density across different communities, and similar size of the modules.

This last observation further supports the application of a thresholding procedure, in contrast to the new trend in the literature which completely avoids the application of a threshold, directly working with fully connected networks, in order to elude the lack of agreement upon the threshold to implement [Schlesinger et al., 2017, Goulas et al., 2015, Bassett et al., 2011, Rubinov and Sporns, 2011]. Hereby, we demonstrate the importance of application of a threshold, as it allows the network to deviate from its random thresholded counterpart, even despite the presence of high degrees of movement, and irrespectively from the pre-processing pipeline in use. Importantly, through the application of an optimal thresholding it is possible to recover the medium-scale structure that would otherwise appear as "lost" as a consequence of motion effects.

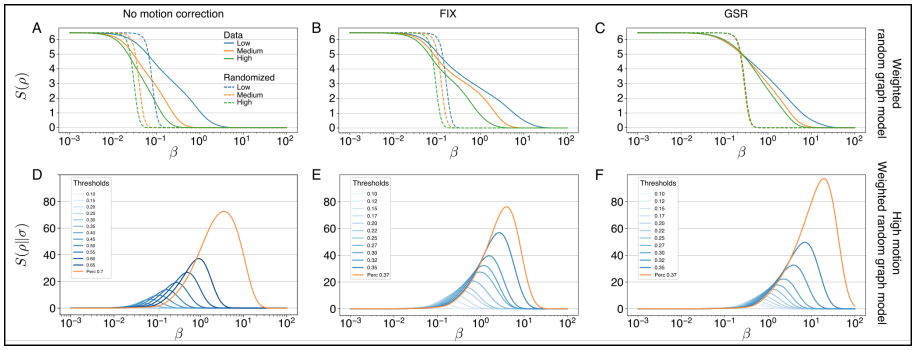

Figure 2.12: Panels A,B,C show the spectral entropies of networks for the pipelines o,FIX and GSR (solid lines), together with their randomized counterpart (CWTERG, dashed lines) over all motion groups. The relative entropies of networks from the high motion group are shown in panels D,E,F where the blue shades correspond to increasing absolute thresholds, while the orange lines correspond to percolation threshold, which has the maximum relative entropy at large scales.

2.6 CONCLUSION

The nature of resting state functional MRI networks based on pairwise association measures, like the Pearson correlation, is of a dense square matrix. Several experimental factors are involved in shaping the properties of these matrices and no consensus exists in the literature on the best practice for the definition and processing of these matrices and the associated connectivity graphs. In the present work, I leveraged some newly introduced tools, critical for making graph-theoretical analyses of networks more robust and theoretically sound [Nicolini et al., 2019], as means to evaluate the effects of contentious debated processing steps over the functional network topology. Importantly, we could bring together two novel precious null models, which for the first time extends the maximum entropy random graph formalism to networks with threshold and real positive weights, and a spectral entropy framework, essential to appreciate the differences of networks with respect to their random versions from local to global scales. This promising approach made it possible to quantitatively determine the effects of experimental factors on the properties of functional networks.

In light of this newly developed approach, we studied how thresholding procedures, motion and correction pipelines are essential factors in shaping the network. The application of a threshold to resting-state networks is now one of the most contentious steps debated in the field. Most studies now resort to the application of a fixed density to networks when studying different populations. However, this approach presents several drawbacks, pointed out by various authors [van den Heuvel et al., 2017a, de Vico Fallani et al., 2017, Bordier et al., 2017]. These pitfalls led to an increasing trend to altogether avoid any sparsification of the studied graphs, thus eluding the issue. Even more striking is the recent finding that the application of a threshold itself could inject some complex structure within the network, thus representing an important confounding artifact [Cantwell et al., 2019].

Here, by means of advanced information theory tools, we have found that the thresholding procedure is an essential step in analysis pipelines and helps to differentiate networks from their random version. Indeed, we hypothesized that if the thresholding procedure would actually inject structure within a network, it would do so also in the random counterparts of the empirical networks evaluated.

Conversely, we show how the role of the threshold itself is crucial and highly beneficial to study the large scale architecture of real-world networks. Importantly, our results point to the existence of an optimal sparsification threshold, and provide a procedure, based on percolation analysis, for its identification

The importance of sparsification can also be appreciated through the evaluation of the effects of motion and different preprocessing pipelines. Importantly, the introduced formalism has proven crucial for the identification of the effects of head movements over all scales of the network. Motion seems, indeed, to increase randomness and to reduce spectral entropies across different scales, bringing the network closer to its random counterpart. However, a reported finding revealed that this motion effect is critically reduced when we apply stringent thresholds, until reaching percolation, where the network, even in presence of strong head movements, is maximally distant from the null model.

Altogether, thanks to this methodological advancement, I could appreciate the importance of some critical pre-processing steps which should be more carefully evaluated when facing complex network analysis applied to functional brain images. These tools are critical to conduct graph theoretical analysis on functional data from different clinical populations, as described in the next chapters of my thesis.

3 FUNCTIONAL CONNECTIVITY ALTERATIONS IN AUD

After tackling a few critical aspects for the application of network theory to the study of functional connectivity, I extended these methods to the analysis of resting state data from AUD patients and healthy controls. As reviewed in the first introductory chapter of this thesis work, the neural mechanisms involved in alcohol addiction are not fully understood, and a number of questions remains open. Moreover, one specific region recently caught the attention of the clinical community, playing a central role for the translation of interoceptive states into decision-making processes: the insular cortex. Here, I first evaluate differences identified between a sample of AUD patients and one of healthy volunteers by means of a graph theoretical approach, with a specific focus on the role played by the insula within the network. The work disseminated here is now under peer-reviewed publication process (Bordier et al. in prep). Following, I will evaluate an independent sample of patients, with the aim to possibly replicate previously discussed findings.

3.1 INCREASED NETWORK CENTRALITY OF THE ANTERIOR INSULA IN EARLY ABSTINENCE

Alcohol addiction is among the most prevalent disorders worldwide, it represents a severe social burden and critical danger for patients. Indeed, 5.3% of all global deaths can be attributed to alcohol consumption [World Health Organization (WHO), 2018]. It is a chronic and relapsing brain disorder, and the prolonged alcohol intake further complicates the identification of neural circuits involved in the rise and maintenance of the disease. Ethanol, the addictive and rewarding substance present in alcoholic beverages,can exert crucial prolonged actions on the brain and desensitize neural circuits. Unfortunately, the reversal of these ef-

fects appears critical. As I extensively disclosed in the first chapter of this these, AUD has been associated to several brain alterations, both at a structural and at a functional level suggesting a complex framework. Altogether, brain alterations identified in this neuropsychiatry disorder, previously reviewed, point towards the severe symptomatology of alcohol-addicted patients, comprising the loss of self-control and reflective-thinking in presence of alcoholic cues, or altered interoception and memory functions. Yet, the lack of clear-cut findings in the field can originate from the high variability of the disorder and in the samples of patients investigated. Indeed, clinical variables such as days of abstinence or age at first drinking can significantly change the underlying functional pathways. This further complicates the identification of clear endophenotypes of AUD, which is crucial for the development of targeted treatments.

The application of graph theoretical approaches to AUD is still in its infancy, and just few studies investigated the topological organization of the alcohol-addicted functional brain [Sjoerds et al., 2015, Morris et al., 2017, Wang et al., 2018, Zhu et al., 2018]. Altogether, these studies mostly addressed local properties such as nodal degree, efficiency, and clustering coefficient, or global topology measures by means of overall functional connectivity and global efficiency. The trend highlighted by these reports is clear when evaluating global metrics, where AUD patients mostly present reduced global efficiency and functional strength when compared to samples of healthy volunteers. Opposite, conflicting results are reported at the local level, with different patterns of increased and decreased nodal efficiency and nodal segregation in separated brain regions involving the reward system, frontal and temporal regions, and the insula [Wang et al., 2018, Wang et al., 2015, Sjoerds et al., 2015]. To the best of our knowledge, no study to date evaluated the functional architecture of the addicted brain with the use of modularity algorithms.

I already thoroughly highlighted in the first introductory chapter of this thesis the important role covered by the modular organization of complex systems, characterized by the presence of subclusters of nodes more tightly connected within themselves, forming so called modules, or communities. This feature ensures an optimal balance between segregation and integration of different regions. A modular network benefits of strong evolutionary advantages, as the subdivision of the

system into separated yet connected modules confers robustness and adaptability [Sporns and Betzel, 2016]. Indeed, a modular networks is more flexible in case of external perturbations, allowing only the impact over specific segregated modules in contrast to a reshape of the whole system when facing an external environmental challenge. However, alterations of the modular organization can rearrange and disrupt the communication pathways between separated neural regions. The disruption in the segregation and integration balance between different brain cortices might, indeed, lead to pathological conditions [Fornito et al., 2016].

Here, we intend to evaluate the modular organization of functional connectivity networks in detoxified alcohol-dependent patients. To achieve this we resort to the application of an InfoMap approach, which, as described in chapter 1, benefits from higher resolution compared to Newman's approach, the mostly applied partition algorithm. Indeed, the detection of differences related to the modular architecture in psychiatric patients has often proven difficult, most likely because of the critical resolution limit of the modularity maximization approach. The important resolution limit of the Newman algorithm might hinder the identification of specific fragmentations in key neural structures, thus hampering the investigation of subtle alterations within functional neural networks. For this reason, in this study we leveraged the benefits of the InfoMap algorithm with a Consensus approach, with the aim to possibly identify functional alterations that could not be previously revealed by means of simple evaluation of local topological metrics. The identification of neural regions presenting an altered integration within the whole systems might be crucial for the identification of therapeutic targets. Ideally, we could, indeed, select the altered structure, subsequently target it for treatment, and evaluate the effects over the whole network in case of an external perturbation aiming the affected region. Hence, we evaluate possible differences at a modular level in a sample of AUD patients, as compared to the healthy functional organization detected in a sample of volunteers.

3.1.1 Methods and Materials

Participants

The investigation was carried out in the framework of the ERA-NET NEURON TRANSALC study (WHO-International Clinical Trials Registry Platform: DRKS00003357). Thirty-five recently detoxified, abstinent AUD patients, all males (age=45±9, abstinence days 21±7, 260±120 [g]/day of alcohol pretreatment), and 37 male healthy volunteers (age=41±10) were recruited for the study. Patients were included if they satisfied AUD diagnostic criteria as listed in the DSM-IV and after completion of medically supervised detoxification (treatment of withdrawal symptoms with short-acting benzodiazepines had to be completed for at least 3 days), with at least 2 weeks of abstinence prior to the MRI session. All participants were assessed by Structured Clinical Interview for DSM-IV to identify patients who met criteria for AUD; participants were excluded from the study if they met criteria for Axis I or II psychiatric disorder within the past 12 months (except alcohol or nicotine dependence), had current use of psychotropic or anticonvulsive medication, had positive urine drug screening (opiates, cannabinoids, benzodiazepines, barbiturates, cocaine, amphetamines), or unstable medical conditions. After this baseline assessment, patients were offered the choice between of two treatment options: either a multi-professional medically-supervised therapy schedule (IWT), or the same therapy schedule together with adjuvant oral Naltrexone (NTX, 50mg per day) in a naturalistic open-label free-choice design. Twenty-nine patients were included in this arm of the study, with 12 subjects receiving IWT only, and 17 NTX. A follow-up fMRI scan was scheduled for all patients two weeks into treatment with either NTX plus treatment as usual or ITW only (M = 15.5 days, SD = 3.5). The study was approved by the local ethics committee in accordance with the Declaration of Helsinki.

Image acquisition and preprocessing

Functional data was acquired with a 3T MR scanner (MAGNETOM Trio, Siemens, Erlangen, Germany), using echo-planar imaging (EPI) and simultaneous acquisition of physiological data. T2* weighted echo-planar images (EPI) were acquired

in a transversal orientation 30° clockwise to AC-PC-line covering the whole brain with the following parameters: TR=1.5 s, TE=28 ms, flip angle = 80°, 24 slices, slice thickness 4 mm, 1 mm gap, voxel dimensions 3 x 3 x 5 mm^{-2}, FOV 192x192 mm^{-2}, 64x64 in-plane resolution. This short TE and the 30° flip to ACPC orientation were chosen to minimize susceptibility artifacts. In total, 240 timepoints were acquired per each participant. Physiological data were acquired with the SIEMENS standard sensors for pulse oximetry and respiration with a sample rate of 50 Hz. During the resting-state scan participants were instructed to keep their eyes closed.

The fMRI data were preprocessed using SPM8 (Welcome Trust Centre for NeuroImaging, London, UK). After discarding the initial 10 volumes of each participant, the remaining volumes were processed to remove physiological confounds (heartbeat, respiration) from the raw data using the Aztec toolbox (7). The resulting corrected volumes were slice-time corrected, head-motion realigned (patients average maximum translation = 0.545±0.465, average maximum rotation= 0.007±0.006; control average maximum translation = 0.502±0.474, average maximum rotation= 0.007±0.007) and normalized to the standard MNI EPI template space (voxel-size resampled to 3x3x3mm^3). The signal related to head movement was removed using a multiple regression model. Potential differences in motion related artifacts between groups were assessed using Framewise Displacement (FD) and DVARS. No significant between-group differences were observed in these metrics (FD: t=0.214, p=0.831; DVARS: t=0.151, p=0.88).

Functional connectivity graphs

Nodes were defined according to the functional template described in [Crossley et al., 2013], comprising 638 cortical and subcortical nodes. BOLD time series were then extracted and averaged for each parceled region, and Pearson correlation coefficients were calculated for all pairs of nodes to compute a functional connectivity matrix for each participant. Finally, subjects' specific adjacency matrices were Z-Fisher transformed and averaged to obtain two group-level functional connectivity matrices for healthy controls and AUD patients. As described in the previous chapter, in order to remove weak and spurious edges from the group-average network we apply a thresholding procedure based on percolation analysis,

to maximize the structural organization that can be extracted from the system. Optimal sparsification thresholds were determined independently in the patient and control to enable unbiased comparison of the respective community structures.

Modular organization and nodal centrality measures

The modular architecture of the functional network was computed using the InfoMap approach [Rosvall and Bergstrom, 2008], based on the optimization of a cost function dubbed map equation. To reduce the effects of degeneracy of solutions - still present in Infomap, although to a lower extent than in the more popular Modularity optimization method - , we resort to a Consensus approach. This method provides a means to compute a stable partition that is representative of the consensus of all nearly-optimal solutions generated by different runs of the community detection algorithm.

First, we generated the consensus matrix (nxn, with n the number of nodes), which is obtained by running the community detection InfoMap method 1000 times and assigning a value to the element t_ij of the matrix that corresponds to the number of times nodes i and j appear in the same community. Second, we ran the community detection algorithm (InfoMap, in our case) on the consensus matrix to generate the consensus partition. The computation of the consensus partition was performed using a modified version of the function provided by the Brain Connectivity Toolbox [Rubinov and Sporns, 2010] adapted to weighted networks. All visual representations of the anatomical distribution of modules and topological parameters were produced using the BrainNet viewer toolbox [Xia et al., 2013] and MRIcron [Rorden and Brett, 2000].

To address the role of all nodes within the overall network, we considered the classification, based on the modular organization, proposed by [Guimera and Amaral, 2005] and described in the chapter 1 of this thesis. According to this, nodes are classified by their within-module degree (proportion of connection of a node to all other nodes belonging to its own module) and their participation coefficient (proportion of connections of a node towards external modules). To assess statistical differences across the two groups, we computed participation coefficient of each node for each participant and ran a t-test, Bonferroni corrected. By means

of this classification it is possible to evaluate the central or peripheral roles that specific regions can play within the overall system.

3.1.2 Results

As a first step, we evaluated global differences in overall functional connectivity strength. This was assessed by the edge-weight distribution between patients and controls, as shown in figure 3.1. The two histograms depict the z-transformed edge distributions for the two groups. Here, we can first observe an important left-shift in the edge distribution of AUD patients, reflecting a reduction in the overall strength. The global functional connectivity strength measured at the subject level was significantly different across the two groups, with patients showing a reduced edge-weight strength, as reflected by the z-Values distribution (t=1.78; p=0.03). In addition, also the global efficiency, a measure of integration of the network, resulted significantly decreased in patients (t=2.186; p=0.015). This reduction in global connectivity is in line with previously reported findings in alcohol dependent patients of a decreased functional strength and efficiency, when explored with a graph theoretical approach [Sjoerds et al., 2015, Morris et al., 2017, Wang et al., 2018, Zhu et al., 2018].

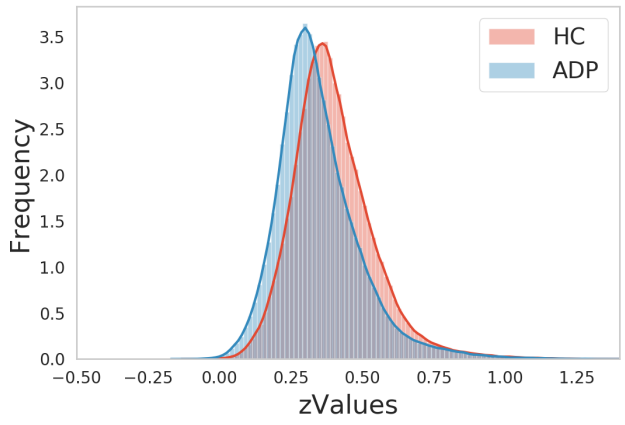

Figure 3.1: Edge-weight distribution of HC and AUD groups. Patients show a right-shift in the distribution, representing a significant reduction in the overall functional connectivity strength (p=0.03).

Disruption of modular organization in alcoholics

Following the application of the InfoMap algorithm, we detected 14 and 21 modules in the control and patient groups respectively, result of a fragmentation and reorganization of certain communities in AUD. Interestingly, the modular struc-

ture for the two groups appears largely consistent, and a significant fragmentation in patients was visible only in a few modules. Figure 3.2 shows the modular structure of the two groups, together with the adjacency matrices re-ordered according to nodes partitions.

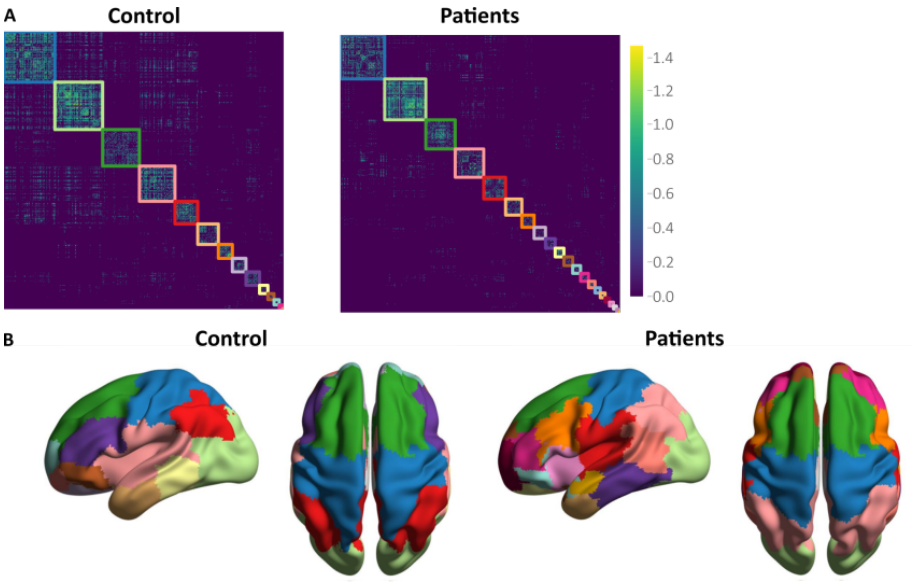

Figure 3.2: Comparison of modular architectures between HC and AUD patients. Panel A: Group-level adjacency matrices for the two groups with nodes re-ordered according to modular membership. Modules are outlined with their respective color represented in community organization mapped on the cortical surface of the brain in panel B.

The fragmentation of two modules most prominently involved is shown in figure 3.3. Among these, we detected a crucial re-organization of the basal ganglia sub-module, a region well-known to play a critical role in substance addiction. In HC this community includes the amygdala, pallidum, putamen, hippocampus, and thalamus. In contrast, these regions are organized into three distinct sub-modules in AUD, the amygdala, the thalamus, and pallidum-putamen. The other structure involved is the supramarginal temporal module. In controls, this community shows dissociation of the anterior part of the insula forming an independent module in patients. From panel B of figure 3.3 we can appreciate this break-up of the insula into two sub-modules in AUD, corresponding to the insular anatomical separation into its anterior and posterior portion (see also figure 1.10 for the anatomical representation). Opposite, in HC all the nodes of this region falls within the same community structure, reflecting

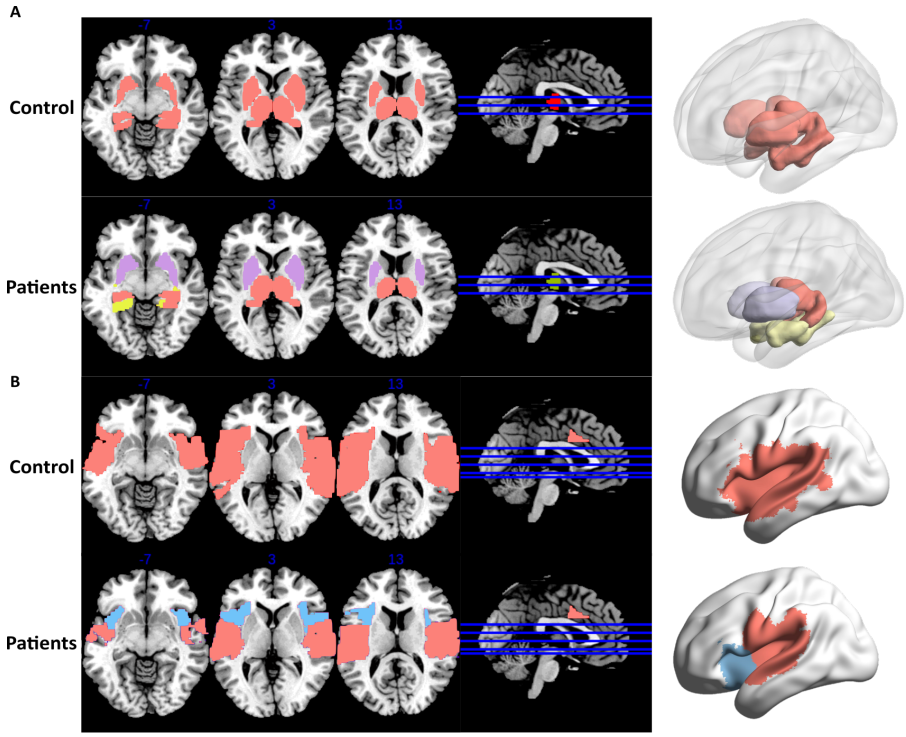

Figure 3.3: Local fragmentations identified in AUD patients compared to HC. Panel A shows the differences in the modular organization in basal ganglia structures. In patients these structures are organized into three separated communities, including amygdala, the thalamus, and pallidum-putamen. Panel B shows the separation of the insular cortex in AUD. The insula is separated into anterior (blue) and posterior (red) sections.

Increased centrality of the anterior insula in AUD

The modular architecture of the brain functional network is essential for the identification of so-called connector hubs, nodes with a higher number of connections pointing towards different modules, thus playing a strong integrative role. To assess this aspect, we addressed the participation coefficient of all nodes in the network, and subsequently evaluated differences between node-wise participation coefficient in patients and controls. Consistent with the overall decreased functional connectivity in AUD, patients show more widespread reduction in participation coefficient as compared to HC, mostly including visual regions, sensory and auditory cortices, and parts of middle frontal gyrus. Yet, some nodes surprisingly show an opposite trend, with an increase in participation coefficient in the patient group, comprising frontal regions, superior parietal areas and, most prominently, the bilateral anterior insula (Figure 3.4). In contrast, the posterior insula exhibits significant reduction in participation coefficient.

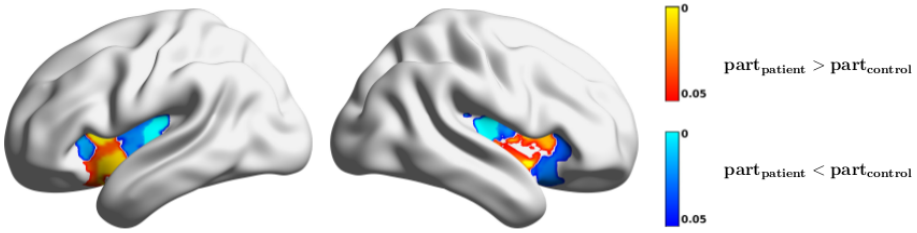

Figure 3.4: Differences in participation coefficients of nodes in the insula cortex mapped on the brain cortical surface. P-values obtained by a one-tailed Student's test, Bonferroni corrected. The anterior insula shows significantly increased centrality in patients, while participation coefficient in the posterior insula is reduced.

Voxel-Based Morphometry

Importantly, this case-control study so far revealed altered functional connectivity organization in basal ganglia structures and the insular cortex. However, as extensively reviewed, these regions were previously reported to show altered gray matter volumes. Specifically, a study from [Senatorov et al., 2014] revealed enlargement of the amygdala and reduction of the insular volume in AUD patients. To rule out the possibility that our results might be influenced by these alterations, we subsequently performed a Voxel-Based Morphometry (VBM) analysis. We found no evidence of significant morphometric differences between patients and controls, thereby excluding potential confounding effects driven by these alterations on functional connectivity organization.

Effect of treatment on network properties

In the combined group of 29 patients participating in treatment, IWT alone or in combination with NTX, we observed a modest but significant increase in the strength of functional connectivity (p=0.007). Interestingly, the initial fragmentation of the supramarginal module was reversed, with the anterior insula reunited with the supramarginal nodes after 2 weeks of treatment (figure 3.5). Similarly, the participation coefficient of the anterior insula showed significant reduction after 2 weeks with a trend towards normalization of its topological centrality. Conversely, the basal module organization remained fragmented over time, and no significant effects on participation coefficient of the nodes included in this module were observed.

Analyses of the two subgroups of patients treated with IWT plus adjunct NTX (n=17) or ITW alone (n=12) showed very consistent results, with recovery of the supramarginal module in both cases, and no significant effects in the basal module.

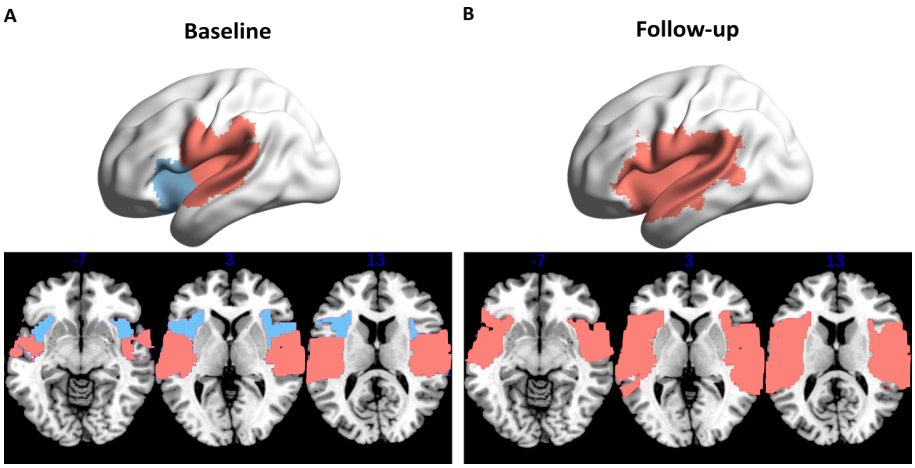

Figure 3.5: Effects of treatment on the basal and supramarginal modules in AUD patients. Panel A shows the fragmentation of the insular cortex before the additional two weeks of treatment. In panel B we observe the normalization of the organization of this module after two weeks of treatment. The modular organization is identical for participants treated only with IWT and for patients treated also with NTX.

3.1.3 Discussion

To the best of our knowledge, this is the first case-control study evaluating the functional modular organization in AUD. Interestingly, we revealed region-specific alterations in the functional architecture of the alcoholic network, assessed in recently detoxified patients. In details, we detected local fragmentations in neural regions already well-known to play a central role in addiction.

First, the basal ganglia structures appeared to break up into separated submodules in the patient group, in contrast to the identification of a single module comprising basal sub-structures in HC. These regions are central in the overall brain reward system, and different studies already identified anomalies in their structure and function in relation to substance addiction [Wrase et al., 2008, Dupuy and Chanraud, 2016, Fritz et al., 2019]. Here, we further proved the altered functional embedding of these subcortical regions within the overall brain network in

AUD. As discussed, the modular architecture is crucial for an efficient information flow of the whole brain system, ensuring an optimal balance of integration and segregation. The identified fragmentation of these regions suggests an abnormal communication among these areas, in line with their role and their functional recruitment as related to the negative emotional states and withdrawal/negative affect stage of addiction [Koob and Volkow, 2016].

A second particular aspect, highlighted by this study, is the role played by the anterior insular cortex within the overall functional network. First of all, we revealed an important fragmentation of the insular region in AUD, which matches the anatomical and functional architecture of this cortical area. Specifically, we observed a separation of the anterior portion of the insula from the rest of the region, in contrast to the organization identified in healthy controls, where all its nodes fall into the same community connected to the superior temporal cortex and some inferior frontal nodes. Importantly, this cortical region recently gained increasing attention in the study of addiction disorders. This area, embedded within the temporal and the frontal lobe (Fig1.10), is the main region of the brain responsible for interoception. Furthermore, thanks to its connections towards more frontal and subcortical areas, the insula plays a critical role in the translation of interoceptive feelings into emotional and decision-making behaviors [Craig, 2009]. In lay terms, this cortical system informs us about the needs and urges of our body, and subsequently sends this information to other cortices as to act and behave accordingly. Surprisingly, its role seems to be crucial for the maintenance of addiction, and the presence of lesions can abruptly interrupt the addictive cycle. This is clear from the findings of Naqvi and colleagues [Naqvi et al., 2007], who observed that patients that experienced damages comprising the insular cortex suddenly quit smoking. From this observation, a number of studies investigate its potential role in drug addiction. For example, task-based functional studies reported increased reactivity of this region in AUD patients elicited by alcohol cues [Naqvi and Bechara, 2009]. This further suggested the importance of this region in drug craving and cue-triggered urges, particularly involving its anterior portion [Craig, 2009].

In line with this concept, we surprisingly revealed an increased centrality of the anterior insula in AUD patients, as revealed by a higher participation coefficient, possibly indicating an exaggerated role of this region in the integration of inte-

roceptive states into emotional and decision making processes in patients [Naqvi and Bechara, 2009].

The effects of protracted abstinence was explored in patients who underwent a standardized therapy program with or without adjuvant naltrexone, an opioid receptor antagonist with demonstrated albeit modest efficacy for relapse prevention [Jonas et al., 2014]. We observed a partial recovery of connectivity strength, and normalization of the structure of the supramarginal module. The participation coefficient of the insular cortex was significantly lower after two weeks of treatment. Importantly, these findings demonstrate that at least some alterations in functional connectivity observed in early withdrawal are actually reversible. Moreover, the observation of a normalization by treatment of the integrative role of the insula suggests a potential mechanism underlying amelioration of the condition.

Whether partial normalization in the strength and structure of functional connectivity networks was driven by continued abstinence, or reflected the phsychoeducational or pharmacological intervention remains unclear from the post-hoc analyses of the two subgroups of patients receiving daily adjunct NTX or IWT only. Normalization of the supramarginal module was observed in both cases, thus suggesting that they are not related to the specific pharmacological mechanism of NTX, but rather reflect the change in the state of the condition during protracted abstinence. These effects appear to be driven by insular connectivity, since no significant changes were observed at the level of the basal module, the latter comprising dopaminergic pathways that are central to the brain reward system. A recent study by Morris et al. [Morris et al., 2017] showed reduced connectivity in AUD patients, consistent with our results, and an effect of NTX on some topological parameters like local efficiency.

Overall, here we importantly revealed, for the first time by means of complex network analysis, the exaggerated centrality that the anterior portion of the insula acquires in AUD patients. Given the novelty of these observations, together with the high variability of the functional architecture in individual patients and healthy volunteers, we subsequently decided to try and validate these conclusions also on a separate dataset comprising alcohol dependent patients. Indeed, functional connectivity studies in humans suffer of the high heterogeneity and variability of brain organization in the overall population; for this reason validation

studies aiming to replicate specific findings in independent cohorts are of critical importance.

3.2 VALIDATION IN A SEPARATE SAMPLE OF AUD PATIENTS

The case-control study previously described assessed functional alterations in the modular architecture in alcohol dependent patients as compared to a sample of healthy volunteers. Noteworthy, this investigation revealed an important fragmentation of specific regions involved in addiction, namely basal ganglia structures and the insular cortex. Furthermore, a significant increase in a topological measure indexing the integrative role of local nodes, the participation coefficient, highlighted an excessively central role of the anterior portion of the insula within the overall functional network. These findings are particularly relevant as they demonstrate, for the first time, that patients with a history of alcohol addiction present specific alterations in the integration and segregation of these key regions.

Replication of results is critically important to increase confidence in neuroimaging findings. Several reports recently tried to focus the attention of scientists over this crucial aspect leading to the subsequent growth of "open science", thus promoting openness, transparency and data sharing in functional neuroimaging [Nickerson, 2018]. Limited reproducibility of neuroimaging studies comes from several sources. For example, even slight changes of the parameters for image preprocessing might impact the final results, as well as different methodological approaches for network analysis can lead to different outcomes. The lack of a well-established unique pipeline from image processing to network construction and evaluation further complicates replicability. For this reason, scientists are asked to be as transparent as possible when disseminating their results, thus giving the chance to other researchers to subsequently evaluate the same findings. Moreover, from these alerts, the presence of freely available neuroimaging datasets is rapidly growing, making neuroscience more accessible to everyone. Yet, the appreciation of functional brain effects in different studies is still challenging, mostly for what concerns human studies. Brain conditions, often studied by means of cross-sectional and case-control studies, are highly heterogeneous and the effects

might be so subtle that we would need very big sample sizes to evaluate specific findings. This is particularly true also when we consider the high variability, both at a structural and functional level, in the brain organization of the global population as well as differences in the origin, development, and maintenance of the investigated psychiatric or neurologic disorders. In the case of brain disorders the lack of replicability is furthermore critical given the subsequent difficulties in the identification of specific altered neural regions that might be perfect target for treatment options. For these reasons, we considered crucial the necessity to further replicate our recent findings also on different cohorts of patients.

In the case of AUD patients local alterations in sub-cortical structures (amygdala, hippocampus, thalamus, etc.) and in the insular cortex were already consistently reported [Wrase et al., 2008, Senatorov et al., 2014, Fritz et al., 2019]. The involvement of the insula in drug addiction gained centrality from the observation of the sudden interruption of smoking-addiction in patients who suffered from a stroke affecting this area [Naqvi et al., 2007]. Thus, detailed investigations related to the functional embedding of this cortical region in addiction is essential, as it might prove to be an optimal target for addiction treatments. Surprisingly, the study disseminated in the previous section is the first in revealing the involvement of these regions, both sub-cortical and cortical, also in the modular organization of the functional brain network in these patients. However, further evaluations should be carried out before assessing possible effects of a treatment targeting these regions.

Hence, I leveraged an independent sample of AUD patients to evaluate whether the specific modular alterations previously identified could be detected also in a separate cohort. Here, I will evaluate the functional strength and modular architecture in this independent group of patients and I will subsequently compare it, qualitatively, to the previously investigated samples of AUD and HC.

3.2.1 Materials and Methods

In this section I will describe the independent sample of AUD patients kindly shared with us by Anneke Goudriaan, from the Arkin Mental Health Institute and from the Amsterdam University Medical Center (UMC), department of Psychiatry

(University of Amsterdam). To distinguish this cohort from the sample of AUD patients previously investigated I will refer to it as AUD_A (Alcohol Use Disorder – Amsterdam). The other sample will be here referred as AUD_T (Alcohol Use Disorder – Transalc). The sample of healthy controls employed here will be the same as the one introduced in the previous section.

Participants

A total of 38 AUD patients were recruited at UMC from addiction treatment centers in the city area of Amsterdam, the Netherlands. Participants recruited were screened with a Composite Diagnostic Interview (CIDI; [World Health Organization (WHO), 1990]) to assess presence and severity of AUD according to the DSM-IV criteria. Inclusion criteria required sobriety for at least three weeks, as confirmed by a urine test. All participants were screened for MR suitability, current psychiatric disorders, including anxiety, major depression and abuse of substances other than alcohol. The study was approved by the local Medical Ethical Committee of the Academic Medical Center of the University of Amsterdam. All participants signed the informed consent form, consistent with the declaration of Helsinki, before participating in the study.

Image acquisition and preprocessing

Resting-state functional images were acquired on a Philip Achieva 3T scanner at the Spinoza Imaging Center, Amsterdam, the Netherlands. Acquisition parameters by means of field-echo EPI sequence were as follow: TE=27.3ms; TR=2s; FOV=240x240mm; 37 slices; slice thickness 3mm; 0.3mm slice gap; flip angle=76.1°. Images were oriented axially along the anterior-posterior commissure to the posterior-commissure (AC-PC) line. Scanning time was 7 minutes, for a total of 210 dynamic volumes acquired. During resting-state scan acquisition participants were asked to keep their eyes closed.

Preprocessing steps were highly similar to those implemented in the previously described study with AUD patients. Functional images were preprocessed with SPM12 (Wellcome Trust Center for NeuroImaging, London, UK). The first 10 volumes for each participant were discarded as to ensure signal stability. Resulting volumes were slice-time corrected, head motion realigned, and normalized to the

standard MNI EPI template space (voxel-size resampled to 3x3x3mm^{-3}). The signal related to head movement, extracted from the image realignment step, was removed by means of a multiple regression model. Given that we did not have any pre-recorded physiological signal for this study, in contrast to the Transalc study, we further extracted time series from white-matter and ventricles regions and added this spurious information to the multiple regression model.

Graph-theoretical analysis

Construction of the network followed the very same procedure previously described in section 3.1.1. All images were parceled according to the functional template described in [Crossley et al., 2013], with a final definition of 638 cortical and subcortical nodes. BOLD time series were subsequently extracted from each node, and Pearson correlation coefficients were calculated for all pairs of nodes. Subjects' specific adjacency matrices underwent a z-Fisher transform and were averaged to obtain the group-level functional connectivity matrix. A percolation approach was implemented as means to discard weak and spurious edges.

The modular architecture was detected with InfoMap [Rosvall and Bergstrom, 2008], employing a consensus approach.

3.2.2 Results

Similar to previous findings, we observed an important reduction in the overall functional connectivity in AUD_A. Through the evaluation of the edge-weight distribution from both groups of patients and HC we detected an even stronger right-shift of the AUD_A group, denoting a strong and significant decrease in functional connectivity (figure 3.6). If compared to the HC group, this reduction appears highly significant (t=9.16; p=2.6^{-13}). This strong significance might be caused by the different acquisition scans, as the simple weight strength can be strongly affected by the intensity of the BOLD signal. Yet, also the evaluation of the binary global efficiency, indexing the efficiency in the information flow and not dependent on the weight strength, revealed a significant reduction in the AUD_A group, in line with our previous report (t=2.63; p=0.01). No differences

between the two patient groups are appreciated in relation to global efficiency (t=0.74; p=0.45).

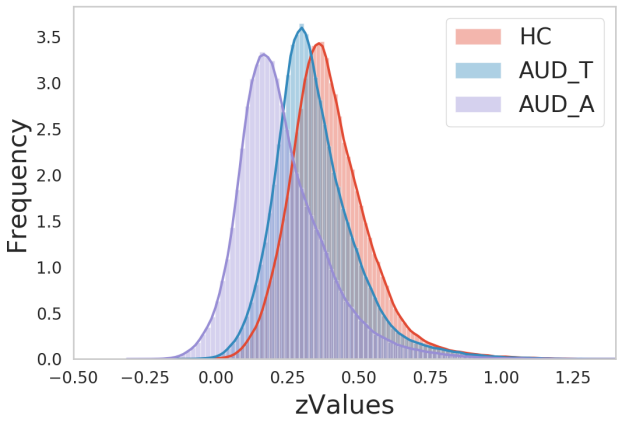

Figure 3.6: Edge-weight distribution of the three experimental groups.

Modular organization

Again, we detected the modular architecture for the second group of patients by means of InfoMap (Figure 3.7). Interestingly, AUD_A did not show a widespread modular fragmentation, revealing a total of 13 modules (range 164 – 6 nodes) denoting the overall functional modularity, a number of communities very similar to the one encountered in HC (13 communities). Observing the overall global modular architecture we can appreciate in this group a different reorganization as compared to HC, mostly related to the frontoparietal network, which seems to present a non-pathological diversification in AUD_A, mostly likely originating from the different acquisition scans and parameters. Yet, specific local fragmentations can be appreciated also in this independent sample of patients.

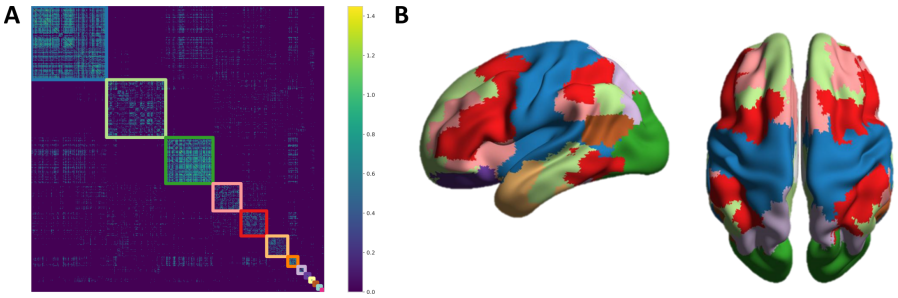

Figure 3.7: Modular architecture in the independent sample of AUD patients. Panel A shows the group-level sparsified adjacency matrix re-ordered according to nodes' modular membership. Panel B represents the community organization mapped on the cortical surface of the brain. The two images are color-matched.

Surprisingly, we could detect also in this patient group specific local fragmentations situated at the level of the basal ganglia structures and the insular cortex (figure 3.8). In details, AUD_A patients presented a re-organization of basal regions even more prominent than the one detected in the AUT_T group. Indeed, here we revealed a division into four different modules comprising pallidum-putamen, the thalamus, and a further fragmentation of the hippocampus, which appears split into two distinct sub-modules, one comprising also the bilateral amygdala. Furthermore, this independent sample of patients revealed a very similar fragmentation of the insular cortex as the one previously described in AUD_T patients. Indeed, the bilateral anterior portion of the insula stands in a separate community, while the more posterior area now lays together with the somatosensory module. Interestingly, as we can appreciate from both panels of figure 3.8, the two groups of AUD patients appears to share the specific local alterations in areas with a key role addiction.

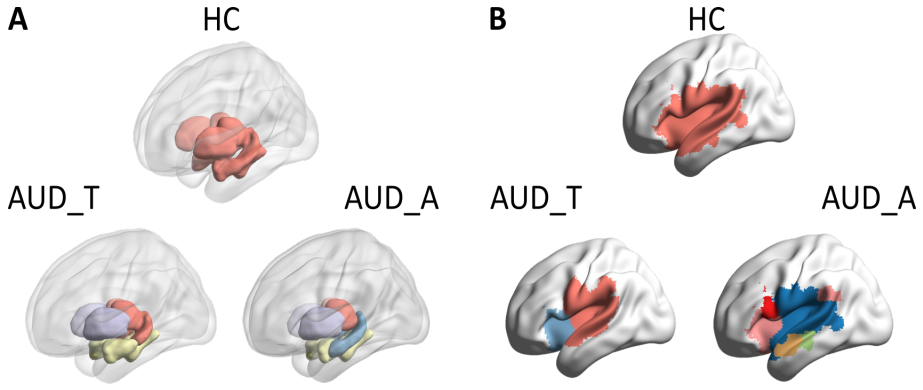

Figure 3.8: Representation of the local modular fragmentations observed in the two independent samples of AUD patients as compared to a sample of HC. Panel A shows the re-organization localized in the basal ganglia structures; Panel B represents the similar fragmentation of the anterior and posterior insula detected in the AUD groups in contrast to HC.

3.2.3 Discussion

This study further supported the involvement of region specific alterations in the overall modular organization of alcohol dependent patients. By means of a data-driven approach we could successfully replicate very similar findings as those already discussed in the previous case-control study. Specifically, we detected

in an independent sample of AUD patients a specific fragmentation of the basal ganglia, subcortical regions with a prominent role in the reward system, and of the insular cortex, a critical area that gained increasing attention for its involvement in addiction disorders. Given the nature of this exploratory study,comprising cohorts of patients acquired in different centers and with different acquisition protocols, we could not test further statistical measures. Yet, these results appear robust across different studies, and interesting in the light of the strongly debated role of the insula in drugs addiction including alcoholism [Senatorov et al., 2014, Sullivan et al., 2013, Gaznick et al., 2013, Scuppa et al., 2019].

In conclusion, I extensively reviewed the central role of the insular cortex as the main interoceptive center of the brain, and its critical involvement in addiction suggests how drug craving and cue-induced urges might be considered as complex interoceptive feelings. Specifically, this information seems to be predominantly processed in the anterior portion of the insula, which appears to have an altered embedding within the overall functional network. The observed separation of this region from the more posterior portion reflects an underlying alteration in the communication of this area. Furthermore, its abnormal integration is also suggested from the identification of an exaggerated integrative role that the anterior insula presents within the system, as highlighted by its significant increase in participation coefficient. These findings, together with the accumulating evidence reported in the scientific literature, point towards a complex involvement of the insula in the control of addictive behaviors [Scuppa et al., 2019]. As already stressed, its specific role in the translation of internal urges into emotional and decision-making processes might be a central aspect driving addiction.

Unfortunately, studies carried out in human patients present critical interpretative issues. Indeed, it is not possible to manipulate and control a number of important variables that might lead to misleading interpretations. Importantly, from these studies it is not possible to assume whether the identified functional alterations are driven by the extended exposure to alcohol, or whether they play a central role as predisposition factors. To answer these questions animal models of alcohol addiction represent a more powerful approach [Meinhardt and Sommer, 2015]. Significantly, a very recent study carried out by Scuppa and colleagues [Scuppa et al., 2019] in our group revealed important alterations of the functional

connectivity in the insular cortex only in rats that were exposed for a prolonged period of time (8 weeks) to ethanol, and such aberrancies were at least partially reversed by a pharmaceutical treatment. This is in line with the second development of our study (Bordier et al in prep) which similarly reported a reversal of insular alterations following a prolonged period of abstinence. Indeed, in the same patients, after few more weeks of detoxification, the role of the insula appeared to be normalized, with a reduction in the participation coefficient and a lack of fragmentation of the anterior portion. Altogether, these findings appear to suggest that the altered role acquired by the insula in addiction can be a consequence of drug intoxication and possibly amenable to treatment. Yet, from the first findings reported from Naqvi and colleagues [Naqvi et al., 2007] it further appears that the role played by the insula is critical for the maintenance of addictive behaviors. Lesions of the insular cortex, indeed, suddenly block craving and cue-induced urges, suggesting that its altered function is necessary for the continuation of addiction disorders.

Now, considering all these findings, a further question arises: can we artificially manipulate the pattern of connectivity of the insular cortex? Would this manipulation reverse and normalize both functional alterations and addictive behaviors? A novel and promising approach might help us in answering these questions, relying on a magnetic stimulation of the brain cortex by means of TMS. From the observation of the critically altered role played by the insular cortex within the whole system, we could ideally evaluate how the effects of a perturbation of the network, targeting this key region, might re-shape the overall topological organization. If successful, this promising approach might represent a possible novel option for treatment of alcohol addiction, hopefully avoiding relapses and improving clinical outcomes. These questions are at the basis of the next thesis chapter. Indeed, after the promising findings reported in these described case-control studies, we aimed to evaluate whether the stimulation of the insular cortex, or the stimulation of addiction-related regions, could reverse the dramatic behavioral and functional connectivity effects of this disorder. Hence, in the next chapter I will report results from two studies, carried out in the framework of the European Sybil-AA consortium, assessing the effects of a magnetic stimulation targeting the insular cortex and the Anterior Cingulate Cortex (ACC), a region part of the salience network

and previously found to be involved in addictive disorders, in AUD patients. The results of these studies will, hopefully, help further elucidate the topological role that the insula acquires in addiction.

4 INTERVENTION STUDIES IN ALCOHOL ADDICTION BY MEANS OF DEEP TMS

The identification of key nodes involved in alcohol addiction networks can be crucial for the development of targeted treatments. With this aim, after the evaluation of altered structures in the resting state networks of alcoholic patients, we tested how focal perturbations of the system could lead to changes in alcohol use and abuse.

In the present chapter, I will describe two studies independently carried out in two different centers: at the Center for Social and Affective Neuroscience (CSAN), university of Linköping (Sweden), and at the Ben-Gurion University of Negev (Israel), respectively. These comprise two human intervention studies, with the aim to challenge resting state networks of alcohol dependent patients, by means of deep Transcranial Magnetic Stimulation (dTMS), a technique recently approved by the FDA for the treatment of depression and obsessive-compulsive disorders. These interventions targeted regions implicated in alcohol addiction: the bilateral insula, and the anterior cingulate cortex (ACC). Together, these studies will address changes in functional connectivity induced by deep rTMS, and evaluate relations of these changes with clinical outcomes. These studies are carried out in the framework of the SyBil-AA consortium ("Systems Biology of Alcohol Addiction: Modeling and validating disease state networks in human and animal brains for understanding pathophysiology and predicting outcomes and improving therapy").

4.1 INTRODUCTION

Besides being the most prevalent psychiatric disorder worldwide, Alcohol Use Disorder (AUD) is a highly heterogeneous disorder and treatment options available are currently lacking. Few medications have been made available for alcoholic

patients, however their efficacy has proven inconclusive. A number of different conditions might influence the clinical outcome in AUD patients, who repeatedly risk to fall into relapse. For example, the efficacy of specific medications seems to be related to genetic factors, duration of the period of abstinence, or age of first onset of addiction [Heilig et al., 2011]. Among these medications, two drugs currently represent a first line treatment for alcohol addiction, namely naltrexone and acamprosate. Naltrexone has been the first pharmacological treatment approved for AUD; both drugs appear to reduce alcohol craving, but the long-lasting neural adaptations induced by chronic alcohol intake seem to be difficult to reverse by means of these pharmacological treatments alone. In addition, a second line treatment for AUD includes the use of disulfiram, an inhibitor of the enymeacetaldehyde dehydrogenase enzyime. However, this drug does not reduce alcohol craving; it functions through the aversive effects that ethanol exerts over the body when taken. By blocking the enzymes responsible for ethanol degradation, disulfiram causes strong hangover symptoms in the patient, discouraging subsequent alcohol intakes. Notably, these strongly aversive effects often lead to poor compliance and discontinuation of pharmacological treatment by the patient.

The limited number of treatment options now available in clinical settings, and their low efficacy in the general patients' population, might be specifically partially due to the lack of a clear understanding of the neurobiological substrates of alcohol addiction.

In previous chapters (1,3), I extensively reviewed the main neural aberrancies most commonly reported in AUD patients, plus some of our most recent findings related to functional connectivity alterations in different samples of patients. Interestingly, brain areas more consistently related to alcohol induced alterations comprise the reward system, together with insular cortices and medial frontal regions [Dupuy and Chanraud, 2016, Camchong et al., 2013]. The identification of neural substrates that might potentially increase the propensity to relapse in patients is crucial for the advance in medication or treatment development for AUD. Ideally, we could interfere with the functional activity of these putative areas in clinical populations, with the aim to reverse the critical neuroadaptations induced by prolonged alcohol intake. Innovative and non-invasive clinical tools now offer the opportunity to alter the cortical excitability of these regions, challenging func-

tional states of the networks. Specifically, recently developed non-invasive neuromodulatory techniques, such as the Transcranial Magnetic Stimulation (TMS) have proven efficacious for the treatment of different psychiatric disorders [Fitzgerald, 2009, Trevizol et al., 2016]. This approach involves the application of a magnetic field that penetrates the skull, and, in turn, induces electric currents that can alter the underlying neuronal excitability [Cho and Strafella, 2009].

Specifically, the use of repetitive TMS can induce cortical changes in excitability, blood flow, or neurotransmitters release. Stimulation of the dorsolateral prefrontal cortex (DLPFC) appears to be effective for the treatment of drug-resistant major depression [Noda et al., 2015], and accumulating evidence now suggest its efficacy also for the treatment of addiction to different substances of abuse [Camprodon et al., 2007, Rapinesi et al., 2016]. Related to addiction, rTMS has been found to specifically alter release of dopamine [Strafella et al., 2001, Strafella et al., 2003, Cho and Strafella, 2009, Malik et al., 2018], a neurotransmitter known to be critically involved in addiction. The study from Strafella and colleagues [Strafella et al., 2001] reported increased release of dopamine in the ipsihemisphere of the TMS stimulation over the DLPFC. This further suggests the utility of neuromodulatory approaches in psychiatric conditions with dopamine dysfunctions. In line with this, the treatment of addiction can benefit from the application of non-invasive rTMS. A number of studies already tested its efficacy in AUD. However, reported findings in the literature are not always consistent across studies, and despite most applications seem to reduce immediate cravings, no real follow-ups have been recorded [Luigjes et al., 2019]. Repeated sessions of rTMS over several weeks proved to be effective in the reduction of alcohol craving [Mishra et al., 2010, De Ridder et al., 2011], but other conflicting findings report no effects on craving after single session stimulations [Herremans et al., 2012, Herremans et al., 2013]. Some evidence, moreover, report efficacy in alcohol craving reductions both after sham and active stimulations [Höppner et al., 2011, Ceccanti et al., 2015]. The different stimulation parameters, comprising current intensity as well as stimulation duration, might significantly hinder the actual effects that rTMS can exerts over AUD patients [Hone-Blanchet et al., 2015]. Specifically, the number of stimulation sessions seems to be particularly crucial, as proven by Herremans and colleagues [Herremans et al., 2015], where reductions in craving were established

only after 15 rTMS sessions. Another impacting factor relates to the use of a cue provoking paradigm, namely the exposure to drug related cue before the rTMS session (such as exposure to their favorite alcoholic drink). Studies that exploited this paradigm were, indeed, the most effective in reducing craving levels [Hone-Blanchet et al., 2015].

All the aforementioned studies picked as target of stimulation the DLPFC. This frontal region is very easy to access through TMS, and seems to be relevant for alcohol craving [Nardone et al., 2012]. However, as previously discussed, other areas are implicated in alcohol addiction, with strong functional and structural alterations, such as the insular cortex and medial frontal regions. Unfortunately, the more classic TMS figure eight coils can only provide focal stimulation of cortical surfaces. The development of more sophisticated coils, the so called H-coils, finally brought about the opportunity to reach brain structures more deeply embedded, such as the insular cortex, or the anterior cingulate cortex [Roth et al., 2002]. The H-coils can induce deeper and wider distribution of the magnetic fields. Thanks to these technical advances, the application of deep repeated TMS (deep rTMS) for the treatment of different disorders is more frequently investigated. Indeed, its application already has FDA approval for the treatment of major depression and obsessive compulsive disorder. Specific coils have been developed, targeting different neural regions deeper in the cortex. For example, by reaching the insular cortex, an H-coil has been proven to actively decrease the dopamine level in the substantia nigra and striatum, with strong implications for its possible use in the treatment of addiction [Malik et al., 2018]. A pioneering study, tested its efficacy in the reduction of cigarettes smoking and by manipulating different variables, such as stimulation intensity or cue-provoking stimuli exposure, tried to determine the optimal settings [Dinur-Klein et al., 2014]. As a result, smoking cessation, maintained for at least 12 weeks after 15 sessions of treatment, was obtained in patients that received an excitatory stimulation (10Hz), together with a cue-exposure just before the deep rTMS sessions. This further suggests that neuromodulations applied while craving can enhance the temporarily change in craving measures and reduce intake of the drug of abuse.

Deep rTMS may provide a means to target the neural substrates we have identified as involved in AUD, and to try and reverse the alterations induced by pro-

longed alcohol exposure. Through this approach, we can attempt to reduce craving levels and relapse rates in AUD. Importantly, using neuroimaging techniques we can further identify possible correlations between clinical and neuronal modifications induced by the treatment.

From this idea, in collaboration with the European consortium Sybil-AA ("Systems Biology of Alcohol Addiction: Modeling and validating disease state networks in human and animal brains for understanding pathophysiology, predicting outcomes and improving therapy") funded within the "Horizon 2020" framework, we specifically evaluated the effects that such perturbations can have on the whole functional connectivity network. Two double-blind, sham-controlled, randomized studies were carried out with identical experimental design and stimulation protocols, with the only difference laying in the area targeted by deep rTMS. A first study, carried out at the Center for Social and Affective Neuroscience (CSAN), university of Linköping (LIU, Sweden), targeted the bilateral insula. Given the strong implications, extensively reviewed, that this cortical region exerts on the mediation of drug rewards and addictive processes, its modulation could be a potential powerful therapeutic strategy to treat addiction. Furthermore, by means of deep rTMS, we may not only manipulate alter the intrinsic functional activity of the insula, but act over its entire circuit, which comprises reciprocal connection to the orbitofrontal cortex, the ACC, thalamus, amygdala, and globus pallidus, all structures importantly implicated in the addiction process.

A second study carried out at the Ben-Gurion University of Negev (BGU, Israel), targeted directly the ACC. Here, an identical protocol tested the effects of treatment sessions over frontal regions, which may play a critical role in alcohol craving, reduced inhibitory control, and relapse to alcohol use. It was, indeed, previously reported that the altered and reduced activation of the ACC in AUD patients could subsequently predict relapse. Furthermore, TMS effects over the ACC proved to be state-dependent, as the lower the baseline activity, the more TMS could increase its activity [Herremans et al., 2016].

Altogether, with these two studies we aim to evaluate the effects of interferences to nodes in then network that appear to play a key role in alcohol addiction. By artificially manipulating brain activity and perturbing the network, we seek to avoid relapse, a critical step in the addiction cycle. Furthermore, we intend to

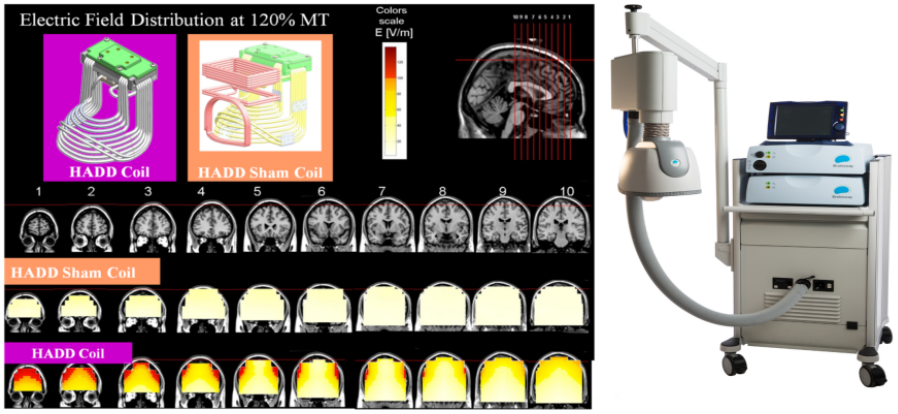

Figure 4.1: Deep TMS model developed by BrainsWay LTD. used for the BGU study

evaluate the effects over the whole network when a focal perturbation is applied to a specific set of nodes.

4.2 MATERIALS AND METHODS

4.2.1 Experimental design

The experimental design was identical for the two studies carried out in two different centers, at the Center for Social and Affective Neuroscience (CSAN), university of Linköping (LIU, Sweden), and at the Ben-Gurion University of Negev (BGU, Israel), respectively.

In both studies, patients seeking treatment were randomized into sessions of either active or sham deep rTMS treatment. Participants underwent a total of 15 rTMS sessions, over 3 weeks (5 sessions per week). High frequency stimulations of 10Hz were delivered at an intensity of 120% of the Motor Threshold (MT), as 50 trains of 30 pulses. Each train had a duration of 3 seconds, with a 20 seconds of inter-train interval, for a total of 1500 pulses delivered over approximately 20 minutes. To ensure adaptations to the repetitive stimulations, the very first two sessions had lower intensity strength, starting from 100% of the MT for the first, and 110% for the second session.

For both stimulations, deep TMS H-coils developed by the Brainsway LTD. (model 102B) were implemented. H-coils are designed to target specific brain regions. Specifically, the study carried out at LIU targeted the bilateral insula, whereas the one carried out at BGU targeted the ACC.

Immediately before and after each deep rTMS session participants filled-out craving questionnaires (Alcohol Urge Questionnaire- AUQ), to evaluate differences in craving scores induced by single treatment sessions. Before undergoing deep rTMS, patients were also exposed to alcohol, by sniffing their favorite drink for two minutes. Exposure to the substance of abuse just before treatment has been proved to increase effectiveness in the reduction of craving induced by stimulation [Dinur-Klein et al., 2014].

In addition to the 3 weeks of dTMS treatment, all participants underwent two MRI sessions, one before the beginning of the treatment period, and a second one at the end of the stimulation sessions.

To evaluate clinical outcomes, patients were followed-up for a total of 12 weeks after the end of the treatment, specifically at 2, 4, 8, and 12 weeks after completion.

Here, both self-reports of heavy drinking days and biomarkers of alcohol use were collected.

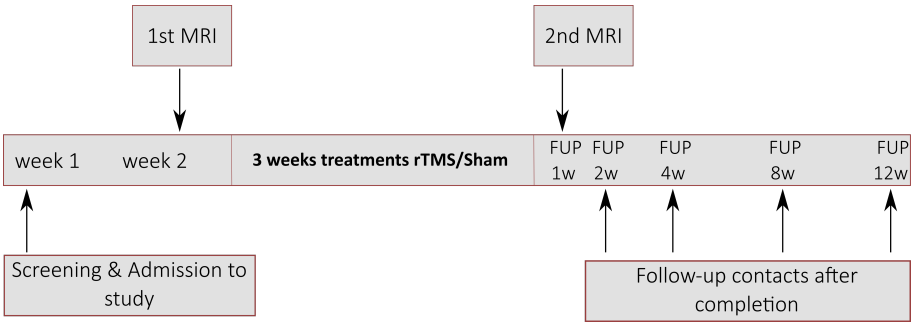

Figure 4.2: Experimental design of the two dTMS studies, carried out over approx. 5 months

4.2.2 Participants and clinical measures

Participants were recruited through local clinics, flyers, and advertisements on the local media, and consisted in patients voluntarily seeking treatment for alcohol use disorder. Exclusion criteria for the admission to the study comprised: MR incompatibility (presence of pacemakers or iron plaques), history of neurological disorders, pregnancy, TMS incompatibility (history of seizures).

Details of the groups recruited at the two sites are reported below. Shortly, for the study carried out at LIU, 50 participants were recruited and screened. Among these, only 41 patients completed all the treatment sessions (mean age 51.7±9.1, 6 females). At BGU, 61 participants were recruited and screened, 51 completed all the deep rTMS treatment sessions (mean age 41±9.8, 15 females).

At first admission, patients were screened for disorder severity, craving, and alcohol consumption. Questionnaires common to both centers included: AUDIT scores and Alcohol Dependence Scale (ADS) for the evaluation of disorder severity before and after the three weeks of treatment, and during follow-up weeks; Penn Alcohol Craving Scale (PACS) at first screening, after the completion of every week of treatment, and at the follow-up weeks.

LIU study also comprised the collection of urine samples, every week for the whole duration of the experimental study, to assess the level of Phosphatidylethanol (Peth), a biomarker for ethanol presence in the body.

All clinical measures were evaluated for changes induced by treatment and over time by mans of repeated measures ANOVAs.

To be admitted to the TMS session, patients were required to be sober. Soberness was estimated through a breathalyzer test. Total abstinence was not required during the entire experimental period. Participants were excluded from the study if: so requested; did no longer meet eligible criteria despite a positive initial screening; did not comply with instructions of treatment staff; were intoxicated by alcohol; developed serious alcohol withdrawal complications (seizures, delirium tremens, anxiety, etc...); became or were found pregnant; showed emergence or worsening of psychiatric symptoms.

4.2.3 MR data acquisition

Imaging parameters were identical for the two studies. At the LIU center, MR images were acquired with a Philips Ingenia 3 Tesla scanner (Philips Healthcare, Best, The Netherlands).

First, a high resolution 3D T1-weighted scan was acquired, with TS=7ms, TE=3.2ms, flip angle=8°, FOV=256x240x170, voxel resolution=1x1x1mm, no slice gap, for a total scantime of 5min and 34sec. Functional resting-state images were acquired with an Echo-Planar Imaging (EPI) sequence. Six dummy volumes were firstly acquired to allow the spin system to reach steady-state longitudinal magnetization and reduce effects of partial saturation. The EPI sequence consisted in: TR=2s, TE=30ms, flip angle=77°, FOV=220x220, in-plane resolution=3.4x3.4, slice thickness=4mm, no slice gap, number of axial slices=32. Functional runs had duration of approximately 12 minutes, for a total of 353 volumes acquired. Before the resting-state images acquisition, participants were asked to perform specific behavioral tasks, while laying in the MR scanner, which are not going to be reported here.

4.2.4 Image preprocessing

Imaging data were preprocessed using SPM12 (Wellcome Trust Center for Neuroimaging, London, UK). Functional volumes were corrected for slice-timing, re-

aligned, normalized to the standard MNI EPI template, and co-registered to the high-resolution image. Structural images were normalized to standard MNI template and segmented, in order to extract subject-specific white matter and CSF masks. Effects of motion were assessed on all scans, by means of Framewise Displacement (FD) and DVARS, computed following Power [Power et al., 2012]. Resting-state volumes were corrected for motion and physiological noise through a method based on principal components analysis, namely aCompCor. The first five principal components from WM and CSF, together with the six standard movement parameters extracted by SPM, were regressed out from the timeseries. A butterworth band-pass filter of 0.01-0.1 Hz was applied to both regressors and timeseries.

4.2.5 Functional connectivity graphs

Functional connectivity graphs were generated in the same way as described in the previous chapters. We parceled the preprocessed data into 638 nodes, following the functional template generated in Crossley [Crossley et al., 2013]. Connectivity matrices for each patient, pre and post rTMS, were generated by means of inter-regional pairwise correlation (based on Pearson coefficient). Following, correlation coefficients were z-Fisher transformed to ensure comparability across individuals. We then computed pre and post-treatment group matrices (Sham vs rTMS) by averaging each individual's adjacency matrix. Finally, to ensure maximization of community detection, we thresholded group matrices through a percolation approach, retaining all the strongest edges that would ensure full connectedness of the matrices, as previously discussed.

4.2.6 Modular organization and graph metrics

As described in the previous studies, we compared modular architectures across deep rTMS conditions as well as before and after stimulation. Modular organization was detected at the group level though the consensus approach of InfoMap, and computed with the igraph-0.7.1 package.

Global and local graph topological metrics were subsequently computed from single-subject sparse adjacency matrices. At the global level, we addressed overall functional connectivity, global efficiency, and matrix density after percolation (as described in previous chapters 2,3). Next, at the local level of every single node, we computed degree centrality, strength centrality, and local efficiency. Related to the modular architecture, at the nodal level, we evaluated participation coefficient, to detect nodes playing more central roles within the global organization. All topological metrics were evaluated by means of paired t-test, to assess within-subjects changes before and after treatment, and through simple 2 tailed t-tests. Furthermore, given the application of a percolation procedure to sparsify individual matrices, which might lead to different edge density across subjects, all statistical tests were carried-out by co-varying for individual matrix density, using analysis of covariance (ANCOVA). Statistical significance of topological metrics, addressing all 638 nodes at the local level was evaluated by means of non-parametric permutations. All reported results are corrected for multiple comparison correction (false discovery rate, [Genovese et al., 2002]). As in the aforementioned studies, all graph topological metrics were computed with the Brain Connectivity Toolbox (BCT).

Furthermore, to estimate functional connectivity changes induced by the treatment, we exploited the Network Based Statistics (NBS) toolbox [Zalesky et al., 2010a]. This toolbox allows to run non-parametric testing over all links in the graph to evaluate statistical differences between groups overcoming the multiple comparison correction problem. We applied paired t-tests to question within-subjects changes in pre and post-stimulations.

4.3 RESULTS LIU STUDY

4.3.1 Clinical data

For the purpose of this study, 50 patients were recruited, only 41 successfully completed all the treatment sessions (mean age 51.7±9). Out of these participants, 20 patients (mean age 50.55±10; 17M/3F) were randomly assigned to the active TMS treatment, and 21 patients (mean age 53.1±7; 17M/4F) to the sham control

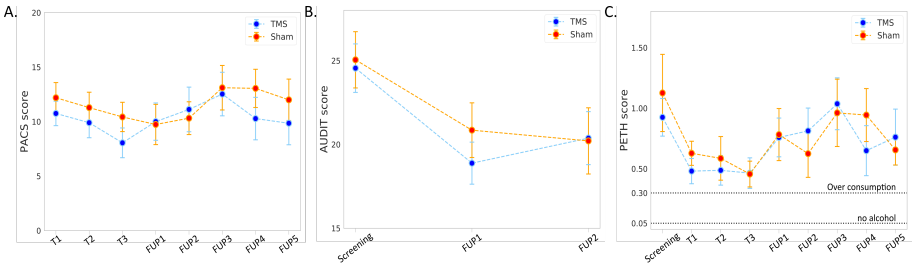

Figure 4.3: Panel A shows scores of PACS during the three treatment weeks and during 5 weeks of follow-up. Panel B shows AUDIT scores evaluated at screening and for the first two follow-up weeks. Panel C shows Peth level measured every week, from screening to follow-up.

condition. The two groups were matched for age (t=0.894, p=0.37) and gender (χ=0.119, p=0.731). Two participants from the TMS condition were subsequently discarded from the analysis due to motion in the MRI sessions (mean FD>0.5mm).

We first evaluated effects of treatment by means of self-reported questionnaires. No treatment effects could be observed in neither PACS nor AUDIT scores. However, significant effects of time could be observed during the treatment period (3 weeks) in PACS scores [$F(1,2)$=5.042, p = 0.009, η^2=0.012]. In contrast, a non-significant increase in scores was found during follow-up [$F(1,4)$=2.156, p=0.079, η^2=0.07]. A strong reduction in AUDIT scores, assessing alcohol consumption and drinking-behaviors, was found for both groups after treatment [$F(1,2)$=37.541, p<0.001, η^2=0.556]. Similar trend was observed when evaluating the presence of ethanol in the body. Peth levels, indeed, did not show any difference across TMS and sham conditions, however an effect of time is found during the three weeks of treatment [$F(1,3)$=17.778, p<0.001, η^2=0.331]. No significant effect was observed during follow-up weeks, where Peth levels increased [$F(1,4)$=1.227, p=0.305, η^2=0.05]. Course of these effects are depicted in figure 4.3.

4.3.2 Effects of TMS on global functional connectivity

To evaluate the effects of deep rTMS of bilateral insula on functional connectivity we ran paired tests between follow-up and pre-treatment conditions, for both sham and active TMS treatments. No differences in the overall functional connectivity were highlighted at the individual level after sham condition, as measured by means of paired t-tests (t=-1.58, p=0.12). No significant differences could be

appreciated either after the active TMS treatment, despite the presence of a tendency in reduced overall functional connectivity (t=1.69, p=0.09). The histograms in figure 4.4 show the group-average edge-weight distribution for both follow-ups when compared to baseline. Considered the well-known, and already discussed, effects that head movements can exert over functional connectivity, we evaluated motion for the experimental groups. No significant differences were observed by Framewise Displacement across groups (pre-sham vs post-sham: t=-1.02, p=0.31; pre-tms vs post-tms: t=0.007, p=0.99).

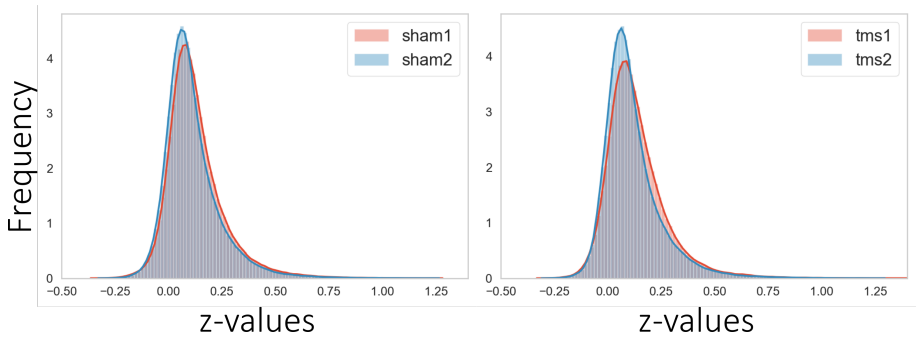

Figure 4.4: Edge-weight distribution for the group-average functional connectivity matrices, comparing follow-up sessions to their respective baseline conditions.

In order to compute subsequent graph topological metrics at the individual level we applied a thresholding procedure based on a percolation approach. The resulting sparse matrices did not reveal differences in edge density across conditions (sham pre vs sham post: t=0.63, p=0.53; tms pre vs tms post: t=1.05, p=0.31). Yet, given that many graph topological metrics can be influenced by different density, in all following tests we used individual density values as a covariate variable.

A similar pattern was observed for global efficiency. No significant differences were identified before and after treatments, but a non-significant trend of reduced global efficiency was present after treatments, predominantly in the active TMS condition (pre-sham vs. post-sham: F=-1.63, p=0.11; pre-tms vs post-tms: F=-1.88, p=0.06).

Details related to the means and standard deviations for all the investigated topological metrics are reported in table 4.1.

	FD (mm)		Functional Connectivity (FC)		Density		Global Efficiency (GE)	
Pre-TMS	0.25±0.1	*t=0.007,*	0.26±0.08	*t=1.69,*	0.14±0.06	*t=0.63,*	0.29±0.05	*F=-1.88,*
Post-TMS	0.25±0.09	*p=0.99*	0.22±0.03	*p=0.09*	0.13±0.06	*p=0.52*	0.26±0.03	*p=0.069*
Pre-Sham	0.21±0.07	*t=-1.024,*	0.25±0.08	*t=-1.582,*	0.13±0.04	*t=1.05,*	0.29±0.05	*F=-1.63,*
Post-Sham	0.24±0.08	*P=0.31*	0.22±0.02	*p=0.12*	0.12±0.03	*p=0.31*	0.26±0.02	*p=0.11*

Table 4.1: Global functional connectivity metrics

4.3.3 Effects of TMS on local functional connectivity

The edge-wise investigation of functional connectivity changes investigated by means of NBS did not reveal any significantly different link, in any direction. Following, we evaluated effects of the treatment on local topological metrics by means of non-parametric paired tests, covaried by density, for all the 638 nodes, and run over 5000 permutations. Thus, all the significant results reported are corrected for multiple comparison correction.

First, we addressed changes in binary degree centrality. A pattern of reduction and increase in degree centrality was present in both sham and TMS conditions before and after treatment. In total, 17 nodes showed reduced degree centrality after both sham and active TMS treatments, comprising mostly right precuneus and postcentral gyrus, hippocampus (right and left), and calcarine regions. In contrast, frontal superior regions, the caudate, and the thalamus presented higher degree centrality after sham stimulation. Active TMS caused an increase in binary degree in 13 nodes, comprising inferior and medial frontal cortices, left angular gyrus, and right inferior parietal cortex.

In line with the reduction of degree centrality in posterior regions, node strength appeared decreased in precuneus and postcentral gyrus, calcarine regions and hippocampus after sham. Conversely, no increase in strength was detected. A very similar pattern was present for the active TMS condition. After treatment, a reduction in nodal strength was present in posterior regions, comprising precentral gyrus, precuneus and postcentral gyrus, calcarine regions, and cuneus.

The pattern of reduction in functional connectivity observed in posterior regions after three weeks of treatment is present also when evaluating local efficiency. In both sham and active TMS conditions, a decrease in nodal efficiency is found

in the precentral gyrus, posterior cingulate, occipital medial regions, and in the supplementary motor area.

4.3.4 Effects of TMS on modular architecture

To assess the overall changes in functional organization induced by TMS at the global level, we investigated the modular structure before and after treatments. First, we checked possible differences at the individual level related to Q modularity, measured with the community Louvain algorithm. Specifically, no differences were present in Q values, co-varied for density, across conditions (pre-tms vs post-tms: F=-0.133, p=0.91; pre-sham vs post-sham: F=0.08, p=0.92). Following, modular organization was generated both at the group and at the individual levels by means of an InfoMap consensus approach. At the group level, we did not observe important differences between conditions. Before treatment the number of communities identified was very similar between sham and active TMS (pre-TMS: 23 modules, ranging from 92 to 4 nodes; pre-sham: 24 modules, ranging from 90 to 2 nodes), whereas at follow-up, we appreciated a reduction in the number of modules detected (post-TMS: 18 modules, ranging from 91 to 8 nodes; post-Sham: 20 modules, ranging from 86 to 7 nodes). However, at the individual level, the number of modules between conditions was not statistically different (pre-tms vs post-tms: t=1.15, p=0.26; pre-sham vs post-sham: t=-0.72, p=0.46).

At the global level, we appreciated specific re-organizations of the modular structure of basal ganglia after sham and active TMS treatments, whereas a re-organization of frontal regions was present only after active TMS treatment (figure 4.5). To evaluate significance of this reorganization, we compared the number of modules belonging to these structures across all individuals' modular partitions. In more detail, for every participant, we extracted modules from basal and superior frontal structures, and compared the number of communities across conditions. The re-organization identified in the basal ganglia appeared statistically significant only after the active TMS treatment (pre-tms vs post-tms: t=2.043, p=0.005; pre-sham vs post-sham: t=-0.476, p=0.61). In contrast, re-organization of superior frontal regions was not significant (pre-tms vs post-tms: tt=1.868, p=0.07; pre-sham vs post-sham: t=1.14, p=0.26).

From each individual partition, we subsequently extracted participation coefficient information for all nodes. At the nodal level, we did not find statistical differences in terms of inter-community participation coefficient for any condition.

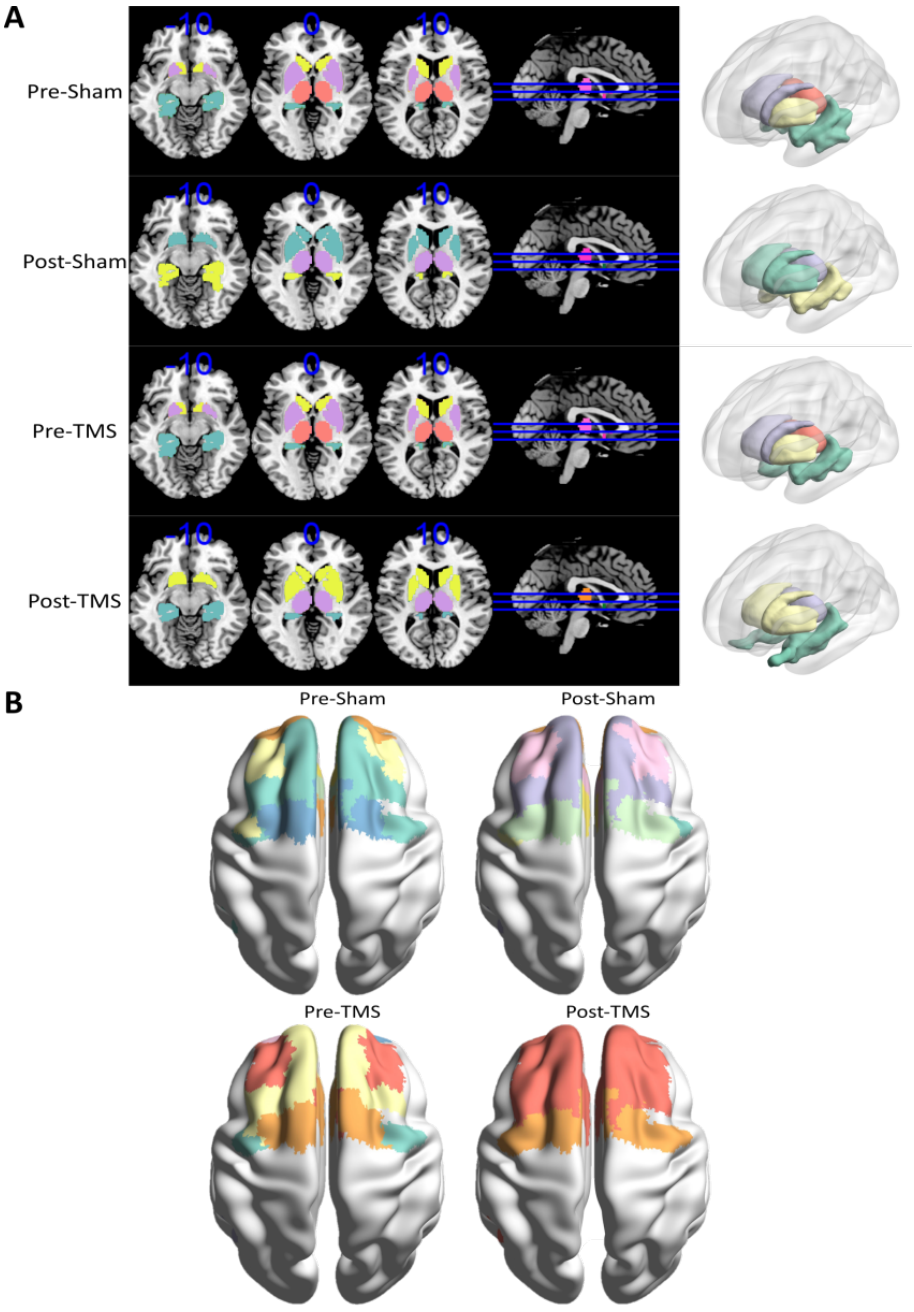

Figure 4.5: Panel A shows modular re-organization of the basal ganglia structures after both treatments. Panel B shows modular re-organization in frontal regions

4.3.5 Effects of TMS on insular connectivity

To evaluate the efficacy of the TMS stimulation over the bilateral insular, we separately evaluated, through post-hoc and hypothesis-driven analysis, degree centrality, strength, local efficiency, and density of insular connections. No differences were reported in any local topological metric across conditions. Related to the modular organization of the insular cortex, one node from the left and right anterior insula were separated in all conditions.

4.3.6 Correlation with clinical variables

After completion of the analysis of functional connectivity changes induced by deep rTMS, we further addressed relations between clinical measures and global functional metrics. For this purpose we conducted partial correlations, co-varying for density.

No relation between global topological metrics (global efficiency, functional connectivity, Q scores) was found at baseline with clinical measures (AUDIT, ADS, PACS). Interestingly, baseline PACS scores, a measure of craving, correlated with global metrics at follow-up, namely with global efficiency (r=-0.403, p=0.01) and with overall functional connectivity (r=-0.463, p=0.004). We further tested possible relations between changes in functional connectivity or global efficiency and changes in craving. The difference between global metrics at follow-up and at baseline did not show any significant correlation with the difference of craving scores at the end of the treatment and at screening. No correlations were identified with clinical variables collected after treatment (Figure 4.6).

Furthermore, we evaluated edge-wise correlations with clinical variables, to identify sub-networks within the system that could possibly be related to clinical response. To this end, we tested for correlations by means of the Network-Based Statistics (NBS; [Zalesky et al., 2010a] toolbox, a precious tool allowing to test all edges in the network with non-paramatric tests. Specifically, we tested for correlations of all functional connectivity links, at the individual level, with clinical variables conducting 5000 non-parametric permutations co-varied with density. No

significant sub-network was found to correlate with either craving scores (PACS) nor severity of the disorder (ADS) at baseline or follow-up.

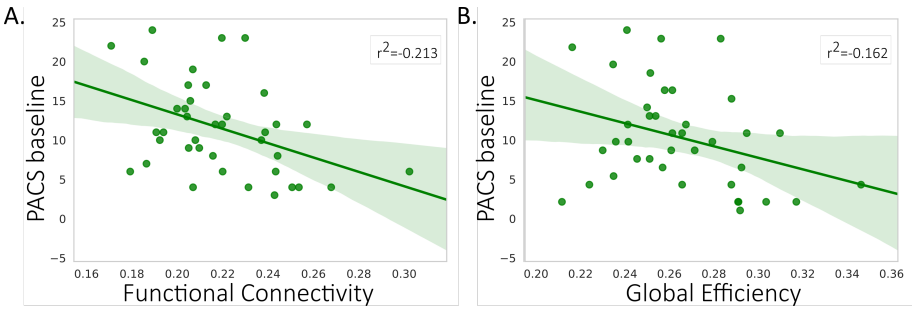

Figure 4.6: Plots showing correlation between PACS at baseline and global metrics at follow-up. Panel A represents correlation between PACS scores and overall functional connectivity (r=-0.463, p=0.004). Panel B shows correlation between PACS and global efficiency (r=-0.403, p=0.01).

4.4 RESULTS BGU STUDY

4.4.1 Clinical Data

At the Israeli research center, 51 participants were recruited for this study. Among these patients only 44 completed the treatment and were randomly assigned to either TMS condition (23 AUD patients, mean age 43±9; 15M/8F) or Sham (21 AUD patients, mean age 41±10; 14M/8F). The two groups were matched for age (t=0.465, p=0.647) and gender (χ=0.01, p=0.917). For the functional imaging analysis two participants from the TMS condition and 4 from sham were discarded due to excessive motion (mean FD>0.5mm).

Only self-reported questionnaires were available for this dataset. Only self-report questionnaires were available for this dataset. Effects of treatment and time were evaluated by means of PACS and AUDIT scores with repeated measures ANOVA. As we can observe from the plot in panel A of figure 4.7, a strong reduction in craving levels, measured by means of PACS scores, is present in both treatment groups. This strong effect of time is strongly significant in both conditions from baseline to the final week of treatment (TMS: [$F(1,21)$=62.036, p<0.0001, η^2=0.74]; Sham: [$F(1,21)$=17.018, p<0.0001, η^2=0.44]). We further observed an interaction between stimulation and time during the three weeks of

treatment [$F(2,84)=3.641$, $p=0.041$, $\eta^2=\eta^2=0.08$]. Examining the two groups separately, we observe a significant reduction of PACS scores during the three weeks of treatment in the TMS group [$F(2,42)=4.003$, $p=0.04$,$\eta^2=0.16$], which is not present in the sham condition [$F(2,42)=0.288$, $p=0.751$,$\eta^2=0.01$]. At follow-up, TMS treatment shows a not-significant trend of increased craving [$F(4,68)=2.598$, $p=0.095$,$\eta^2=0.13$]. Opposite, this trend in increased PACS scores appears significant during the follow-up period in the sham condition [$F(4,64)=4.547$, $p=0.01$,$\eta^2=0.22$].

Clinical results are represented in figure 4.7.

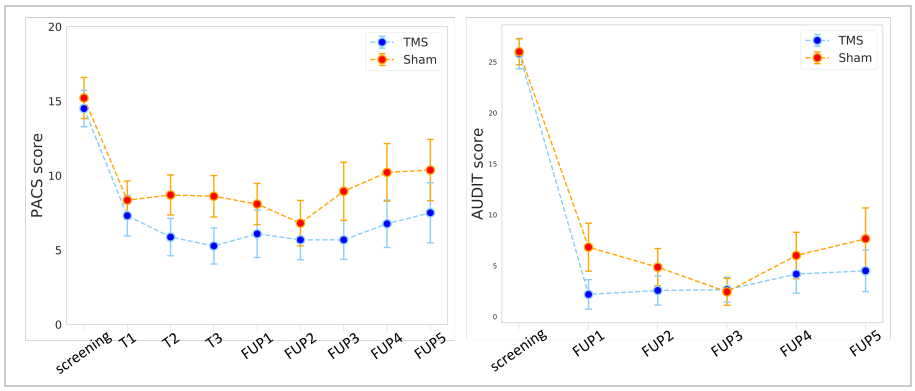

Figure 4.7: Panel A shows PACS craving scores during treatment and at follow-up. Panel B shows AUDIT scores at screening and after treatment.

4.4.2 Effects of TMS on global functional connectivity

Similar to the previous study we evaluated the effects of deep TMS over global functional connectivity measures by means of paired tests between follow-up and pre-treatment conditions. No significant differences were present after either TMS or Sham in overall functional connectivity strength (pre-tms vs. post-tms: $t=0.04$, $p=0.96$; pre-sham vs. post-sham: $t=0.24$, $p=0.8$). Histograms in figure 4.8 show the group-average edge-weight distribution for both conditions at follow-up as compared to the baseline groups. To ensure that the overall functional connectivity at the subjects' level was not influenced by the presence of head movements, we tested whether the groups moved differently as measured by FD. No differences across any condition were present in terms of motion (pre-tms vs. post-tms: $t=0.33$, $p=0.73$; pre-sham vs post-sham: $t=0.03$, $p=0.26$).

	FD (mm)		Functional Connectivity (FC)		Density		Global Efficiency (GE)	
Pre-TMS	0.23±0.07	*t=0.33,*	0.25±0.03	*t=0.04,*	0.18±0.05	*t=0.3,*	0.29±0.03	*F=0.012,*
Post-TMS	0.24±0.08	*p=0.87*	0.25±0.03	*p=0.96*	0.18±0.06	*p=0.76*	0.29±0.03	*p=0.99*
Pre-Sham	0.26±0.1	*t=0.03,*	0.24±0.05	*t=0.24,*	0.16±0.07	*t=0.409,*	0.29±0.03	*F=0.239,*
Post-Sham	0.27±0.08	*P=0.96*	0.24±0.05	*p=0.8*	0.17±0.08	*p=0.8*	0.29±0.04	*p=0.81*

Table 4.2: Global functional connectivity metrics

As already discussed in the previous studies, we applied a thresholding procedure based on percolation as to obtain graphs both at the group and at the individual level. No differences were found in edge density across conditions at the individual level (pre-tms vs. post-tms: t=0.3, p=0.76; pre-sham vs post-sham: t=0.409, p=0.76). To ensure comparability across conditions when evaluating topological metrics at the individual level we used density values as a covariate variable.

Differences in global efficiency were measured in thresholded graphs, covarying for density. As observed with the overall functional connectivity strength, no differences were found across conditions in global efficiency (pre-tms vs. post-tms: F=0.012, p=0.99; pre-sham vs. post-sham: F=0.239, p=0.81). Details related to the global topological metrics are described in table 4.2.

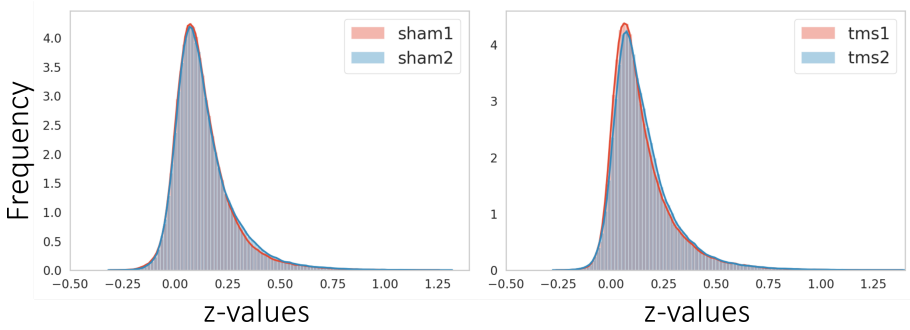

Figure 4.8: Edge-weight distribution for the group-average functional connectivity matrices, comparing follow-ups sessions to their baseline conditions.

4.4.3 Effects of TMS on local functional connectivity

As addressed in the LIU study, we evaluated treatment effects over local topological metrics by means of non-parametric paired tests, covaried by density, for all

638 nodes, over 5000 permutations. Thus, only results significant after multiple comparison correction are reported here.

We tested differences induced by treatment in degree centrality and nodal strength. Here, we could only identify a reduction in both binary and weighted degree after treatment with a sham condition in 10 nodes, surviving FDR correction (t>2.5), involving occipital regions (bilateral lingual gyrus, bilateral medial occipital cortex, and bilateral calcarine sulcus). No changes surviving multiple comparison correction are present after the real TMS condition for any node. Similarly, we did not identify changes in the nodal local efficiency for neither sham nor TMS groups.

4.4.4 Effects of TMS on modular architecture

For the evaluation of changes induced by three weeks of deep rTMS treatment at a global scale we further assessed the modular architecture in all conditions. First, we looked for differences at the individual level in modularity measured with Q scores extracted by means of the community Louvain algorithm. No changes are present for Q values, when co-varying for density, after active TMS (F=0.766, p=0.448) or after sham (F=0.659, p=0.514). To further evaluate the overall communities' organization we detected the modular architecture by means of InfoMap with a consensus approach, both at the group and at the individual level. At the group level no important differences were found when comparing follow-up conditions to their baseline. For the TMS condition, 15 modules were identified before treatment, with modules size ranging from 178 to 5 nodes. Similar, after active TMS treatment 15 modules are found, ranging from 179 to 4 nodes. A greater number of modules is detected in the sham condition before treatment (18 communities, ranging from 143 to 3 nodes), and after treatment (20 communities, ranging from 158 to 3 nodes). The modular architecture was overall highly similar among all conditions (figure 4.9). In line with this, no differences in the number of modules detected at the individual level are present (pre-tms vs- post-tms: p=0.24; pre-sham vs. post-sham: p=0.41). Opposite to what observed in the LIU dataset, frontal regions showed very similar organization in all conditions, with 3 to 4 communities. Sub-cortical structures were identical before both active and sham treatments, with important fragmentations of the basal ganglia. Pallidum and

putamen structures are found to be always part of one single module, whereas thalamus, caudate, and hippocampus are separated into different communities in all conditions.

From the global functional architecture we could detect changes in the different roles played by nodes within the whole network by measuring participation coefficient at the individual level. Here, we could only detect few significant changes surviving FDR, mostly showing a reduction in the participation coefficient in specific nodes after active TMS. Specifically, only three nodes comprising the right caudate and right hippocampus shows a reduction in participation coefficient after active TMS.

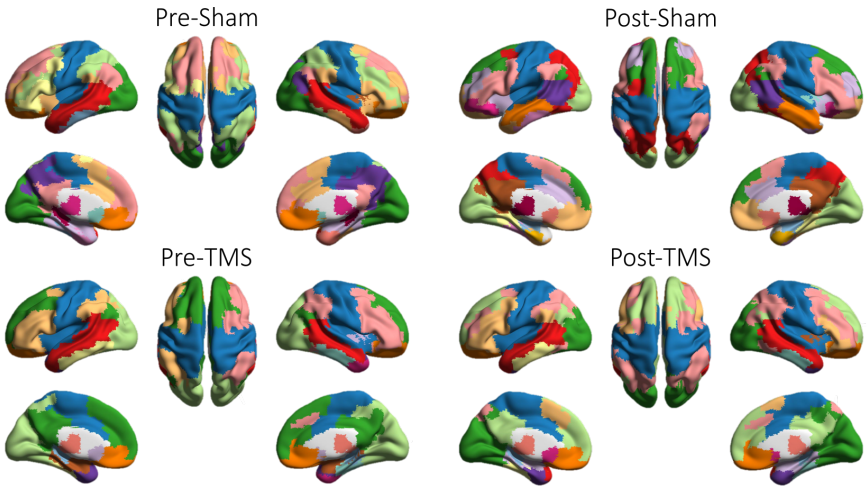

Figure 4.9: Modular architecture detected with InfoMap for all conditions before and after deep rTMS treatment.

4.4.5 Effects of TMS on insular and ACC connectivity

This study aimed to target the anterior cingulate cortex by means of deep rTMS. As reviewed, the ACC is part of the salience network, strongly connected to the insular cortex, a central hub in addiction. Thus, we further evaluated changes in the ACC and in the insular connectivity following treatment as a post-hoc data-driven analysis. No differences could be identified in any local topological metrics in either the insular cortex nor in the ACC after sham or TMS treatments.

Related to the modular organization of the insular cortex, we observe a fragmentation of the anterior insular from its posterior portion only in the sham conditions

(both pre and post). In the active TMS group, all nodes of the insula fall within the same community, together with somatosensory cortices.

4.4.6 Correlations with clinical data

Following the analysis of the functional connectivity topological organization from a local to a global scale, we evaluated possible correlations between clinical variables (AUDIT, PACS, ADS) and global metrics (global efficiency, functional connectivity, and Q values). Given the dependency of these metrics on graph sparsity, we ran partial correlations co-varied for density.

Interestingly, PACS scores, measuring craving, negatively correlated with the global efficiency (r=-0.403, p=0.004) and functional connectivity at baseline (r=-0.354, p=0.013). Furthermore, global efficiency was found to negative correlate with ADS, scores reflecting the severity of alcohol dependence (r=-0.435, p=0.004). ADS scores strongly correlated also with the overall functional connectivity at baseline (r=-0.438, p=0.004; figure 4.10). No correlations were identified with AUDIT scores and topological measures at baseline. Interestingly, at follow-up, only functional connectivity and global efficiency for the real TMS treated group negatively correlated with PACS scores collected at the end of the last week of treatment (r=-0.5, p=0.03 and r=-0.479, p=0.04, respectively).

We further tested the presence of correlations between the change in functional connectivity and efficiency at follow-up compared to their baselines with the change in craving scores at the end of the treatment and at screening. In line with the relation present between global metrics and craving at follow-up in the real TMS condition, a significant correlation was present only between the change in functional connectivity (δ_{FC}) and global efficiency (δ_{GE}) with the change in craving for the TMS treated group (tms δ_{FC}: r=-0.551, p=0.015; TMS δ_{GE}: r=-0.574, p=0.01; Sham δ_{FC}: r=-0.078, p=0.79; Sham δ_{GE}: r=-0.165, p=0.574; figure 4.11).

Following, we evaluated correlations between all functional edges and clinical variables by means of 5000 non-parametric permutations conducted with the NBS toolbox. Here, we revealed a correlation between functional connectivity matrices at the individual level and PACS scores at baseline (t=3.1, p=0.049, figure 4.12). The sub-network identified comprised 372 functional links, including widespread

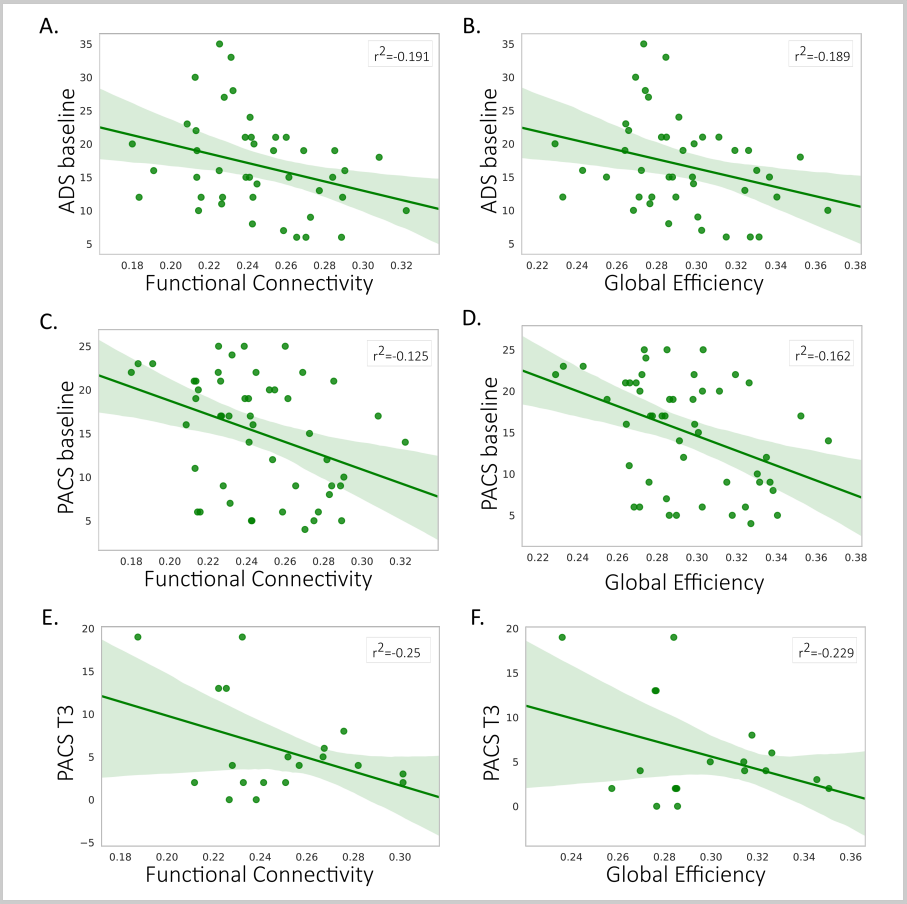

Figure 4.10: Plots showing identified correlations between clinical measures and global metrics at baseline. Panel A shows correlation between global functional connectivity and ADS scores at baseline (r=-0.435, p=0.004**). Panel B represents correlation between global efficiency and ADS (r=-0.438, p=0.004**). Panels C and D show correlation between topological metrics and craving PACS scores (global efficiency: r=-0.403, p=0.004**; functional connectivity: r=-0.354, p=0.013). Panels E and F show correlations identified for the real TMS treatment group at follow-up between craving scores at the third week of treatment with functional connectivity (r=-0.5, p=0.03) and global efficiency (r=-0.479, p=0.04). ** indicates tests surviving Bonferroni correction.

cortico-cortical connections. In detail, highest significances are found in interhemispheric frontal connections . In contrast, no relation was found between functional connectivity at follow-up and clinical variables, neither at baseline nor during follow-up.

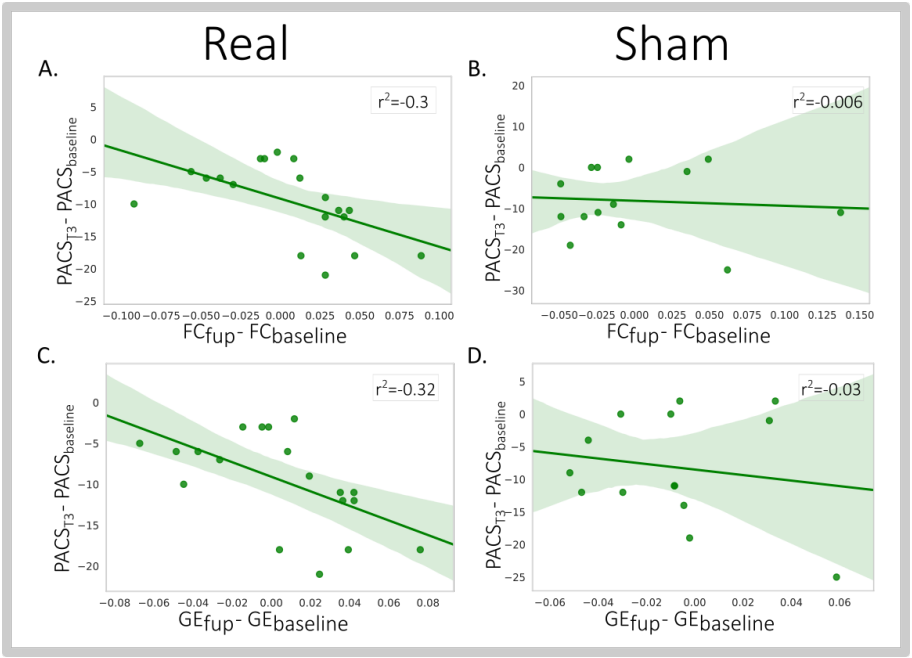

Figure 4.11: Correlations changes in connectivity and craving for active TMS and sham. Panels A and C show correlation between the change in global metrics (functional connectivity and global efficiency, respectively; follow-up minus baseline) and the changes in craving scores (PACS at T_3 minus PACS at screening). Significant relations are found only for the active TMS treated group δ_{FC}: r=-0.551, p=0.015; δ_{GE}: r=-0.574, p=0.01). Panels B and D show the same relations but investigated in the sham group (δ_{FC}: r=-0.078, p=0.79; Sham δ_{GE}: r=-0.165, p=0.574).

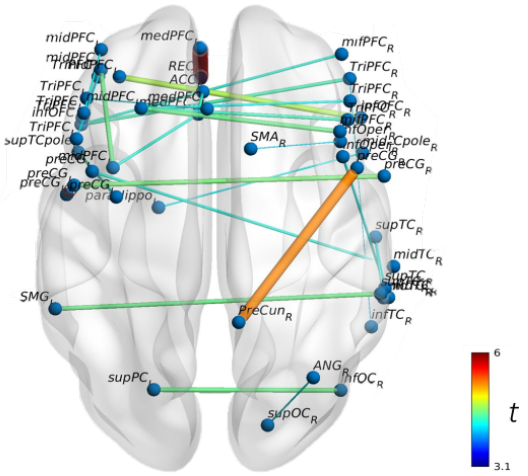

Figure 4.12: Graphical representation mapped on the brain surface of the strongest functional connections correlating with craving scores at baseline. Statistical measures are computed by means of partial correlations co-varied for density.

4.5 DISCUSSION

The aim of these two studies, carried out with an identical design but in different research centers, was to evaluate the efficacy of a possible novel treatment for alcohol dependence disorder, targeting specific regions involved in addiction. The first study performed at the University of Linköping in Sweden (LIU), aimed to target the bilateral insula, a cortical region crucial in craving and addictive behaviors [Naqvi and Bechara, 2009, Naqvi and Bechara, 2010]. In contrast, the second study, developed at the Ben-Gurion University in Israel (BGU), employed a TMS coil targeting the anterior cingulate cortex (ACC), key part of the salience network fundamental in the top-down control of conscious behaviors, such as drug urges. Interestingly, only one of the two studies here evaluated revealed a significant treatment effect. Indeed, it appears evident that the stimulation of the ACC, as assessed at BGU, reduces craving to a greater and significant extent after a protracted treatment with an active deep rTMS stimulation. Reductions in both craving and disorder severity scores (measured by means of PACS and AUDIT, respectively) are evident as an effect of time in both treatment groups. Indeed, we clearly observed a strong and significant reduction during treatment, as compared to the baseline self-reports. Yet, this reduction is more significantly prominent in the active TMS condition, reflecting potential efficacy of this treatment in modulating alcohol craving, one of the most dramatic factors inducing patients towards subsequent relapse. Importantly, this effect appeared to be present, to a lesser extent, also after three months, in contrast to patients assigned to the sham condition who show increasing patterns of craving at a much faster rate during the follow-up period.

Conversely, we could not demonstrate any clinical effect of this novel treatment in the first study here evaluated, where the bilateral insular cortex was targeted with deep rTMS. Indeed, in the LIU study we revealed a general reduction in all clinical variables, comprising craving scores (PACS) and alcohol disorder severity scales (AUDIT), regardless of the treatment condition. In details, patients were asked to try and remain abstinent during the three weeks of treatment, still they would not have been excluded from the trial if found drinking small amounts of alcohol. As proved by the presence of ethanol in urine samples collected in the LIU

study, patients assigned to both the active TMS and the sham conditions strongly reduced their alcohol intakes during the three weeks when they daily went to the clinic to receive deep rTMS treatment. However, ethanol concentrations appear to increase, in both conditions, just after the end of the trial, when they were not supposed to be present daily in a hospital setting. This is similarly observed in patients recruited at the BGU center, where craving and severity scores appear to increase (not statistically significant) during follow-up weeks. Altogether, this specific clinical results seems to suggest a placebo effect induced by the clinical setting where patients were supposed to go to every day for the duration of the treatment.

Repeated Transcranial Magnetic Stimulation represents a novel and promising technique to treat several psychiatric disorders, including depression, obsessive-compulsive disorders, and perhaps addiction [Fitzgerald, 2009, Trevizol et al., 2016]. To date, only a few studies have investigated the effects of rTMS in reducing craving symptoms in AUD patients, reporting contrasting results. Importantly, all these studies targeted left or right dorsolateral prefrontal cortex (DLPFC; [Mishra et al., 2010, Herremans et al., 2012, Höppner et al., 2011, Herremans et al., 2015, Mishra et al., 2015]). In details, findings reported from these previous studies suggest that one single session of rTMS does not show efficacy in reducing craving scores [Höppner et al., 2011, Herremans et al., 2012], and a trend towards reduction appears from both active and sham stimulations. In contrast, successful reduction of craving is prominent only after at least 10-15 treatment sessions [Mishra et al., 2010, Mishra et al., 2015, Herremans et al., 2015]. These three studies reported, indeed, an amelioration of addictive behaviors. However, only the first study from Mishra and colleagues [Mishra et al., 2010] also included a sham-controlled group which did not reveal significant reductions in craving after 10 rTMS stimulation sessions. Efficacy of the treatment is further reported after 10 [Mishra et al., 2015] and 15 sessions [Herremans et al., 2015], as measured by a decrease in self-reported craving scores by AUD patients. Yet, these two studies did not include a sham-control group.

All previous studies, studies stimulated the right or left DLPFC. The choice of stimulation of this frontal cortical region is related to several factors, among these the ease in reaching it with conventional rTMS coils, and the accumulating

evidence of its efficacy for the treatment of other psychiatric disorders such as depression [Loo and Mitchell, 2005]. Moreover, it was proven that the repeated stimulation of the frontal cortex has modulatory effects over the dopaminergic system, facilitating the release of dopamine [Strafella et al., 2001]. For this reason, the stimulation of this region in disorders showing alteration in the dopaminergic system, such as addiction, appears promising. Interestingly, a pilot study employing a deep TMS over the DLPFC in AUD patients reported a significant reduction in the dopamine transporter availability in caudate and putamen only after active TMS treatment as compared to sham [Addolorato et al., 2017]. No effects on craving measures were present; however this study only reports findings from very few participants (5 active TMS, 6 sham) and clinical outcomes are to be interpreted with caution. Another pilot study evaluated the efficacy of the deep TMS H-coil over the medial PFC on AUD patients, and successfully reported a manipulation in the release of dopamine in active TMS as compared to sham [Ceccanti et al., 2015]. Furthermore, this study identified a reduction in both craving measures and in alcohol drinking days in both stimulation groups (sham and active), yet this change was more prominent and significantly different only in patients who underwent an active TMS as compared to patients assigned to sham. However, similar to the study from Addolorato [Addolorato et al., 2017], this pilot study only presents findings related to a very small sample of patients (9 active TMS, 9 sham).

Altogether, the existing scientific literature does prove that magnetic stimulation of frontal cortical regions can manipulate the dopaminergic system, but results related to a reduction in craving measures are conflicting.

With the two sham-controlled longitudinal studies evaluated in this chapter we significantly shed more light over the potential efficacy of this novel treatment based on deep TMS. Specifically, the stimulation of the ACC appears promising for the treatment of alcohol addiction, as suggested by a significant reduction in craving scores. Another interesting aspect, in line with previous studies, comes from the number of treatment sessions necessary to induce a reduction in addictive-behaviors. In the BGU study, indeed, the differentiation between the active rTMS and the sham condition appears only at the end of the second week of treatment, after 10 consecutive treatment sessions, as already indicated by [Mishra et al.,

2010, Herremans et al., 2015, Mishra et al., 2015]. At the end of the third week, after the 15^{th} stimulation, the difference in craving between the two groups is further increased. Yet, it is important to state that the clinical effect here evaluated, despite being significant, does not appear to be particularly prominent, given the lack of a big effect size. For this aspect, the limited number of participants should be taken into account. Specifically, patients are still being recruited at the BGU center, aiming to collect more valuable data for the purpose of this clinical study.

In relation to the effects of deep rTMS treatments over the functional connectivity organization in alcohol dependent patients, only one of the two studies here evaluated proved some significant modulations in reward-related regions after stimulations. Specifically, the deep stimulation of the bilateral insula, despite the lack of efficacy in the clinical outcomes, appeared to significantly re-organize sub-cortical regions as well as frontal cortices. We previously proved that AUD patients present a substantial fragmentation in sub-cortical basal ganglia structures (Bordier et al. in prep; chapter 3 of this thesis). Both samples of patients from the LIU and BGU studies present similar fragmentation thus providing independent corroborating evidence. However, only patients from the LIU sample revealed a statistically significant re-organization of the basal structures after active stimulation of the insular cortex, with a tendency towards a reduction in fragmentation. Importantly, the insula has reciprocal connections towards these regions, forming a key pathway in the brain reward-system [Craig, 2009, Malik et al., 2018]. From these findings, it appears that stimulation of this cortical area would be effective in modulating the organization in these central reward-related regions. Yet, another interesting observation comes from the non-statistically significant re-organization of these sub-cortical structures also in the sham treated group. Indeed, we observed a rearrangement of specific structures (i.e. caudate, pallidum, putamen) very similar to the one observed in patients treated with real TMS. It is possible that this subtle functional re-organization relates to the reduction of alcohol intake that these patients experience during the three weeks of treatment. As reported in the previous chapter of this thesis (chapter 3) we already observed in AUD patients a substantial re-organization of reward-related regions after several weeks of detoxification, irrespectively of the treatment option received (IWT or IWT+NTX; Bordier et al in prep.). Furthermore, in this TMS study, patients

were supposed to go daily to a clinic to receive treatment. Here, they would find themselves in a supportive clinical setting, and they would consistently interact with experienced and caring clinical staff. It is likely that the combination of the reduction in alcohol intake and a supportive environment might help in the re-organization of functional brain regions strictly involved in reward processes. However, such manipulation might not be strong or protracted enough as to result in significant clinical and behavioral changes. The modulatory effects induced by a stimulation of the insula by means of a deep TMS H-coil over sub-cortical regions (pallidum and striatum) was already reported by a pilot study from Malik and colleagues [Malik et al., 2018]. This study revealed reductions in dopamine levels after one session of low frequency stimulations in healthy volunteers, and thus suggested the possibility to employ such stimulation as a treatment for addiction. However, the present study involved high frequency stimulation, as suggested by the efficacy in reducing craving measures in smokers, reported by Dinur-Klein and colleagues [Dinur-Klein et al., 2014]. It might be possible that the application of a more protracted low-frequency stimulation to the insular cortex in AUD patients could show stronger long-term efficacy as suggested by Malik and colleagues [Malik et al., 2018]. The active stimulation employed in the LIU study, further induced re-organization of superior frontal regions, fundamental for the top-down control of impulsive behaviors. This might additionally suggest the efficacy of the stimulation in manipulating the underlying functional organization of the network. Unfortunately these perturbations of the system do not prove to be sufficient to show clinical long-term effects. In contrast, we could not identify important changes in the functional connectivity networks from the BGU study, wich involved the stimulation of the ACC. Basal structures were found to be similarly fragmented in this sample of patients, with no re-organization after active stimulation despite the positive clinical outcome defined by craving scales. This suggests that the alterations in these sub-cortical regions is neither sufficient nor necessary for the improvement in craving for these patients.

A secondary interesting result from these studies lays in the observation of a significant relation of clinical variables with functional connectivity topological metrics. Specifically, in the BGU study we revealed a significant correlation between alcohol dependence severity (ADS) and both global efficiency and overall func-

tional connectivity strength. Furthermore, craving scores measured with the PACS questionnaire correlated with global efficiency and overall functional connectivity, and with the functional connectivity strength of a widespread brain sub-network. The relation of alcohol dependence severity with whole-brain functional network alterations were similarly reported by Sjoerds and colleagues [Sjoerds et al., 2015]. Of important notice, we observed that functional brain networks show lower efficiency and functional strength with higher severity of alcohol dependence and self-reported urges. Another critical findings comes from the correlation reported between changes in connectivity and changes in craving. Specifically, the more functional connectivity – and global efficiency – improved as a consequence of treatment, the more craving was reduced after three weeks of active TMS stimulation. Yet, the increase in overall functional strength is not significant after delivery of TMS, thus possibly suggesting that by significantly increasing the functional connectivity in AUD we could induce a further reduction of addictive-behaviors in AUD patients.

At a local scale, craving measures significantly correlated, with a negative direction, with a sub-network comprising widespread cortical connections more prominently located in frontal areas. Interestingly, task-based studies already identified a relation of craving urges with functional frontal activation [Myrick et al., 2004, Grüsser et al., 2004, Heinz et al., 2009]. Notably, also the changes in activation of prefrontal regions observed in alcohol-dependent patients when observing alcohol-related images appeared to significantly correlate with craving self-reported scores [Myrick et al., 2004].

However, these significant relations are present here only in one sample of AUD patients (from the BGU study). Unfortunately, given the nature of these clinical studies, we cannot disentangle whether these effects are related to the toxic effect that ethanol exerts on the brain or whether they play a role as a predisposition factor. Moreover, the number of participants in these two clinical studies is limited (43 patients BGU; 41 patients LIU) and we could be under-powered for an examination of specific relations between clinical variables and functional related measures in both samples. Yet, the identification of specific correlation patterns can represent an important factor that should be further addressed in other samples of AUD patients, as well as in other addictive disorders. Importantly, it should

be more carefully evaluated whether these functional alterations related to craving and addiction severity might be a possible target for treatment options.

To conclude, in these two clinical studies we aimed to evaluate the efficacy of a possible novel treatment for alcohol addiction, by means of transcranial magnetic stimulation of the insular cortex and the ACC. Contrary to our expectations, the application of deep TMS did not reveal specific functional connectivity changes that could be translated into a clinical outcome. Thanks to the induction of excitability changes in the cortex, it is thought that an active TMS stimulation might be able to induce long-term functional changes and plasticity in the human brain. Yet, the two studies here investigated did not prove prominent functional effects. Importantly, in both studies we observed an important reduction in craving and disorder severity for both stimulation conditions. Yet, only stimulations targeting the ACC proved efficacy in more significantly reducing craving in the active TMS group. Moreover, this was the only group furthermore proving partial stability during follow-up months, whereas both craving and alcohol consumptions significantly increased in the sham group and in both conditions for the LIU study. This effect subsequently indicates that deep high-frequency rTMS of medial frontal regions can reduce alcohol craving. Further investigations should be carried out in order to better understand the duration of these stimulation effects and whether this promising approach may become an established treatment for alcohol dependent patients.

5 KETAMINE-INDUCED ALTERATIONS AND REVERSAL BY RISPERIDONE

In the present thesis I methodically addressed the application of a complex graph-theoretical approach to resting-state functional networks. After the closer evaluation of some methodological open questions in the network science world, I applied graph theoretical methods to different clinical datasets. Specifically, I investigated alterations in brain functional connectivity underlying AUD, and identified brain areas that may be amenable to therapeutic targeting through neuromodulatory approaches. Importantly, the alterations investigated so far were related to long-lasting effects or longitudinal observations. Neural effects of alcohol on AUD patients are studied after prolonged substance intake, whereas treatments efficacy is addressed after few weeks of deep TMS. The concepts and methods I have developed may be useful to study the effects of other drugs of abuse, and therapeutic approaches more conventional than TMS.

Here, I will apply the graph theoretical framework to evaluate the effects of acute administration of ketamine, a multifaceted drug whose effects on brain function are still the subject of investigation. Ketamine is a psychotomimetic drug with strong abuse liability. However, at higher doses it can be employed as an anesthetic and sedative. In addition, its use as a powerful antidepressant has been recently approved by the Food and Drug Administration (FDA). Ketamine is currently the only drug with acute efficacy in Major Depression, an effect that may be related to its activity on NMDA glutamate receptors. On the other side, this very same influence of ketamine over the glutamatergic system makes it a pharmacological model of psychosis. Indeed, the symptomatology of sub-anesthetic doses of ketamine is similar to that experienced by patients under acute psychosis. How a single drug may have such a wide repertoire of effects remains a fascinating question.

Here, I will evaluate the acute perturbations that ketamine can exert over the brain's functional connectivity organization, in healthy participants who received an intravenous injection of the drug while lying in the MR scanner, to disentangle

the neural pathways that may play a role in diverse effects of the drug. Moreover, I will describe how pretreatment with certain pharmacological agents modulate the alterations induced by ketamine on resting-state functional connectivity.

5.1 INTRODUCTION

Ketamine is an anesthetic and psychotomimetic drug, acting as an antagonist of N-methyl-D-aspartate receptors (NMDAr), one of the main glutamate neuroreceptors. When taken at sub-anesthetic levels, this drug evokes a pattern of psychotic symptoms very similar to those experienced by patients affected by schizophrenia. This observation provided the basis of a novel hypothesis for schizophrenia, involving dysfunctional glutamatergic neurotransmission underlying the disorder. Growing evidence support glutamate involvement in psychosis, driven by a reduction in functionality of NMDAr [Howers et al., 2015, Pilowsky et al., 2006]. Through pharmacological Magnetic Resonance Imaging (phMRI) techniques, we may reveal brain circuits alterations evoked by ketamine, and corroborate the NMDAr physiopathological role in schizophrenia [Bifone and Gozzi, 2012]. This ketamine model of psychosis is now well supported by evidence indicating rapid effects on brain functional activations, which correlates with dissociative and negative symptoms [Deakin et al., 2008, Stone et al., 2012, De Simoni et al., 2013].

Besides the chance to evaluate acute effects induced by a blockade of the glutamatergic system, phMRI techniques are relevant for the evaluation of pharmacological pretreatments. With the study of modulatory effects of different pharmacological agents over ketamine-evoked activations, we may provide clearer understanding for novel antipsychotic mechanisms. Specifically, the evaluation of pretreatment effects with agents acting on the glutamatergic system or NMDAr can better elucidate the underlying psychotomimetic pharmacological mechanisms. Few studies addressed this possibility in healthy humans, reporting controversial results.

In detail, these investigations demonstrated specific attenuations of ketamine-induced functional alterations with a pretreatment of lamotrigine and risperidone [Deakin et al., 2008, Doyle et al., 2013, Joules et al., 2015, Shcherbinin et al., 2015].

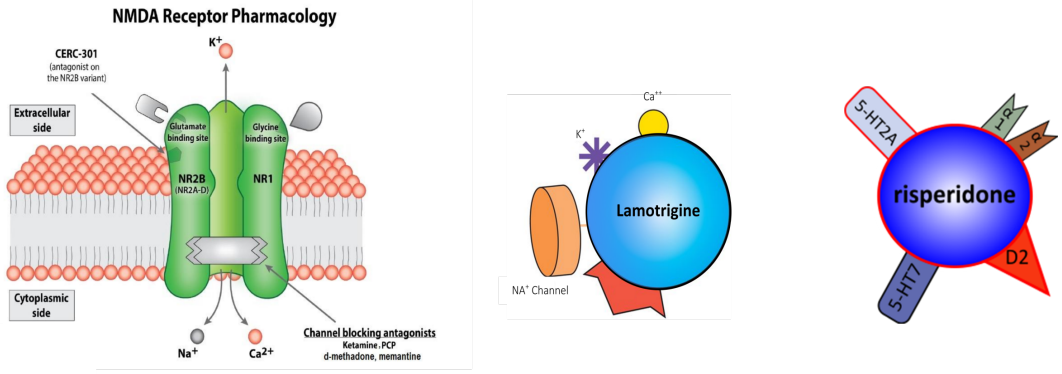

Figure 5.1: Representation of NMDA receptor pharmacology showing target for ketamine, together with lamotrigine and risperidone pharmacodynamics.

First evidence reported a reversal of ketamine-evoked effects after a pre-treatment with lamotrigine [Deakin et al., 2008, Doyle et al., 2013]. Conversely, a modulatory activity induced by a pre-treatment with risperidone but not with lamotrigine was revealed by subsequent studies [Shcherbinin et al., 2015, Joules et al., 2015]. Of interest, risperidone is one of the most common atypical antipsychotics used for the treatment of schizophrenia. This compound acts as an antagonist of the serotoninergic 5-HT2A receptor, and shows high affinities with the dopamine D2 receptor. Through its action over 5-HT2A receptors, risperidone indirectly reduces glutamate release, and enhances NMDAr functionality [Meltzer et al., 2011, Konradsson et al., 2006]. Conversely, lamotrigine, an anticonvulsant used for the treatment of epileptic seizures and bipolar disorder, acts on sodium ion channels and attenuates glutamate release with no action over NMDAr [Large et al., 2005].

Here, we applied advanced graph theoretical methods to evaluate how ketamine can affect the large scale organization of brain functional connectivity and how risperidone and lamotrigine can modulate these alterations. Two previous studies already assessed modulatory effects in this same dataset [Doyle et al., 2013, Joules et al., 2015]. By means of univariate and multivariate BOLD signal analysis, as well as more complex pattern recognition algorithms, they reported a modulatory effect mostly driven by risperidone.

In addition to the already assessed techniques, graph theoretical approaches allow investigation of complex topological properties of the functional brain network, with no need of a priori hypothesis. We can evaluate brain systems perturbations induced by pharmacological challenges, thus revealing drug mechanisms at a

functional brain network level. Through this advanced methodological technique, we can identify changes and alterations in network integration and segregation, by addressing brain modular organization, a fundamental topological property of complex networks, which makes the system more robust and resistant to perturbations [Sporns and Betzel, 2016]. Related to psychosis, modular fragmentations of specific cortical regions, serving primary cognitive functions, seems to underlie schizophrenia [Bordier et al., 2018]. In this framework, the evaluation of ketamine effects over functional modular organization, and the possible reversal of these alterations by antipsychotic drugs, can be promising.

5.2 MATERIALS AND METHODS

5.2.1 Participants

Twenty right-handed male volunteers were recruited for this double blind, randomized, placebo-controlled, partial cross-over design study. All participants were screened and excluded if they had history of neurological and psychiatric disorders. Furthermore, volunteers were excluded from the study if they had history of illicit drugs abuse, excessive alcohol, cigarettes or caffeine consumption. Four participants withdrew during the study, hence, only 16 volunteers (mean age 25.8 years, SD=5.7) completed all four sessions. All subjects gave written informed consent to participate in the study, approved by the Wandsworth Research Ethics Committee (090/H0803/48). Further details about participants recruitment, as well as exclusion criteria, can be found in Doyle [Doyle et al., 2013] and Joules [Joules et al., 2015].

5.2.2 Experimental design

The study was carried out over four different sessions, each separated by at least 10 days. At each session, participants received a single oral dose of either lamotrigine (300 mg), risperidone (2 mg) or placebo (ascorbic acid, for two sessions). Four hours after the oral intake of the compounds, during the broad maximum

plasma exposure of the two drugs, volunteers received an intravenous infusion of either saline (one session) or ketamine, to a target plasma level of 75 $ngml^{-1}$. In total, four combinations were administered: placebo and saline (PLA-SAL), placebo and ketamine (PLA-KET), risperidone and ketamine (RIS-KET), lamotrigine and ketamine (LAM-KET). Two imaging procedures were undertaken at each session, the first 1h 30m after the oral compounds intake (oral only measurements), the second 4h 15m post-oral dose. The intravenous infusion was administered 5 minutes after the beginning of the second imaging procedure (figure 5.2).

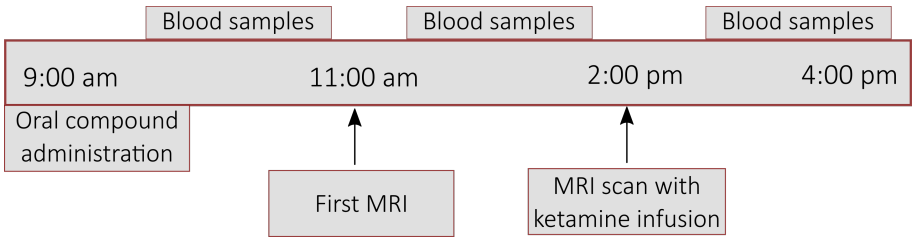

Figure 5.2: Timeline for each experimental session. The study included a total of four session per participant. Four compound combinations were administered during these sessions, separated by at least 10 days.

5.2.3 Ketamine infusion

A sub-anesthetic dose of racemic ketamine was administered intravenously, based on the Clements 250 model [Absalom et al., 2007]. The drug was infused to reach a target plasma level of 75 $ngml^{-1}$, adjusted for each participant's weight and height. A dose of 0.12±0.003 mg/kg was delivered during the first minute followed by a pseudo-continuous infusion of approximately $0.31^{mg/kg/h}$. More details concerning ketamine infusion can be found in Doyle [Doyle et al., 2013] and Joules [Joules et al., 2015].

5.2.4 Image acquisition

MR images were acquired using a 3T General Electric Signa HDx scanner. Gradient-echo echo-planar imaging (EPI) was used to acquire at each session a 15 minutes, eyes open, resting state BOLD phMRI scan, with a total of 450 volumes of 38 near-axial slices (3 mm thickness, 0.3 mm inter-slice gap, TE=30 ms, TR=2000 ms,

FA=75°, in-plane resolution=3.3 mm, matrix size=64x64, field of view=21.1 x 21.1 cm). The compound infusion was administered 5 minutes after the start of the scan session. Additionally, a high-resolution gradient-echo scan was performed resulting in 43 near-axial slices (3 mm thickness, 0.33 mm inter-slice gap, TE=30 ms, TR=2000 ms, FA=90°, in-plane resolution=3.3 mm, matrix size=128x128, field of view=24x24 cm).

5.2.5 Image preprocessing

Imaging data were preprocessed using SPM12 (Wellcome Trust Center for Neuroimaging, London, UK) and FSL. Volumes were corrected for slice-timing, head-motion realigned (mcflirt) with FSL tools. Coregistration to the high-resolution image, and normalized to the standard MNI EPI template space were carried out with SPM12. The structural images were segmented into grey matter, white matter (WM) and cerebrospinal fluid (CSF) tissue types. Linear regression was used to regress out nuisance signal parameters from the time-series, specifically the mean ventricles and WM signals, and the six motion parameters. Given the known impact of motion on the functional timeseries [Power et al., 2012], and the potential confounds arising from movements following an intravenous infusion, the effects of motion was assessed for all the pre- and post- conditions. Analysis of Framewise Displacement and DVARS, computed following Power [Power et al., 2012], did not show any difference between conditions. A butterworth band-pass filter of 0.01 -0.1 Hz was subsequently applied. Pre- and post-infusion conditions were defined as the first 150 and the last 150 volumes acquired (out of 450 volumes), corresponding to 5 minutes of data, respectively. Pre-infusion conditions only measure the presence of the oral compounds, whereas the post-infusion corresponds to the period 5 to 10 minutes after the bolus administration.

5.2.6 Functional Connectivity graphs

We parceled the preprocessed conditions into 638 nodes, extracted by the functional template generated in Crossley [Crossley et al., 2013]. A study exploiting

this same dataset [Joules et al., 2015] adopted a smaller number of parcels to build the connectivity graph (116 ROIs). Here, we chose to implement a larger template, taking advantage of the relatively uniform distribution of parcel size and accuracy in their delineation. The connectivity matrices were estimated by computing pairwise inter-regional correlation for each individual and each condition. We subsequently transformed the correlation coefficients to Fisher's zscore, and computed a group level functional connectivity matrix, by averaging each individual's adjacency matrix. We sparsified the matrices for each condition prior to community detection. Several methods are discussed in the literature for the reduction of matrix density and removal of weakest edges [van den Heuvel et al., 2017a]; here we opted to use a percolation approach, as we have recently proved the ability of this thresholding method to maximize the modular information that can be extracted from the network [Bordier et al., 2017]. This approach initially removes all the weakest edges, stopping when the graph's largest component starts breaking apart; we identify such point as the optimal threshold, preserving the network structure and connectedness. The contrasts used to address ketamine induced effects and the modulation of the pharmacological compounds were:

- Ketamine effect: PLA-SAL vs PLA-KET
- Risperidone modulations: PLA-KET vs RIS-KET
- Lamotrigine modulations: PLA-KET vs LAM-KET

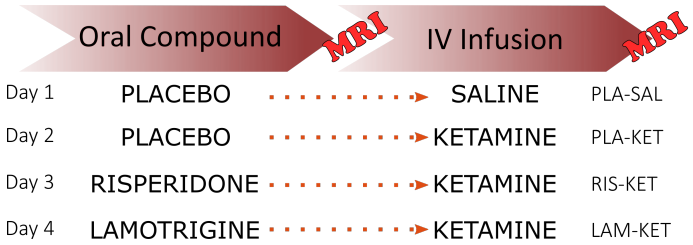

Figure 5.3: Four combinations of drug compounds administered during the four study sessions.

5.2.7 Network Based Statistics (NBS)

Here, we tested for global differences in functional connectivity induced by ketamine and their modulations by different pharmacological compounds. To that

end, we exploited the use of the Network Based Statistics (NBS) toolbox [Zalesky et al., 2010a]. The NBS is a powerful tool to evaluate edge level statistical differences between groups, overcoming the multiple comparison correction problem by performing mass-univariate testing on all graph edges. We applied paired t-tests, to test differences between conditions. Thresholds were set starting from t >3.1 with 5000 permutations on every connection. Contrasts were set in order to detect both increase and decrease of connectivity strength across conditions.

5.2.8 Modular organization

Several methods have been proposed to identify the community structure of complex networks [Newman, 2004, Rosvall and Bergstrom, 2008]. Here, we implemented the InfoMap approach [Rosvall and Bergstrom, 2008], to overcome the resolution limit from which the most widely used approach, Newman's Modularity [Newman, 2004] suffer [Good et al., 2010]. The InfoMap method is based on the minimization of the description length of a random walker defined on the network through a set of heuristics. This approach, however, suffers of degeneracy of nearly-optimal solutions, namely substantially different partitions might present very similar values of the fitness function [Good et al., 2010]. To overcome this important limitation, we applied a consensus approach to generate a stable partition. This is representative of all nearly-optimal solutions generated by different runs of the algorithm [Lancichinetti and Fortunato, 2012]. Here we used the InfoMap implementation available in the igraph-0.7.1 package [Csardi and Nepusz, 2006].

5.2.9 Network metrics

From the single-subject sparsified adjacency matrices, we extracted topological metrics to evaluate changes in the global and local functional organization. The overall functional connectivity was measured as the mean of all non-zero elements of the matrix [van den Heuvel et al., 2017a]. This global metric gives a measure of the overall network strength. Another global metric evaluated at the subject level comprises network density. As described in chapter 1, the density of a matrix is

measured as the proportion of all links present in the network over the number of all possible edges 1.1. Here, we measured network density for all subjects after the application of the percolation threshold. We next evaluated the degree centrality, a local metric, for every node in the network. The degree centrality *(k)* refers to the sum of all the edges attached to a given node [Sporns et al., 2004]. Nodes presenting higher *k* tend to play a more central role in the network, acquiring the name of "network hubs". We addressed statistical significance across conditions for the degree centrality through 10000 paired-test permutations. All reported results are corrected for multiple comparison correction (false discovery rate, [Genovese et al., 2002]). All visual representations of anatomical distribution of modules and significant sub-networks identified through NBS were produced using the BrainNet viewer toolbox [Xia et al., 2013].

5.3 RESULTS

5.3.1 Effects of ketamine on brain functional connectivity

To address the effects of ketamine per se on brain functional connectivity, we compared the PLA-KET condition (ketamine with placebo pre-treatment) with the PLA-SAL (saline infusion following placebo oral intake). The histogram depicted in figure 5.4 shows the edge-weight distribution for the two conditions, evaluating global effects of a ketamine infusion. Functional strength was significantly different across the two conditions (t-test, p=0.001), with a global decreased connectivity induced by ketamine. After the percolation thresholding procedure applied to all participants, no differences were observed in the global density of the two groups (p=0.2236).

Sub-network differences

A paired t-test, implemented within the NBS toolbox, identified a significantly weaker sub-component in PLA-KET compared to PLA-SAL (p corrected=0.0026, figure 5.4). Specifically, this sub-network comprised links within the occipital lobe (mostly comprising the calcarine and lingual fissures, and occipital middle

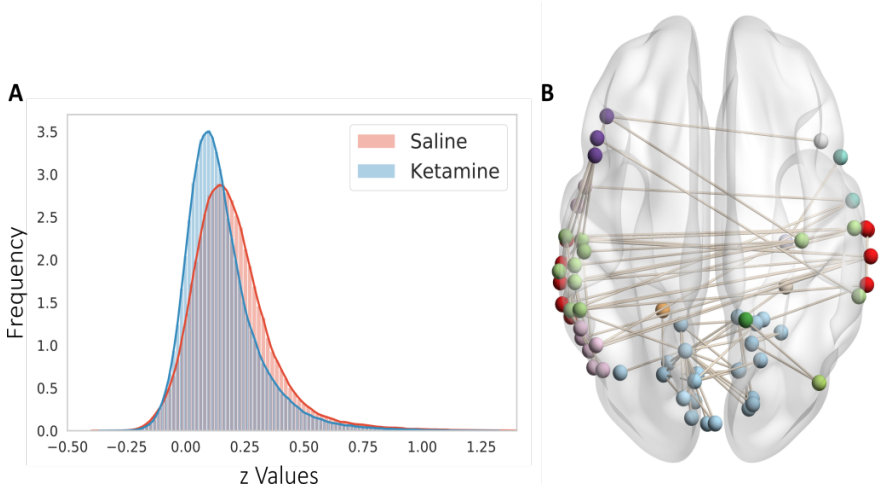

Figure 5.4: A. Histogram representing functional strength distribution for the saline condition (in red) and for the ketamine condition (in blue). B. Sub-network identified with NBS showing decreased functional connectivity strength induced by ketamine.

cortex) and interhemispheric temporal connections, for a total of 81 edges involved, with a T-statistic of t=4. Importantly, when comparing the two placebo conditions (placebo pre-Ket and placebo pre-Sal) with PLA-SAL, no differences were identified for any comparison (t=3.1, p corrected=0.260, p corrected=0.735, respectively). These contrasts were crucial to evaluate both within and between sessions stability.

Nodal centrality and modular organization

Ketamine induced a pattern of both increased and decreased nodal degree centrality. After fdr correction, 54 nodes presented decreased degree centrality in PLA-KET compared to PLA-SAL as seen in figure 5.5. In line with the decreased functional connectivity strength identified by the NBS, these nodes comprised mostly occipital medial regions, calcarine and lingual fissures, parahippocampal gyrus, temporal inferior and medial cortices, together with left inferior frontal nodes. Fourteen nodes showed an increased nodal centrality induced by ketamine. These nodes comprised left and right thalamus, some nodes from the supramarginal gyrus and the inferior parietal cortex.

Next, we implemented the consensus *InfoMap* community detection to identify optimal modular partitions for all experimental conditions. Overall, we observed a general fragmentation of the modular organization in PLA-KET. We identified 18 communities for the PLA-SAL condition, with communities size ranging from

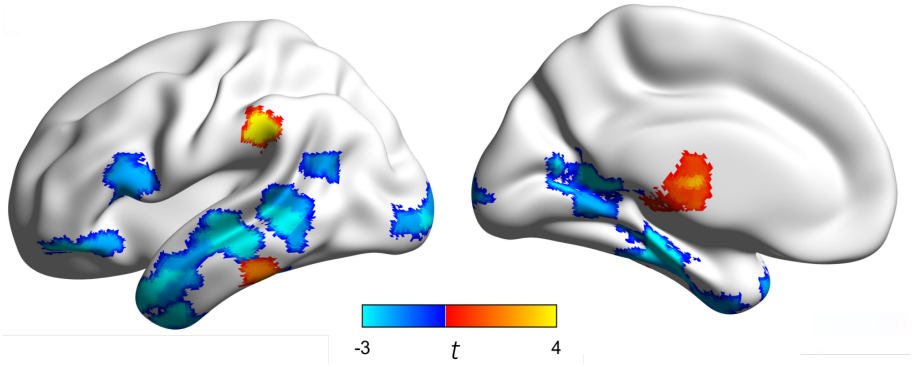

Figure 5.5: Nodes with altered degree centrality in ketamine. Brain areas represented in blue show reduction of centrality induced by ketamine; red areas reflect increase of centrality after ketamine injection.

108 to two nodes, and 30 communities for PLA-KET, with sizes ranging from 87 to 2 nodes. Cortical regions showing greater fragmentations comprised the medial temporal cortex (1 module in PLA-SAL, 4 modules in PLA-KET), auditory and language cortical regions (2 modules in PLA-SAL, 6 modules in PLA-KET), and prefrontal cortices (1 module in PLA-SAL, 3 modules in PLA-KET; figure 5.6).

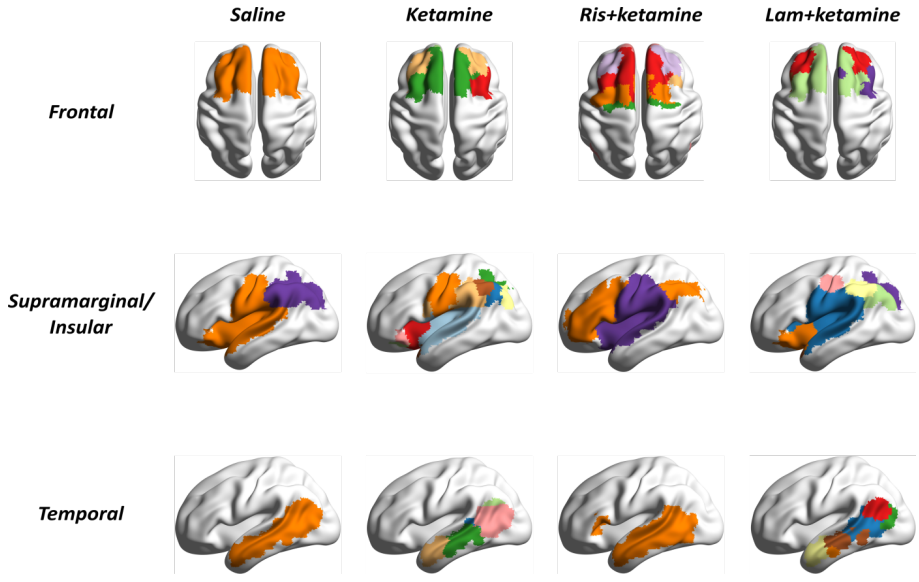

Figure 5.6: Representation on the brain cortical surface of modular organization in superior frontal regions (upper row), auditory and language cortices (middle row), and in temporal poles (bottom row) for all conditions.

5.3.2 Modulatory effects of risperidone

To evaluate whether risperidone could modulate ketamine effects, we compared PLA-KET to RIS-KET. Overall functional connectivity was not affected by a risperidone pre-treatment (p=0.5266), with RIS-KET showing a very similar distribution of edge weights as PLA-KET (figure 5.7). No differences in the density of matrices at percolation was present (p=0.2205).

Sub-network differences

Two sub-networks with weaker connectivity strength in PLA-KET compared to RIS-KET were identified by a paired t-test conducted with the NBS (p=0.0298, p=0.0042), with a t=4, as seen in figure 5.7. The first sub-network comprised 13 edges, involving the middle occipital connections, with lingual and calcarine fissures links. The second sub-network included 33 edges, comprising interhemispheric temporal connections. Interestingly, these sub-networks highly overlap the decreased connectivity connections induced by ketamine when compared to PLA-SAL.

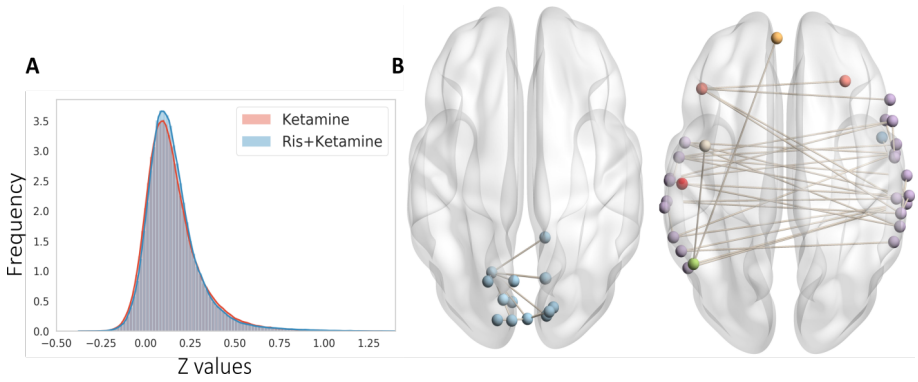

Figure 5.7: Panel A shows the edge-weight distribution of PLA-KET and RIS-KET conditions; Panel B represents two sub-networks with reduction of functional connectivity strength in PLA-KET, compared to RIS-KET, namely sub-networks where ketamine-induced alterations were reversed by risperidone.

Nodal centrality and modular organization

A pattern similar to the PLA-SAL and PLA-KET contrast was identified also concerning degree centrality. RIS-KET revealed higher k compared to PLA-KET in 50 nodes, comprising temporal medial, inferior, and superior regions, calcarine

fissure, parahippocampal gyrus and inferior frontal nodes. Greater centrality in PLA-KET was instead present only in 6 nodes, involving the parietal cortex. In addition, modular organization was substantially modulated by risperidone pre-treatment. The consensus InfoMap approach identified 19 communities for RIS-KET, with sizes ranging from 87 to 3 nodes. Interestingly, the fragmentation of the medial temporal cortex observed in PLA-KET was reversed by risperidone. Similar to PLA-SAL, in RIS-KET the middle temporal cortex was reunited within one community. Moreover, a re-organization of language and auditory cortices was observed in RIS-KET, with the unification of angular and inferior parietal regions to inferior frontal regions. On the contrary, no effect was present in the fragmentation of superior frontal regions as seen in figure 5.6.

5.3.3 Modulatory effects of lamotrigine

The comparison of PLA-KET with the LAM-KET condition, to evaluate possible reversed effects of lamotrigine, did not yield any significant difference in the overall functional connectivity, nor density (respectively, p=8929, p=0.2631).

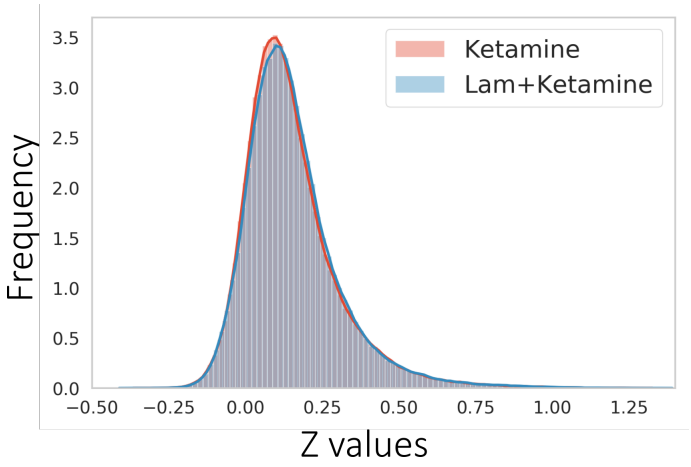

Figure 5.8: Comparison of edge-weight distribution for conditions PLA-KET and LAM-KET.

Sub-network differences

By testing different thresholds (t=2.5, t=3.1, t=3.5, t=4), we did not identify any significant result through the implementation of a paired t-test with the NBS, neither for a decrease nor an increase in connectivity strength.

Nodal centrality and modular organization

Despite the lack of differences at a functional connectivity strength level, 21 nodes presented higher k centrality in LAM-KET compared to PLA-KET. These nodes comprised temporal medial and superior cortices, and precentral gyrus. In contrast, no region showed lower k in LAM-KET compared to the ketamine condition.

The application of Consensus InfoMap revealed a partial reorganization of the modular structures in ketamine with a lamotrigine pre-treatment. LAM-KET presented 18 communities with size ranging from 96 to 4 nodes. Fragmentation of specific regions was, however, still present with lamotrigine pre-treatment. The temporal cortical community showed a low degree of re-organization, being still organized into 4 different communities in LAM-KET. The language/auditory cortex still presents fragmentation, specifically in the supramarginal and angular gyrus. Fragmentations and asymmetries were still present also concerning frontal regions (Figure 5.6).

5.4 DISCUSSION

Here, we addressed ketamine-evoked alterations over brain functional connectivity as well as their modulations induced by different pharmacological agents. Through the implementation of network theory, we could study whole brain connectivity with no necessity of *a priori* hypotheses. Moreover, the evaluation of the overall organization and functional interaction among different brain regions can better elucidate the architecture and global changes induced by pharmacological agents. The modular brain organization, for example, has a strong biological meaning in making the overall system more robust and adaptable to perturbations [Sporns, 2018]. Its evaluation during a ketamine challenge might reveal the reaction of the system to such a strong perturbation. As expected, we revealed substantial changes over brain functional fluctuations induced by a ketamine infusion, by means of a graph theoretical approach. Of interest, these functional alterations were differently modulated by pre-treatments with two different pharmacological agents.

Considering the ketamine effects alone, we first observed a significant reduction in overall functional connectivity strength induced by ketamine (PLA-KET) when compared to a placebo condition (PLA-SAL). This reflects previous evidence showing a marked effect of the drug over BOLD signal in healthy human volunteers [Deakin et al., 2008, Driesen et al., 2013, De Simoni et al., 2013], which allows for its use as a model to investigate psychotomimetic mechanisms. Moreover, the global fragmentation that we observed in the modular organization reflects the strong effect that ketamine exerts. The PLA-KET condition, indeed, revealed an overall disruption of functional modules, with a total number of 30 communities, against the 18 communities identified in PLA-SAL. Of important notice, head motion, a major confound known to affect functional connectivity strength, [Power et al., 2012, Van Dijk et al., 2012], was not statistically different among conditions. This could rule out the possibility that increased in-scanner movements possibly induced by ketamine could drive alterations in functional couplings.

By means of a network approach, we revealed specific alterations localized in occipital regions and in interhemispheric temporal connections. Temporal cortices, besides being central regions to memory formation and consolidation, seem to underpin various aspects of psychosis, such as the occurrence of auditory verbal hallucinations [Alderson-Day et al., 2015]. In detail, alterations in auditory interhemispheric connectivity seem to play a specific role in hallucinations emergence [Ćurčić-Blake et al., 2017]. This is consistent with the behavioral effects induced by a ketamine exposure, which include reduction of contextual processing, memory consolidation deficits, as well as auditory hallucinations. Of interest, auditory hallucinations during ketamine exposure seem to be amplified by the reduced perceptual environment of the MR scanner [Powers III et al., 2015]. This is also in line with findings already reported by different studies involving a ketamine challenge in healthy volunteers, where a correlation with dissociative scales was related to reductions in temporal auditory network strength [Deakin et al., 2008, Niesters et al., 2012, Joules et al., 2015]. Furthermore, the high NMDAr expression within the temporal cortex may explain such alterations in functional connectivity [Niesters et al., 2012]. Similarly, the observed effects in connectivity strength within the visual occipital network possibly represent perceptual distortions common in both ketamine-induced behaviors and psychosis. Indeed, specific functional orga-

nization alterations within these primary sensory areas are also present in patients with schizophrenia [Bordier et al., 2018]. Similar disruptions in occipital regions are widely reported in ketamine studies [Joules et al., 2015, Mueller et al., 2018], possibly underlying a similar disruption of sensory information processing shared by schizophrenia and ketamine challenges.

In light of the similarities observed between psychosis and ketamine-evoked symptomatology as well as functional alterations, the modulation of ketamine-induced changes by pharmacological agents might help understand the mechanism of action of antipsychotic drugs. Risperidone is a common antipsychotic used to treat schizophrenia. Here, during one session, participants received an oral dose of risperidone a few hours before the ketamine injection, with the aim to test whether an antipsychotic could prevent ketamine effects. When compared to PLA-KET, brain network analysis revealed that the condition of ketamine pre-treated with the antipsychotic (RIS-KET) presented higher functional strength in two sub-networks, namely the occipital and temporal interhemispheric networks. Importantly, these connections matched almost entirely the same links that ketamine affected when compared to the placebo-control condition. Moreover, when we addressed the modular architecture in RIS-KET, we observed normalizations in sensory cortices, mostly in temporal and supramarginal communities, which appeared fragmented in the ketamine condition. In contrast, higher-order frontal regions did not show changes when ketamine was pre-treated with risperidone, likewise showing a disrupted organization very similar to the one induced by ketamine. It is interesting to notice that risperidone seemed to prevent some, but not all, critical alterations induced by the NMDAr antagonist, mostly involving sensory cortices.

Given the nature of ketamine as a selective antagonist of NMDAr, thus exerting a strong action over glutamatergic transmission, we could also expect a specific modulation of its activity through the pre-treatment of lamotrigine, a common anticonvulsant known to strongly suppress glutamate release [Goa et al., 1993]. It is important to notice, however, that lamotrigine does not have effects over NMDAr. In the present study, we revealed that lamotrigine pre-treatment (LAM-KET) does not reverse any of the alterations observed in PLA-KET, despite its strong glutamatergic actions. Lack of efficiency of lamotrigine modulatory effects were

already reported through machine learning algorithms assessing nodes centrality [Joules et al., 2015]. Here, we importantly replicated such effect also in modular brain organization, a topological feature crucial for network robustness to perturbations. The presence of modulatory activities by an established antipsychotic may suggest the use of ketamine for the evaluation of the effectiveness of new antipsychotic agents. Future studies can test the efficacy of typical antipsychotics, such as haloperidol, in normalizing ketamine brain changes. Identification of specific pre-treatment patterns may help understand their pharmacological mechanisms of action. Unfortunately, the limited number of participants in the present study made it difficult to assess possible correlations between functional connectivity and behavioral effects of ketamine.

6 CONCLUSIONS AND FUTURE DIRECTIONS

The rise of network neuroscience, applied to resting-state functional MRI in recent years, has led to novel understanding of the topological organization of the brain, in both healthy and pathological conditions. The application of advanced and complex analysis techniques based on graph theoretical approaches has proven precious for the identification of aberrancies in the topological organization of brain connectivity in several neurological and neuropsychiatric disorders. By means of network science tools we can importantly evaluate the interactions of elements in the brain, at all scales, from a local to a global perspective. A particularly relevant opportunity that this approach hands to neuroscience is the possibility to detect the modular architecture of the functional brain, a critical feature of complex networks which confers robustness and stability to the system. The study of the modular organization in pathological conditions may be critical for the understanding of the altered segregation and integration of neural areas in the functional network. In this work I focused on the evaluation of the altered functional organization of cortical and subcortical brain regions in one of the most prevalent neuropsychiatric disorders worldwide: alcohol addiction.

Before applying graph theoretical methods to the clinical studies evaluated in this thesis, I tackled some critical open questions present in the novel and complex field of network neuroscience. The application of this approach to functional brain studies is still in its infancy, and several crucial aspects need to be more thoroughly assessed. As a first and important contribution of this work, I could prove the importance and necessity of one of the most debated steps in the processing of functional brain networks, namely the application of a threshold for the sparsification of connectivity graphs. For this purpose, I leveraged some advanced, newly introduced tools based on the maximum entropy random graph formalism, which allows a more robust application of graph-theoretical analysis to the study of complex resting-state brain systems. By means of these powerful information

theory tools, I clarified the role of thresholding, a problem that has baffled the neuroscientific community for a long time. Particularly, the contribution of this project revealed two specific critical findings related to this methodological and conceptual aspect. First of all, from my observations it is clear that the application of a threshold is fundamental for the revelation of large-scale structures within the system. Only by applying more stringent thresholding it is possible to appreciate a significant difference of an empirical network from its randomized counterpart. Second, I demonstrated from first principles the existence of an optimal thresholding point, where the real network is maximally distant from random. Specifically, this point is found at percolation. Hence, the application of a percolation threshold allows an optimal balance between the removal of spurious connections and the maximization of the information that can be extracted from the system. A further critical outcome of this methodological study, discussed in chapter 2 of this thesis, comes from the finding of the importance of thresholding to mitigate the impact of motion and motion-correction effects on the functional connectivity organization. Importantly, I proved that, irrespectively of the presence of motion artifacts and irrespectively of the specific denoising strategy applied, the percolation threshold always maximizes the distance of the empirical network from its randomized counterpart.

In the second part of this thesis, I leveraged these novel developments to evaluate the functional connectivity alterations underlying clinical populations of alcohol dependent patients. Here, of important notice, I managed to replicate very similar findings in two independent samples of Alcohol Use Disorder (AUD) patients. Specifically, I revealed how the functional embedding of distinct neural regions involved in reward and addictive processes is critically altered in these populations of patients. Through the detection of the modular architecture of the resting alcoholic brain I demonstrated the aberrant segregation of sub-cortical basal structures and of the insular cortex. In greater detail, key regions that are part of the sub-cortical brain reward system, such as the amygdala, thalamus, and striatum, showed substantial fragmentation in their modular organization in two independent samples of AUD, opposite to what is observed in healthy subjects. Another striking findings reported from this clinical study lays in the identification of the altered role played by the insular cortex within the overall brain net-

work. Interestingly, the insula has recently caught the attention of scientists and clinicians for its centrality in addictive disorder, given its role in the translation of interoceptive feelings, such as drug urges, into decision-making and addictive behaviors. Notably, from the clinical studies addressed in this thesis, I demonstrated altered integration and segregation of the anterior portion of the insula. Indeed, these bilateral nodes present an exaggerated integrative role within the system. It is therefore suggested that this increased integration sub-served by the insula may underlie some addictive behaviors. This observation becomes critical in light of a lack of an effective treatment for AUD. Indeed, the identification of the central role of the insula is hypothesized to be a possible promising target for treatment options. In line with these findings I evaluated the effects of a putative novel treatment for AUD based on the application of a deep Transcranial Magnetic Stimulation (TMS), targeting this central region.

Repetitive TMS has recently gained popularity given its efficacy for the treatment of some psychiatric disorders, such as major depression or obsessive-compulsive disorders. Here, I specifically studied the efficacy and the stimulation-induced changes on functional connectivity in two separate studies involving the deep stimulation of the bilateral insula and the anterior cingulate cortex (ACC), a cortical region involved in addiction and presenting reciprocal connections with the insular cortex. Surprisingly, only one of the two studies reported a significant positive clinical readout. Indeed, the deep stimulation of the ACC importantly reduced craving during three weeks of deep TMS stimulations. This reduction appeared evident also during follow-up months, where patients treated with an active TMS condition maintained lower craving scores as compared to patients assigned to a sham stimulation. Unfortunately, this was not evident after a treatment targeting the bilateral insular cortex. In this case, all participants, independently from the delivery of an active or sham stimulation, reduced their alcohol intakes during three weeks of treatment, but increased amounts of drinking immediately after, as revealed by the follow-up reports. However, the stimulation of the insular cortex further revealed a re-arrangement of sub-cortical basal structures, which were previously found to be fragmented in all the AUD samples of patients studied in this thesis. It is therefore possible that in this specific case the stimulation was

effective in recovering some of the brain functional alterations, but not sufficient to translate into a positive clinical outcome.

Altogether, the preliminary results reported in my thesis appear promising. The next steps will include the evaluation of these effects on bigger samples of patients, together with a better understanding of the duration of these clinical readouts.

In conclusion, the work carried out in this PhD thesis gives significant contributions both from a methodological aspect and from a clinical perspective. We importantly bring to the network neuroscience community novel findings to improve analysis of functional graphs, involving the application of an optimal thresholding approach. On the other side, by leveraging these innovative conceptual understanding we revealed brain functional alterations in AUD patients, thus providing novel insights of potential value for treatment of this complex neuropsychiatric disorder.

APPENDIX A

In the following section, I summarize fundamental notations for a better understanding of the classical exponential random graph model formalism, followed by a more detailed explanation of the two null models introduced in chapter 2 (CWTERG and CWTECM).

CLASSICAL MAXIMUM ENTROPY RANDOM GRAPH MODELS

We let $\mathbf{G}$ denote a network in a random graph ensemble $\mathcal{G}$, and $\mathbf{G}^\star$ an observed empirical network. The ensemble $\mathcal{G}$ consists of all networks with the same number of nodes N and of the same type (undirected, weighted etc.) as $\mathbf{G}^\star$, including $\mathbf{G}^\star$ itself. Our goal is to find an analytical description of the random graphs $\mathbf{G}$ that share the same network descriptors of $\mathbf{G}^\star$, and to eventually be able to sample networks from the ensemble. In other words, we look for the functional form of the probability distribution $P(\mathbf{G})$ over the ensemble $\mathcal{G}$, for which the values of descriptors are on average as close as possible to those of the empirical network. We denote the chosen descriptors by $\mathbf{C}^\star = \mathbf{C}(\mathbf{G}^\star)$. These are network-related quantities, like the number of links, the total weight, or the node and strength sequences, and are instrumental in shaping the analytic form of the ensemble. By standard probability arguments, the expected value of the descriptors $\mathbf{C}(\mathbf{G})$ over the ensemble $\mathcal{G}$ are found as

$$\langle \mathbf{C}(\mathbf{G}) \rangle = \int_{\mathbf{G}\in\mathcal{G}} \mathbf{C}(\mathbf{G}) P(\mathbf{G}). \tag{6.1}$$

The functional form of $P(\mathbf{G})$ can be obtained by Shannon entropy maximization subjected to the constraints represented by $\mathbf{C}$. This procedure is rooted in Jaynes's Maximum Entropy formalism [Jaynes, 1957], a statistical mechanics principle that leads to exact expressions for the probability of occurrence of any graph model.

A standard derivation [Squartini and Garlaschelli, 2017, Park and Newman, 2004] shows that the solution of constrained entropy maximization problem is found by introducing a vector of Lagrange multipliers θ, one for each of the constraints in $\mathbf{C}$. The resulting conditional probability reads:

$$P(\mathbf{G}|\theta) = \frac{e^{-H(\mathbf{G},\theta)}}{Z(\theta)} \tag{6.2}$$

where $H(G,\theta)$ is the graph Hamiltonian, defined as a linear combination of constraints:

$$H(\mathbf{G},\theta) = \sum_{a} \theta_a C_a(\mathbf{G}) = \theta \cdot \mathbf{C}(\mathbf{G}) \tag{6.3}$$

and the denominator $Z(\theta)$ is a normalizing quantity called *partition function*, defined by marginalization over all networks $\mathbf{G}$ in the ensemble $\mathcal{G}$:

$$Z(\theta) = \int_{\mathbf{G}\in\mathcal{G}} e^{-H(\mathbf{G},\theta)}. \tag{6.4}$$

The above results show that the graph probability $P(G|\theta)$ depends on the Lagrange multipliers θ, and that it is a function of the constraints considered.

For model fitting purpose, it can be shown [Squartini and Garlaschelli, 2017] that the log-likelihood

$$\mathcal{L}(\theta) = \log P(\mathbf{G}^\star|\theta) = -H(\mathbf{G}^\star|\theta) - \log Z(\theta) \tag{6.5}$$

is maximized by the particular value $\theta^\star$ such that the ensemble average $\langle C\rangle_{\theta^\star}$ of each constraint equals the empirical value $C(\mathbf{G}^\star)$ measured on the real network:

$$\langle C\rangle^\star = \int_{\mathbf{G}\in\mathcal{G}} \mathbf{C}(\mathbf{G})P(\mathbf{G}|\theta^\star) = \mathbf{C}(\mathbf{G}^\star). \tag{6.6}$$

For maximum-entropy ensembles, the maximum likelihood principle indicates the choice of parameters that meet the constraints, and defines a procedure for model fitting: either by maximizing the log-likelihood from Eq. 6.5 by means of gradient based numerical optimization methods [Nocedal and Wright, 2006], or alternatively by solving the system of nonlinear equations defined by Eq. 6.6.

In the following, we show a practical application of this approach to a class of null models suitable for the description of resting-state brain connectivity.

RANDOM NETWORKS WITH FIXED LINK NUMBER AND WEIGHT

We introduce the random graph model that fixes the average total number of links $L^\star$ and the average total weight $W^\star$, together with an external threshold parameter t with the name of *Continuous Weighted Thresholded Enhanced Random Graph Model*. This model is obtained by a Hamiltonian that explicitly enforces these two constraints:

$$H_{\text{CWTERG}}(\mathbf{G}|\alpha,\beta) = \sum_{i<j} \alpha\Theta(w_{ij}-t) + \beta w_{ij}\Theta(w_{ij}-t), \tag{6.7}$$

where the Lagrangian multipliers θ of the problem are the two scalars, α and β. This Hamiltonian is designed to weight the contribution of binary links with the term α and the contribution of weighted links with the term β. The role of the threshold parameter t becomes clear if a dense network is fed in the model, and its null network is sought for as a function of the threshold. Degrees of a network are sum of binary variables, and the Heaviside function Θ is exactly centered at t, taking values one or zero if the edge weight exceeds the cut-off threshold. Similarly, the threshold t shapes the sequence of nodes strength, by contributing with a factor $\sum_j w_{ij}$ for weights greater than the cut-off t. For notation clarity, a change of variables can be performed and the original Lagrangian multipliers are replaced by their exponentiated counterparts, namely the variables $x = e^{-\alpha}$ and $y = e^{-\beta}$.

The partition function Z_{CWTERG} is obtained from the marginalization over all networks in the ensemble as in Eq. 6.4. A simple calculation for this case (see ref. [Squartini and Garlaschelli, 2017]) yields:

$$Z_{\text{CWTERG}} = \int_0^\infty e^{-H_{\text{CWTERG}}(\mathbf{G})}\, dw' \tag{6.8}$$

$$= t + \frac{e^{-\alpha-\beta t}}{\beta} = \frac{-xy^t + t\log y}{\log y} \tag{6.9}$$

The expected number of binary links is found by taking the derivatives of the free energy [Park and Newman, 2004], $F = -\log Z$ with respect to α, the Lagrangian multiplier pertaining the binary links. Similarly, the expected total weight is the derivative with respect to β of the free energy. As a result for the CWTERG we get the expressions for the link probability and expected weight, relatively:

$$\frac{\partial F}{\partial \alpha} = \langle L \rangle = \frac{1}{\beta t e^{\alpha+\beta t} + 1} = \frac{x y^t}{x y^t - t \log y} \tag{6.10}$$

$$\frac{\partial F}{\partial \beta} = \langle W \rangle = \frac{\beta t + 1}{\beta(\beta t e^{\alpha+\beta t} + 1)} = \frac{x y^t \left(-t \log y + 1\right)}{\left(-x y^t + t \log y\right) \log\left(y\right)} \tag{6.11}$$

Fitting the CWTERG model to empirical networks requires one to simultaneously solve a system of two nonlinear equations, and finding the values of the Lagrangian multipliers x, y such that:

$$\begin{cases} L^\star &= \frac{x y^t}{x y^t - t \log y} \\ W^\star &= \frac{x y^t (-t \log y + 1)}{(-x y^t + t \log y) \log(y)} \end{cases} \tag{6.12}$$

Alternatively, and in a completely complementary fashion, one can maximize the log-likelihood of the model $\mathcal{L}_{\text{CWTERG}}$, calculated as the logarithm of the conditional probability $P(\mathbf{G}|x, y)$:

$$\begin{aligned} \mathcal{L}_{\text{CWTERG}}(\mathbf{G}|x, y) =& L(\mathbf{G}) \log x + W(\mathbf{G}) \log y \\ &- \binom{N}{2} \log\left(t - \frac{x y^t}{\log y}\right). \end{aligned} \tag{6.13}$$

RANDOM NETWORKS WITH FIXED DEGREES AND STRENGTHS

The CWTERG model describes the ensemble of networks whose total weight and number of links are constrained to some empirical values. Hence it can be considered an extension of the Erdős-Renyi random graph model to thresholded weighted networks. However, this model only describes networks with uniform connectivity patterns, as it is not considering the heterogeneity of the degrees and strengths.

The Continuous Weighted Thresholded Enhanced Configuration Model (CTWECM) overcomes this problem by defining a Hamiltonian

$$H_{\text{CWTECM}}(\mathbf{G}|\boldsymbol{\alpha},\boldsymbol{\beta}) = \sum_{i<j}(\alpha_i+\alpha_j)\Theta(w_{ij}-t)+ \\ (\beta_i+\beta_j)w_{ij}\Theta(w_{ij}-t). \tag{6.14}$$

where α_i, β_i are the Lagrangian multipliers. The structural form of the Hamiltonian of the CWTECM is the same as the one of the CWTERG, but now the probability $P(\mathbf{G}|\boldsymbol{\alpha},\boldsymbol{\beta})$ can be factorized over all pairs of nodes as follows:

$$P(\mathbf{G}|\boldsymbol{\alpha},\boldsymbol{\beta}) = \prod_{i<j}\frac{e^{-[\alpha_i+\alpha_j+w_{ij}(\beta_i+\beta_j)]\theta(w_{ij}-t)}}{Z_{\text{CWTECM}}} \tag{6.15}$$

where here $Z_{\text{CWTECM}} = t + \frac{e^{-\alpha_i-\alpha_j-t(\beta_i+\beta_j)}}{\beta_i+\beta_j}$.

With the change of variables $x_i = e^{-\alpha_i}$, $y_i = e^{-\beta_i}$ the expected link probability and expected link weight have the same form found in Eq. 6.10, and are obtained by the first derivatives of the free energy with respect to the Lagrange multipliers α_i and β_j as follows:

$$\frac{\partial F}{\partial \alpha_i} = \langle a_{ij}\rangle = \frac{x_i x_j\left(y_i y_j\right)^t}{x_i x_j\left(y_i y_j\right)^t - \log\left(y_i y_j\right)^t} \tag{6.16}$$

$$\frac{\partial F}{\partial \beta_i} = \langle w_{ij}\rangle = \frac{x_i x_j\left(y_i y_j\right)^t\left[\log\left(y_i y_j\right)^t - 1\right]}{\left[x_i x_j\left(y_i y_j\right)^t - \log\left(\left(y_i y_j\right)^t\right)\right]\log\left(y_i y_j\right)}. \tag{6.17}$$

The expected degree and strengths are found by summing the link probability and the expected link weights over all remaining nodes:

$$\langle k_i\rangle = \sum_{i\neq j}\langle a_{ij}\rangle \tag{6.18}$$

$$\langle s_i\rangle = \sum_{i\neq j}\langle w_{ij}\rangle \tag{6.19}$$

and at the optimal parameters $\alpha_i^\star, \beta_i^\star$ they equal their empirical counterparts $\langle k_i \rangle_{\alpha^\star,\beta^\star} = k_i^\star$ and $\langle s_i \rangle_{\alpha^\star,\beta^\star} = s_i^\star$. Similarly to the CWTECM, the optimal parameters can be found by maximization of a log-likelihood function that reads:

$$\mathcal{L}_{\text{CWTECM}}(\mathbf{G}|x,y) = \sum_i s_i(\mathbf{G}) \log y_i + k_i(\mathbf{G}) \log x_i + \sum_{i<j} \log\left(\frac{\log(y_i y_j)}{t\left(\log(y_i y_j)\right) - x_i x_j \left(y_i y_j\right)^t}\right). \tag{6.20}$$

BIBLIOGRAPHY

[Absalom et al., 2007] Absalom, A., Lee, M., Menon, D., Sharar, S., De Smet, T., Halliday, J., Ogden, M., Corlett, P., Honey, G., and Fletcher, P. (2007). Predictive performance of the domino, hijazi, and clements models during low-dose target-controlled ketamine infusions in healthy volunteers. *British journal of anaesthesia*, 98(5):615–623.

[Achard and Bullmore, 2007] Achard, S. and Bullmore, E. (2007). Efficiency and Cost of Economical Brain Functional Networks. *PLoS Computational Biology*, 3(2).

[Addolorato et al., 2017] Addolorato, G., Antonelli, M., Cocciolillo, F., Vassallo, G. A., Tarli, C., Sestito, L., Mirijello, A., Ferrulli, A., Pizzuto, D. A., Camardese, G., et al. (2017). Deep transcranial magnetic stimulation of the dorsolateral prefrontal cortex in alcohol use disorder patients: effects on dopamine transporter availability and alcohol intake. *European Neuropsychopharmacology*, 27(5):450–461.

[Alderson-Day et al., 2015] Alderson-Day, B., McCarthy-Jones, S., and Fernyhough, C. (2015). Hearing voices in the resting brain: A review of intrinsic functional connectivity research on auditory verbal hallucinations. *Neuroscience & Biobehavioral Reviews*, 55:78–87.

[Alexander-Bloch et al., 2012] Alexander-Bloch, A., Lambiotte, R., Roberts, B., Giedd, J., Gogtay, N., and Bullmore, E. (2012). The discovery of population differences in network community structure: New methods and applications to brain functional networks in schizophrenia. *Neuroimage*, 59(4):3889–3900.

[Alexander-Bloch et al., 2010] Alexander-Bloch, A. F., Gogtay, N., Meunier, D., Birn, R., Clasen, L., Lalonde, F., Lenroot, R., Giedd, J., and Bullmore, E. T. (2010). Disrupted modularity and local connectivity of brain functional networks in childhood-onset schizophrenia. *Frontiers in systems neuroscience*, 4:147.

[Ambite et al., 2015] Ambite, J. L., Tallis, M., Alpert, K., Keator, D. B., King, M., Landis, D., Konstantinidis, G., Calhoun, V. D., Potkin, S. G., Turner, J. A., et al. (2015). Schizconnect: virtual data integration in neuroimaging. In *International Conference on Data Integration in the Life Sciences*, pages 37–51. Springer.

[American Psychiatric Association, 2013] American Psychiatric Association (2013). *Diagnostic and statistical manual of mental disorders: DSM-5*. Autor, Washington, DC, 5th ed. edition.

[Anderson and Cohen, 2013] Anderson, A. and Cohen, M. S. (2013). Decreased small-world functional network connectivity and clustering across resting state networks in schizophrenia: an fMRI classification tutorial. *Front. Hum. Neurosci.*, 7(September):520.

[Avena-Koenigsberger et al., 2018] Avena-Koenigsberger, A., Misic, B., and Sporns, O. (2018). Communication dynamics in complex brain networks. *Nature Reviews Neuroscience*, 19(1):17.

[Azondekon et al., 2018] Azondekon, R., Harper, Z. J., and Welzig, C. M. (2018). Combined meg and fmri exponential random graph modeling for inferring functional brain connectivity. *arXiv preprint arXiv:1805.12005*.

[Bassett et al., 2008] Bassett, D. S., Bullmore, E., Verchinski, B. A., Mattay, V. S., Weinberger, D. R., and Meyer-Lindenberg, A. (2008). Hierarchical organization of human cortical networks in health and schizophrenia. *J. Neurosci.*, 28(37):9239–9248.

[Bassett et al., 2011] Bassett, D. S., Wymbs, N. F., Porter, M. A., Mucha, P. J., Carlson, J. M., and Grafton, S. T. (2011). Dynamic reconfiguration of human brain networks during learning. *Proceedings of the National Academy of Sciences*, 108(18):7641–7646.

[Beckmann et al., 2005] Beckmann, C. F., DeLuca, M., Devlin, J. T., and Smith, S. M. (2005). Investigations into resting-state connectivity using independent component analysis. *Philos. Trans. R. Soc. Lond. B. Biol. Sci.*, 360:1001–1013.

[Behzadi et al., 2007] Behzadi, Y., Restom, K., Liau, J., and Liu, T. T. (2007). A component based noise correction method (compcor) for bold and perfusion based fmri. *Neuroimage*, 37(1):90–101.

[Betzel and Bassett, 2017] Betzel, R. F. and Bassett, D. S. (2017). Generative models for network neuroscience: prospects and promise. *J. R. Soc. Interface*, 14(136):20170623.

[Bifone and Gozzi, 2012] Bifone, A. and Gozzi, A. (2012). Neuromapping techniques in drug discovery: pharmacological MRI for the assessment of novel antipsychotics. *Expert Opinion on Drug Discovery*, 7(11):1071–1082.

[Biswal et al., 1995] Biswal, B., Zerrin Yetkin, F., Haughton, V. M., and Hyde, J. S. (1995). Functional connectivity in the motor cortex of resting human brain using echo-planar mri. *Magn. Reson. Med.*, 34:537–541.

[Bleuler, 1950] Bleuler, E. (1950). Dementia praecox or the group of schizophrenias.

[Bordier et al., 2017] Bordier, C., Nicolini, C., and Bifone, A. (2017). Graph Analysis and Modularity of Brain Functional Connectivity Networks: Searching for the Optimal Threshold. *Frontiers in Neuroscience*, 11.

[Bordier et al., 2018] Bordier, C., Nicolini, C., Forcellini, G., and Bifone, A. (2018). Disrupted modular organization of primary sensory brain areas in schizophrenia. *NeuroImage: Clinical*, 18:682–693.

[Bullmore and Sporns, 2009] Bullmore, E. and Sporns, O. (2009). Complex brain networks: graph theoretical analysis of structural and functional systems. *Nature reviews neuroscience*, 10(3):186.

[Burgess et al., 2016] Burgess, G. C., Kandala, S., Nolan, D., Laumann, T. O., Power, J. D., Adeyemo, B., Harms, M. P., Petersen, S. E., and Barch, D. M. (2016). Evaluation of denoising strategies to address motion-correlated artifacts in resting-state functional magnetic resonance imaging data from the human connectome project. *Brain connectivity*, 6(9):669–680.

[Calhoun et al., 2009] Calhoun, V. D., Eichele, T., and Pearlson, G. (2009). Functional brain networks in schizophrenia: a review. *Front. Hum. Neurosci.*, 3(August):17.

[Camchong et al., 2013] Camchong, J., Stenger, A., and Fein, G. (2013). Resting-state synchrony during early alcohol abstinence can predict subsequent relapse. *Cerebral Cortex*.

[Camprodon et al., 2007] Camprodon, J. A., Martínez-Raga, J., Alonso-Alonso, M., Shih, M.-C., and Pascual-Leone, A. (2007). One session of high frequency repetitive transcranial magnetic stimulation (rtms) to the right prefrontal cortex transiently reduces cocaine craving. *Drug and alcohol dependence*, 86(1):91–94.

[Cantwell et al., 2019] Cantwell, G., Liu, Y., Maier, B. F., Schwarze, A. C., Serván, C. A., Snyder, J., and St-Onge, G. (2019). Thresholding normally distributed data creates complex networks.

[Cardenas et al., 2007] Cardenas, V. A., Studholme, C., Gazdzinski, S., Durazzo, T. C., and Meyerhoff, D. J. (2007). Deformation-based morphometry of brain changes in alcohol dependence and abstinence. *Neuroimage*, 34(3):879–887.

[Çetin et al., 2014] Çetin, M. S., Christensen, F., Abbott, C. C., Stephen, J. M., Mayer, A. R., CaÃ±ive, J. M., Bustillo, J. R., Pearlson, G. D., and Calhoun, V. D. (2014). Thalamus and posterior temporal lobe show greater inter-network connectivity at rest and across sensory paradigms in schizophrenia. *NeuroImage*, 97:117–126.

[Ceccanti et al., 2015] Ceccanti, M., Inghilleri, M., Attilia, M. L., Raccah, R., Fiore, M., Zangen, A., and Ceccanti, M. (2015). Deep tms on alcoholics: effects on cortisolemia and dopamine pathway modulation. a pilot study. *Canadian journal of physiology and pharmacology*, 93(4):283–290.

[Chang and Lenzenweger, 2005] Chang, B. P. and Lenzenweger, M. F. (2005). Somatosensory processing and schizophrenia liability: proprioception, exteroceptive sensitivity, and graphesthesia performance in the biological relatives of schizophrenia patients. *Journal of abnormal psychology*, 114(1):85.

[Chanraud et al., 2007] Chanraud, S., Martelli, C., Delain, F., Kostogianni, N., Douaud, G., Aubin, H.-J., Reynaud, M., and Martinot, J.-L. (2007). Brain morphometry and cognitive performance in detoxified alcohol-dependents with preserved psychosocial functioning. *Neuropsychopharmacology*, 32(2):429.

[Chanraud et al., 2011] Chanraud, S., Pitel, A.-L., Pfefferbaum, A., and Sullivan, E. V. (2011). Disruption of functional connectivity of the default-mode network in alcoholism. *Cerebral cortex*, 21(10):2272–2281.

[Chase et al., 2011] Chase, H. W., Eickhoff, S. B., Laird, A. R., and Hogarth, L. (2011). The neural basis of drug stimulus processing and craving: an activation likelihood estimation meta-analysis. *Biological psychiatry*, 70(8):785–793.

[Chikama et al., 1997] Chikama, M., McFarland, N. R., Amaral, D. G., and Haber, S. N. (1997). Insular cortical projections to functional regions of the striatum correlate with cortical cytoarchitectonic organization in the primate. *Journal of Neuroscience*, 17(24):9686–9705.

[Cho and Strafella, 2009] Cho, S. S. and Strafella, A. P. (2009). rtms of the left dorsolateral prefrontal cortex modulates dopamine release in the ipsilateral anterior cingulate cortex and orbitofrontal cortex. *PloS one*, 4(8):e6725.

[Chung and Clark, 2014] Chung, T. and Clark, D. B. (2014). Insula white matter volume linked to binge drinking frequency through enhancement motives in treated adolescents. *Alcoholism: Clinical and Experimental Research*, 38(7):1932–1940.

[Cimini et al., 2019] Cimini, G., Squartini, T., Saracco, F., Garlaschelli, D., Gabrielli, A., and Caldarelli, G. (2019). The statistical physics of real-world networks. *Nature Reviews Physics*, 1(1):58.

[Ciric et al., 2017] Ciric, R., Wolf, D. H., Power, J. D., Roalf, D. R., Baum, G. L., Ruparel, K., Shinohara, R. T., Elliott, M. A., Eickhoff, S. B., Davatzikos, C., et al. (2017). Benchmarking of participant-level confound regression strategies for the control of motion artifact in studies of functional connectivity. *Neuroimage*, 154:174–187.

[Claus et al., 2011] Claus, E. D., Ewing, S. W. F., Filbey, F. M., Sabbineni, A., and Hutchison, K. E. (2011). Identifying neurobiological phenotypes associated with alcohol use disorder severity. *Neuropsychopharmacology*, 36(10):2086.

[Cole et al., 2010] Cole, D. M., Smith, S. M., and Beckmann, C. F. (2010). Advances and pitfalls in the analysis and interpretation of resting-state fmri data. *Frontiers in systems neuroscience*, 4:8.

[Cortes et al., 2018] Cortes, C. R., Grodin, E. N., Mann, C. L., Mathur, K., Kerich, M., Zhu, X., Schwandt, M., Diazgranados, N., George, D. T., Momenan, R., et al. (2018). Insula sensitivity to unfairness in alcohol use disorder. *Alcohol and Alcoholism*, 53(3):201–208.

[Courtney et al., 2013] Courtney, K. E., Ghahremani, D. G., and Ray, L. A. (2013). Fronto-striatal functional connectivity during response inhibition in alcohol dependence. *Addiction biology*, 18(3):593–604.

[Craig, 2009] Craig, A. D. (2009). How do you feel–now? the anterior insula and human awareness. *Nature reviews neuroscience*, 10(1).

[Crossley et al., 2013] Crossley, N. A., Mechelli, A., Vertes, P. E., Winton-Brown, T. T., Patel, A. X., Ginestet, C. E., McGuire, P., and Bullmore, E. T. (2013). Cognitive relevance of the community structure of the human brain functional coactivation network. *Proceedings of the National Academy of Sciences*.

[Csardi and Nepusz, 2006] Csardi, G. and Nepusz, T. (2006). The igraph software package for complex network research. *InterJournal*, Complex Systems:1695.

[Ćurčić-Blake et al., 2017] Ćurčić-Blake, B., Ford, J. M., Hubl, D., Orlov, N. D., Sommer, I. E., Waters, F., Allen, P., Jardri, R., Woodruff, P. W., David, O., Mulert, C., Woodward, T. S., and Aleman, A. (2017). Interaction of language, auditory and memory brain networks in auditory verbal hallucinations. *Progress in Neurobiology*, 148:1–20.

[Damoiseaux et al., 2006] Damoiseaux, J. S., Rombouts, S. A. R. B., Barkhof, F., Scheltens, P., Stam, C. J., Smith, S. M., and Beckmann, C. F. (2006). Consistent resting-state networks across healthy subjects. *Proc. Natl. Acad. Sci. U.S.A.*, 103:13848–13853.

[De Domenico and Biamonte, 2016] De Domenico, M. and Biamonte, J. (2016). Spectral entropies as information-theoretic tools for complex network comparison. *Phys. Rev. X*, 6:041062.

[de Haan et al., 2012] de Haan, W., van der Flier, W. M., Koene, T., Smits, L. L., Scheltens, P., and Stam, C. J. (2012). Disrupted modular brain dynamics reflect cognitive dysfunction in alzheimer's disease. *Neuroimage*, 59(4):3085–3093.

[De Ridder et al., 2011] De Ridder, D., Vanneste, S., Kovacs, S., Sunaert, S., and Dom, G. (2011). Transient alcohol craving suppression by rtms of dorsal anterior cingulate: an fmri and loreta eeg study. *Neuroscience letters*, 496(1):5–10.

[De Simoni et al., 2013] De Simoni, S., Schwarz, A. J., Daly, O. G. O., Marquand, A. F., Brittain, C., Gonzales, C., Stephenson, S., Williams, S. C. R., and Mehta, M. A. (2013). Test–retest reliability of the BOLD pharmacological MRI response to ketamine in healthy volunteers. *NeuroImage*, 64:75–90.

[de Vico Fallani et al., 2017] de Vico Fallani, F., Latora, V., and Chavez, M. (2017). A topological criterion for filtering information in complex brain networks. *PLoS computational biology*, 13(1):e1005305.

[Deakin et al., 2008] Deakin, J. F. W., Lees, J., McKie, S., Hallak, J. E. C., Williams, S. R., and Dursun, S. M. (2008). Glutamate and the Neural Basis of the Subjective Effects of Ketamine. *Archives of General Psychiatry*, 65(2):154.

[Del Felice et al., 2016] Del Felice, A., Bellamoli, E., Formaggio, E., Manganotti, P., Masiero, S., Cuoghi, G., Rimondo, C., Genetti, B., Sperotto, M., Corso, F., et al. (2016). Neurophysiological, psychological and behavioural correlates of rtms treatment in alcohol dependence. *Drug and alcohol dependence*, 158:147–153.

[Demirakca et al., 2011] Demirakca, T., Ende, G., Kämmerer, N., Welzel-Marquez, H., Hermann, D., Heinz, A., and Mann, K. (2011). Effects of alcoholism and continued abstinence on brain volumes in both genders. *Alcoholism: Clinical and Experimental Research*, 35(9):1678–1685.

[Dinur-Klein et al., 2014] Dinur-Klein, L., Dannon, P., Hadar, A., Rosenberg, O., Roth, Y., Kotler, M., and Zangen, A. (2014). Smoking cessation induced by deep

repetitive transcranial magnetic stimulation of the prefrontal and insular cortices: a prospective, randomized controlled trial. *Biological psychiatry*, 76(9):742–749.

[Doyle et al., 2013] Doyle, O. M., Simoni, S. D., Schwarz, A. J., Brittain, C., Williams, S. C. R., and Mehta, M. A. (2013). Quantifying the Attenuation of the Ketamine Pharmacological Magnetic Resonance Imaging Response in Humans: A Validation Using Antipsychotic and Glutamatergic Agents. pages 151–160.

[Driesen et al., 2013] Driesen, N. R., McCarthy, G., Bhagwagar, Z., Bloch, M., Calhoun, V., D'Souza, D. C., Gueorguieva, R., He, G., Ramachandran, R., Suckow, R. F., et al. (2013). Relationship of resting brain hyperconnectivity and schizophrenia-like symptoms produced by the nmda receptor antagonist ketamine in humans. *Molecular psychiatry*, 18(11):1199.

[Dupuy and Chanraud, 2016] Dupuy, M. and Chanraud, S. (2016). Imaging the addicted brain: alcohol. In *International review of neurobiology*, volume 129, pages 1–31. Elsevier.

[Durazzo et al., 2011] Durazzo, T. C., Tosun, D., Buckley, S., Gazdzinski, S., Mon, A., Fryer, S. L., and Meyerhoff, D. J. (2011). Cortical thickness, surface area, and volume of the brain reward system in alcohol dependence: relationships to relapse and extended abstinence. *Alcoholism: Clinical and Experimental Research*, 35(6):1187–1200.

[Esfahlani and Sayama, 2018] Esfahlani, F. Z. and Sayama, H. (2018). A percolation-based thresholding method with applications in functional connectivity analysis. In *International Workshop on Complex Networks*, pages 221–231. Springer.

[Fede et al., 2019] Fede, S. J., Grodin, E. N., Dean, S. F., Diazgranados, N., and Momenan, R. (2019). Resting state connectivity best predicts alcohol use severity in moderate to heavy alcohol users. *Neuroimage: clinical*, 22:101782.

[Fitzgerald, 2009] Fitzgerald, P. B. (2009). Repetitive transcranial magnetic stimulation treatment for depression: lots of promise but still lots of questions. *Brain Stimulation: Basic, Translational, and Clinical Research in Neuromodulation*, 2(4):185–187.

[Fornito et al., 2015] Fornito, A., Zalesky, A., and Breakspear, M. (2015). The connectomics of brain disorders. *Nature Reviews Neuroscience*, 16(3):159.

[Fornito et al., 2016] Fornito, A., Zalesky, A., and Bullmore, E. (2016). *Fundamentals of brain network analysis.*

[Fornito et al., 2012] Fornito, A., Zalesky, A., Pantelis, C., and Bullmore, E. T. (2012). Schizophrenia, neuroimaging and connectomics. *Neuroimage*, 62(4):2296–2314.

[Fox et al., 2005] Fox, M. D., Snyder, A. Z., Vincent, J. L., Corbetta, M., Van Essen, D. C., and Raichle, M. E. (2005). The human brain is intrinsically organized into dynamic, anticorrelated functional networks. *Proceedings of the National Academy of Sciences*, 102(27):9673–9678.

[Fox et al., 2009] Fox, M. D., Zhang, D., Snyder, A. Z., and Raichle, M. E. (2009). The global signal and observed anticorrelated resting state brain networks. *Journal of neurophysiology*, 101(6):3270–3283.

[Friston and Frith, 1995] Friston, K. J. and Frith, C. D. (1995). Schizophrenia: a disconnection syndrome. *Clin Neurosci*, 3(2):89–97.

[Friston et al., 1996] Friston, K. J., Williams, S., Howard, R., Frackowiak, R. S., and Turner, R. (1996). Movement-related effects in fmri time-series. *Magnetic resonance in medicine*, 35(3):346–355.

[Fritz et al., 2019] Fritz, M., Klawonn, A. M., and Zahr, N. M. (2019). Neuroimaging in alcohol use disorder: From mouse to man. *Journal of neuroscience research*.

[Gallos et al., 2012] Gallos, L. K., Makse, H. a., and Sigman, M. (2012). A small world of weak ties provides optimal global integration of self-similar modules in functional brain networks. *Proc. Natl. Acad. Sci. U. S. A.*, 109(8):2825–2830.

[Garcia et al., 2018] Garcia, J. O., Ashourvan, A., Muldoon, S., Vettel, J. M., and Bassett, D. S. (2018). Applications of community detection techniques to brain graphs: Algorithmic considerations and implications for neural function. *Proceedings of the IEEE*, 106(5):846–867.

[Gazdzinski et al., 2005] Gazdzinski, S., Durazzo, T. C., and Meyerhoff, D. J. (2005). Temporal dynamics and determinants of whole brain tissue volume changes during recovery from alcohol dependence. *Drug and alcohol dependence*, 78(3):263–273.

[Gaznick et al., 2013] Gaznick, N., Tranel, D., McNutt, A., and Bechara, A. (2013). Basal ganglia plus insula damage yields stronger disruption of smoking addiction than basal ganglia damage alone. *nicotine & tobacco research*, 16(4):445–453.

[Genovese et al., 2002] Genovese, C. R., Lazar, N. A., and Nichols, T. (2002). Thresholding of statistical maps in functional neuroimaging using the false discovery rate. *Neuroimage*, 15(4):870–878.

[Goa et al., 1993] Goa, K. L., Ross, S. R., and Chrisp, P. (1993). Lamotrigine. *Drugs*, 46(1):152–176.

[Goldstein et al., 2009] Goldstein, R. Z., Bechara, A., Garavan, H., Childress, A. R., Paulus, M. P., Volkow, N. D., et al. (2009). The neurocircuitry of impaired insight in drug addiction. *Trends in cognitive sciences*, 13(9):372–380.

[Good et al., 2010] Good, B. H., De Montjoye, Y.-A., and Clauset, A. (2010). Performance of modularity maximization in practical contexts. *Physical Review E*, 81(4):046106.

[Gordon et al., 2018] Gordon, E. M., Lynch, C. J., Gratton, C., Laumann, T. O., Gilmore, A. W., Greene, D. J., Ortega, M., Nguyen, A. L., Schlaggar, B. L., Petersen, S. E., et al. (2018). Three distinct sets of connector hubs integrate human brain function. *Cell reports*, 24(7):1687–1695.

[Goulas et al., 2015] Goulas, A., Schaefer, A., and Margulies, D. S. (2015). The strength of weak connections in the macaque cortico-cortical network. *Brain Structure and Function*, 220(5):2939–2951.

[Grant and Chamberlain, 2016] Grant, J. E. and Chamberlain, S. R. (2016). Expanding the definition of addiction: DSM-5 vs. ICD-11. *CNS spectrums*, 21(4):300–3.

[Griffanti et al., 2017] Griffanti, L., Douaud, G., Bijsterbosch, J., Evangelisti, S., Alfaro-Almagro, F., Glasser, M. F., Duff, E. P., Fitzgibbon, S., Westphal, R.,

Carone, D., et al. (2017). Hand classification of fmri ica noise components. *Neuroimage*, 154:188–205.

[Grodin et al., 2018] Grodin, E. N., Sussman, L., Sundby, K., Brennan, G. M., Diazgranados, N., Heilig, M., and Momenan, R. (2018). Neural correlates of compulsive alcohol seeking in heavy drinkers. *Biological Psychiatry: Cognitive Neuroscience and Neuroimaging*, 3(12):1022–1031.

[Grüsser et al., 2004] Grüsser, S. M., Wrase, J., Klein, S., Hermann, D., Smolka, M. N., Ruf, M., Weber-Fahr, W., Flor, H., Mann, K., Braus, D. F., et al. (2004). Cue-induced activation of the striatum and medial prefrontal cortex is associated with subsequent relapse in abstinent alcoholics. *Psychopharmacology*, 175(3):296–302.

[Guimera and Amaral, 2005] Guimera, R. and Amaral, L. A. N. (2005). Functional cartography of complex metabolic networks. *nature*, 433(7028):895.

[Hallquist and Hillary, 2019] Hallquist, M. N. and Hillary, F. G. (2019). Graph theory approaches to functional network organization in brain disorders: A critique for a brave new small-world. *Network Neuroscience*, 3(1):1–26.

[Heilig and Egli, 2006] Heilig, M. and Egli, M. (2006). Pharmacological treatment of alcohol dependence: target symptoms and target mechanisms. *Pharmacology & therapeutics*, 111(3):855–876.

[Heilig et al., 2011] Heilig, M., Goldman, D., Berrettini, W., and O'Brien, C. P. (2011). Pharmacogenetic approaches to the treatment of alcohol addiction. *Nature Reviews Neuroscience*, 12(11):670–684.

[Heinz et al., 2009] Heinz, A., Beck, A., Grüsser, S. M., Grace, A. A., and Wrase, J. (2009). Identifying the neural circuitry of alcohol craving and relapse vulnerability. *Addiction biology*, 14(1):108–118.

[Herremans et al., 2012] Herremans, S., Baeken, C., Vanderbruggen, N., Vanderhasselt, M.-A., Zeeuws, D., Santermans, L., and De Raedt, R. (2012). No influence of one right-sided prefrontal hf-rtms session on alcohol craving in recently detoxified alcohol-dependent patients: results of a naturalistic study. *Drug and alcohol dependence*, 120(1-3):209–213.

[Herremans et al., 2013] Herremans, S., Vanderhasselt, M.-A., De Raedt, R., and Baeken, C. (2013). Reduced intra-individual reaction time variability during a go–nogo task in detoxified alcohol-dependent patients after one right-sided dorsolateral prefrontal hf-rtms session. *Alcohol and alcoholism*, 48(5):552–557.

[Herremans et al., 2016] Herremans, S. C., De Raedt, R., Van Schuerbeek, P., Marinazzo, D., Matthys, F., De Mey, J., and Baeken, C. (2016). Accelerated hf-rtms protocol has a rate-dependent effect on dacc activation in alcohol-dependent patients: An open-label feasibility study. *Alcoholism: Clinical and Experimental Research*, 40(1):196–205.

[Herremans et al., 2015] Herremans, S. C., Van Schuerbeek, P., De Raedt, R., Matthys, F., Buyl, R., De Mey, J., and Baeken, C. (2015). The impact of accelerated right prefrontal high-frequency repetitive transcranial magnetic stimulation (rtms) on cue-reactivity: an fmri study on craving in recently detoxified alcohol-dependent patients. *PLoS One*, 10(8):e0136182.

[Hone-Blanchet et al., 2015] Hone-Blanchet, A., Ciraulo, D. A., Pascual-Leone, A., and Fecteau, S. (2015). Noninvasive brain stimulation to suppress craving in substance use disorders: review of human evidence and methodological considerations for future work. *Neuroscience & Biobehavioral Reviews*, 59:184–200.

[Höppner et al., 2011] Höppner, J., Broese, T., Wendler, L., Berger, C., and Thome, J. (2011). Repetitive transcranial magnetic stimulation (rtms) for treatment of alcohol dependence. *The World Journal of Biological Psychiatry*, 12(sup1):57–62.

[Howers et al., 2015] Howers, O., McCutcheon, R., and Stone, J. M. (2015). Glutamate and dopamine in schizophrenia: an update for the 21st century. *Journal of Psychopharmachology*, 29(2):97–115.

[Jaynes, 1957] Jaynes, E. T. (1957). Information theory and statistical mechanics. *Phys. Rev.*, 106(4):620–630.

[Jenkinson et al., 2002] Jenkinson, M., Bannister, P., Brady, M., and Smith, S. (2002). Improved optimization for the robust and accurate linear registration and motion correction of brain images. *Neuroimage*, 17(2):825–841.

[Jenkinson et al., 2012] Jenkinson, M., Beckmann, C. F., Behrens, T. E., Woolrich, M. W., and Smith, S. M. (2012). Fsl. *Neuroimage*, 62(2):782–790.

[Johann et al., 2003] Johann, M., Wiegand, R., Kharraz, A., Bobbe, G., Sommer, G., Hajak, G., Wodarz, N., and Eichhammer, P. (2003). Repetitiv transcranial magnetic stimulation in nicotine dependence. *Psychiatrische Praxis*, 30(Suppl 2):129–131.

[Jonas et al., 2014] Jonas, D. E., Amick, H. R., Feltner, C., Bobashev, G., Thomas, K., Wines, R., Kim, M. M., Shanahan, E., Gass, C. E., Rowe, C. J., et al. (2014). Pharmacotherapy for adults with alcohol use disorders in outpatient settings: a systematic review and meta-analysis. *Jama*, 311(18):1889–1900.

[Jones et al., 2013] Jones, D. K., Knösche, T. R., and Turner, R. (2013). White matter integrity, fiber count, and other fallacies: the do's and don'ts of diffusion mri. *Neuroimage*, 73:239–254.

[Joules et al., 2015] Joules, R., Doyle, O. M., Schwarz, A. J., O'Daly, O. G., Brammer, M., Williams, S. C., and Mehta, M. A. (2015). Ketamine induces a robust whole-brain connectivity pattern that can be differentially modulated by drugs of different mechanism and clinical profile. *Psychopharmacology*, 232(21-22):4205–4218.

[Jung et al., 2007] Jung, Y. C., Jang, D.-P., Namkoong, K., Ku, J., Kim, J.-J., Park, S., Cho, Z.-H., Kim, Y.-B., and Lee, E. (2007). Shape deformation of the insula in alcoholics: reduction of left–right asymmetry. *Neuroreport*, 18(17):1787–1791.

[Kashtan and Alon, 2005] Kashtan, N. and Alon, U. (2005). Spontaneous evolution of modularity and network motifs. *Proceedings of the National Academy of Sciences*, 102(39):13773–13778.

[Kawamoto and Rosvall, 2015] Kawamoto, T. and Rosvall, M. (2015). Estimating the resolution limit of the map equation in community detection. *Physical Review E*, 91(1):012809.

[Konradsson et al., 2006] Konradsson, Å., Marcus, M. M., Hertel, P., Svensson, T. H., and Jardemark, K. E. (2006). Inhibition of the glycine transporter glyt-1

potentiates the effect of risperidone, but not clozapine, on glutamatergic transmission in the rat medial prefrontal cortex. *Synapse*, 60(2):102–108.

[Koob, 2011] Koob, G. F. (2011). Theoretical frameworks and mechanistic aspects of alcohol addiction: alcohol addiction as a reward deficit disorder. In *Behavioral neurobiology of alcohol addiction*, pages 3–30. Springer.

[Koob, 2013] Koob, G. F. (2013). Addiction is a reward deficit and stress surfeit disorder. *Frontiers in psychiatry*, 4:72.

[Koob and Volkow, 2010] Koob, G. F. and Volkow, N. D. (2010). Neurocircuitry of addiction. *Neuropsychopharmacology*, 35(1):217.

[Koob and Volkow, 2016] Koob, G. F. and Volkow, N. D. (2016). Neurobiology of addiction: a neurocircuitry analysis. *The Lancet Psychiatry*, 3(8):760–773.

[Kühn and Gallinat, 2011] Kühn, S. and Gallinat, J. (2011). Common biology of craving across legal and illegal drugs–a quantitative meta-analysis of cue-reactivity brain response. *European Journal of Neuroscience*, 33(7):1318–1326.

[Lam et al., 2008] Lam, R. W., Chan, P., Wilkins-Ho, M., and Yatham, L. N. (2008). Repetitive transcranial magnetic stimulation for treatment-resistant depression: a systematic review and metaanalysis. *The Canadian Journal of Psychiatry*, 53(9):621–631.

[Lancichinetti and Fortunato, 2012] Lancichinetti, A. and Fortunato, S. (2012). Consensus clustering in complex networks. *Sci. Rep.*, 2:336.

[Large et al., 2005] Large, C. H., Webster, E. L., and Goff, D. C. (2005). The potential role of lamotrigine in schizophrenia. *Psychopharmacology*, 181(3):415–436.

[Lerman-Sinkoff and Barch, 2016] Lerman-Sinkoff, D. B. and Barch, D. M. (2016). Network community structure alterations in adult schizophrenia: Identification and localization of alterations. *NeuroImage Clin.*, 10:96–106.

[Li et al., 2009] Li, C.-s. R., Luo, X., Yan, P., Bergquist, K., and Sinha, R. (2009). Altered impulse control in alcohol dependence: neural measures of stop signal performance. *Alcoholism: Clinical and Experimental Research*, 33(4):740–750.

[Lindquist et al., 2019] Lindquist, M. A., Geuter, S., Wager, T. D., and Caffo, B. S. (2019). Modular preprocessing pipelines can reintroduce artifacts into fmri data. *Human brain mapping*.

[Liu et al., 2008] Liu, Y., Liang, M., Zhou, Y., He, Y., Hao, Y., Song, M., Yu, C., Liu, H., Liu, Z., and Jiang, T. (2008). Disrupted small-world networks in schizophrenia. *Brain*, 131(4):945–961.

[Lohse et al., 2014] Lohse, C., Bassett, D. S., Lim, K. O., and Carlson, J. M. (2014). Resolving Anatomical and Functional Structure in Human Brain Organization: Identifying Mesoscale Organization in Weighted Network Representations. *PLoS Computational Biology*, 10(10).

[Loo and Mitchell, 2005] Loo, C. K. and Mitchell, P. B. (2005). A review of the efficacy of transcranial magnetic stimulation (tms) treatment for depression, and current and future strategies to optimize efficacy. *Journal of affective disorders*, 88(3):255–267.

[Lowe et al., 1998] Lowe, M., Mock, B., and Sorenson, J. (1998). Functional connectivity in single and multislice echoplanar imaging using resting-state fluctuations. *Neuroimage*, 7(2):119–132.

[Lowe et al., 2000] Lowe, M. J., Dzemidzic, M., Lurito, J. T., Mathews, V. P., and Phillips, M. D. (2000). Correlations in low-frequency bold fluctuations reflect cortico-cortical connections. *Neuroimage*, 12(5):582–587.

[Luigjes et al., 2019] Luigjes, J., Segrave, R., de Joode, N., Figee, M., and Denys, D. (2019). Efficacy of invasive and non-invasive brain modulation interventions for addiction. *Neuropsychology review*, 29(1):116–138.

[Lynall et al., 2010] Lynall, M. E., Bassett, D. S., Kerwin, R., McKenna, P. J., Kitzbichler, M., Muller, U., and Bullmore, E. (2010). Functional connectivity and brain networks in schizophrenia. *J Neurosci*, 30(28):9477–9487.

[Makris et al., 2008] Makris, N., Oscar-Berman, M., Jaffin, S. K., Hodge, S. M., Kennedy, D. N., Caviness, V. S., Marinkovic, K., Breiter, H. C., Gasic, G. P., and Harris, G. J. (2008). Decreased volume of the brain reward system in alcoholism. *Biological psychiatry*, 64(3):192–202.

[Malik et al., 2018] Malik, S., Jacobs, M., Cho, S.-S., Boileau, I., Blumberger, D., Heilig, M., Wilson, A., Daskalakis, Z. J., Strafella, A. P., Zangen, A., et al. (2018). Deep tms of the insula using the h-coil modulates dopamine release: a crossover [11 c] phno-pet pilot trial in healthy humans. *Brain imaging and behavior*, 12(5):1306–1317.

[Maslov and Sneppen, 2002] Maslov, S. and Sneppen, K. (2002). Specificity and stability in topology of protein networks. *Science*, 296(5569):910–913.

[Maurage et al., 2012] Maurage, P., Joassin, F., Philippot, P., Heeren, A., Vermeulen, N., Mahau, P., Delperdange, C., Corneille, O., Luminet, O., and De Timary, P. (2012). Disrupted regulation of social exclusion in alcohol-dependence: an fmri study. *Neuropsychopharmacology*, 37(9):2067.

[McGhie and Chapman, 1961] McGhie, A. and Chapman, J. (1961). Disorders of attention and perception in early schizophrenia. *Br. J. Med. Psychol.*, 34(2):103–116.

[Mechtcheriakov et al., 2007] Mechtcheriakov, S., Brenneis, C., Egger, K., Koppelstaetter, F., Schocke, M., and Marksteiner, J. (2007). A widespread distinct pattern of cerebral atrophy in patients with alcohol addiction revealed by voxel-based morphometry. *Journal of Neurology, Neurosurgery & Psychiatry*, 78(6):610–614.

[Meinhardt and Sommer, 2015] Meinhardt, M. W. and Sommer, W. H. (2015). Post-dependent state in rats as a model for medication development in alcoholism. *Addiction biology*, 20(1):1–21.

[Meltzer et al., 2011] Meltzer, H. Y., Bonaccorso, S., Bobo, W. V., Chen, Y., and Jayathilake, K. (2011). A 12-month randomized, open-label study of the metabolic effects of olanzapine and risperidone in psychotic patients: influence of valproic acid augmentation. *The Journal of clinical psychiatry*, 72(12):1602–1610.

[Mendes et al., 2019] Mendes, N., Oligschläger, S., Lauckner, M. E., Golchert, J., Huntenburg, J. M., Falkiewicz, M., Ellamil, M., Krause, S., Baczkowski, B. M., Cozatl, R., Osoianu, A., Kumral, D., Pool, J., Golz, L., Dreyer, M., Haueis, P., Jost, R., Kramarenko, Y., Engen, H., Ohrnberger, K., Gorgolewski, K. J., Farrugia, N., Babayan, A., Reiter, A., Schaare, H. L., Reinelt, J., Röbbig, J., Uhlig,

M., Erbey, M., Gaebler, M., Smallwood, J., Villringer, A., and Margulies, D. S. (2019). A functional connectome phenotyping dataset including cognitive state and personality measures. *Scientific Data*, 6.

[Meunier et al., 2010] Meunier, D., Lambiotte, R., and Bullmore, E. T. (2010). Modular and hierarchically modular organization of brain networks. *Frontiers in neuroscience*, 4:200.

[Meunier et al., 2009] Meunier, D., Lambiotte, R., Fornito, A., Ersche, K., and Bullmore, E. T. (2009). Hierarchical modularity in human brain functional networks. *Frontiers in neuroinformatics*, 3:37.

[Mishra et al., 2010] Mishra, B. R., Nizamie, S. H., Das, B., and Praharaj, S. K. (2010). Efficacy of repetitive transcranial magnetic stimulation in alcohol dependence: a sham-controlled study. *Addiction*, 105(1):49–55.

[Mishra et al., 2015] Mishra, B. R., Praharaj, S. K., Katshu, M. Z. U. H., Sarkar, S., and Nizamie, S. H. (2015). Comparison of anticraving efficacy of right and left repetitive transcranial magnetic stimulation in alcohol dependence: a randomized double-blind study. *The Journal of neuropsychiatry and clinical neurosciences*, 27(1):e54–e59.

[Monterosso et al., 2001] Monterosso, J. R., Flannery, B. A., Pettinati, H. M., Oslin, D. W., Rukstalis, M., O'Brien, C. P., and Volpicelli, J. R. (2001). Predicting treatment response to naltrexone: the influence of craving and family history. *The American Journal on Addictions*, 10(3):258–268.

[Morris et al., 2017] Morris, L. S., Baek, K., Tait, R., Elliott, R., Ersche, K. D., Flechais, R., Mcgonigle, J., Murphy, A., Nestor, L. J., Orban, C., Passetti, F., Paterson, L. M., Rabiner, I., Reed, L., Smith, D., Suckling, J., Taylor, E. M., Bullmore, E. T., Lingford-Hughes, A. R., Deakin, B., Nutt, D. J., Sahakian, B. J., Robbins, T. W., and Voon, V. (2017). Naltrexone ameliorates functional network abnormalities in alcohol-dependent individuals. *Addiction Biology*, 23:425–436.

[Mueller et al., 2018] Mueller, F., Musso, F., London, M., de Boer, P., Zacharias, N., and Winterer, G. (2018). Pharmacological fMRI: Effects of subanesthetic ketamine on resting-state functional connectivity in the default mode network,

salience network, dorsal attention network and executive control network. *NeuroImage: Clinical*.

[Müller-Oehring et al., 2014] Müller-Oehring, E. M., Jung, Y.-C., Pfefferbaum, A., Sullivan, E. V., and Schulte, T. (2014). The resting brain of alcoholics. *Cerebral cortex*, 25(11):4155–4168.

[Murphy and Fox, 2017] Murphy, K. and Fox, M. D. (2017). Towards a consensus regarding global signal regression for resting state functional connectivity MRI. *NeuroImage*, 154.

[Muschelli et al., 2014] Muschelli, J., Nebel, M. B., Caffo, B. S., Barber, A. D., Pekar, J. J., and Mostofsky, S. H. (2014). Reduction of motion-related artifacts in resting state fmri using acompcor. *Neuroimage*, 96:22–35.

[Myrick et al., 2004] Myrick, H., Anton, R. F., Li, X., Henderson, S., Drobes, D., Voronin, K., and George, M. S. (2004). Differential brain activity in alcoholics and social drinkers to alcohol cues: relationship to craving. *Neuropsychopharmacology*, 29(2):393.

[Naqvi and Bechara, 2009] Naqvi, N. H. and Bechara, A. (2009). The hidden island of addiction: the insula. *Trends in neurosciences*, 32(1):56–67.

[Naqvi and Bechara, 2010] Naqvi, N. H. and Bechara, A. (2010). The insula and drug addiction: an interoceptive view of pleasure, urges, and decision-making. *Brain Structure and Function*, 214(5-6):435–450.

[Naqvi et al., 2007] Naqvi, N. H., Rudrauf, D., Damasio, H., and Bechara, A. (2007). Damage to the insula disrupts addiction to cigarette smoking. *Science*, 315(5811):531–534.

[Nardone et al., 2012] Nardone, R., Bergmann, J., Christova, M., Lochner, P., Tezzon, F., Golaszewski, S., Trinka, E., and Brigo, F. (2012). Non-invasive brain stimulation in the functional evaluation of alcohol effects and in the treatment of alcohol craving: a review. *Neuroscience Research*, 74(3-4):169–176.

[Newman, 2004] Newman, M. E. (2004). Fast algorithm for detecting community structure in networks. *Physical review E*, 69(6):066133.

[Nickerson, 2018] Nickerson, L. D. (2018). Replication of resting state-task network correspondence and novel findings on brain network activation during task fmri in the human connectome project study. *Scientific reports*, 8(1):17543.

[Nicolini and Bifone, 2016] Nicolini, C. and Bifone, A. (2016). Modular structure of brain functional networks: breaking the resolution limit by surprise. *Sci.Rep.*, 6:19250.

[Nicolini et al., 2017] Nicolini, C., Bordier, C., and Bifone, A. (2017). Community detection in weighted brain connectivity networks beyond the resolution limit. *Neuroimage*, 146:28–39.

[Nicolini et al., 2019] Nicolini, C., Forcellini, G., Minati, L., and Bifone, A. (2019). Scale-resolved analysis of brain functional connectivity networks with spectral entropy. *bioRxiv*, page 813162.

[Nicolini et al., 2018] Nicolini, C., Vlasov, V., and Bifone, A. (2018). Thermodynamics of network model fitting with spectral entropies. *Phys. Rev. E*, 98:022322.

[Niesters et al., 2012] Niesters, M., Khalili-Mahani, N., Martini, C., Aarts, L., van Gerven, J., van Buchem, M. A., Dahan, A., and Rombouts, S. (2012). Effect of Subanesthetic Ketamine on Intrinsic Functional Brain Connectivity. *Anesthesiology*, 117(4):868–877.

[Nocedal and Wright, 2006] Nocedal, J. and Wright, S. (2006). *Numerical optimization*. Springer Science & Business Media.

[Noda et al., 2015] Noda, Y., Silverstein, W. K., Barr, M., Vila-Rodriguez, F., Downar, J., Rajji, T. K., Fitzgerald, P., Mulsant, B. H., Vigod, S., Daskalakis, Z. J., et al. (2015). Neurobiological mechanisms of repetitive transcranial magnetic stimulation of the dorsolateral prefrontal cortex in depression: a systematic review. *Psychological medicine*, 45(16):3411–3432.

[Obando and De Vico Fallani, 2017] Obando, C. and De Vico Fallani, F. (2017). A statistical model for brain networks inferred from large-scale electrophysiological signals. *Journal of The Royal Society Interface*, 14(128):20160940.

[Park and Newman, 2004] Park, J. and Newman, M. E. J. (2004). Statistical mechanics of networks. *Phys. Rev. E*, 70(6):066117.

[Patel et al., 2014] Patel, A. X., Kundu, P., Rubinov, M., Jones, P. S., Vértes, P. E., Ersche, K. D., Suckling, J., and Bullmore, E. T. (2014). A wavelet method for modeling and despiking motion artifacts from resting-state fmri time series. *Neuroimage*, 95:287–304.

[Pilowsky et al., 2006] Pilowsky, L., Bressan, R., Stone, J., Erlandsson, K., Mulligan, R., Krystal, J., and Ell, P. (2006). First in vivo evidence of an nmda receptor deficit in medication-free schizophrenic patients. *Molecular psychiatry*, 11(2):118.

[Power et al., 2012] Power, J. D., Barnes, K. A., Snyder, A. Z., Schlaggar, B. L., and Petersen, S. E. (2012). Spurious but systematic correlations in functional connectivity MRI networks arise from subject motion. *NeuroImage*, 59(3):2142–2154.

[Power et al., 2011] Power, J. D., Cohen, A. L., Nelson, S. M., Wig, G. S., Barnes, K. A., Church, J. A., Vogel, A. C., Laumann, T. O., Miezin, F. M., Schlaggar, B. L., et al. (2011). Functional network organization of the human brain. *Neuron*, 72(4):665–678.

[Power et al., 2015] Power, J. D., Schlaggar, B. L., and Petersen, S. E. (2015). Recent progress and outstanding issues in motion correction in resting state fmri. *Neuroimage*, 105:536–551.

[Powers III et al., 2015] Powers III, A. R., Gancsos, M. G., Finn, E. S., Morgan, P. T., and Corlett, P. R. (2015). Ketamine-Induced Hallucinations. *Psychopathology*, 48:376–385.

[Pruim et al., 2015] Pruim, R. H., Mennes, M., van Rooij, D., Llera, A., Buitelaar, J. K., and Beckmann, C. F. (2015). Ica-aroma: A robust ica-based strategy for removing motion artifacts from fmri data. *Neuroimage*, 112:267–277.

[Pynn and DeSouza, 2013] Pynn, L. K. and DeSouza, J. F. (2013). The function of efference copy signals: implications for symptoms of schizophrenia. *Vision research*, 76:124–133.

[Rando et al., 2011] Rando, K., Hong, K.-I., Bhagwagar, Z., Li, C.-S. R., Bergquist, K., Guarnaccia, J., and Sinha, R. (2011). Association of frontal and posterior

cortical gray matter volume with time to alcohol relapse: a prospective study. *American Journal of Psychiatry*, 168(2):183–192.

[Rapinesi et al., 2016] Rapinesi, C., Del Casale, A., Di Pietro, S., Ferri, V. R., Piacentino, D., Sani, G., Raccah, R. N., Zangen, A., Ferracuti, S., Vento, A. E., et al. (2016). Add-on high frequency deep transcranial magnetic stimulation (dtms) to bilateral prefrontal cortex reduces cocaine craving in patients with cocaine use disorder. *Neuroscience letters*, 629:43–47.

[Rehm et al., 2015] Rehm, J., Anderson, P., Barry, J., Dimitrov, P., Elekes, Z., Feijão, F., Frick, U., Gual, A., Gmel, G., Kraus, L., Marmet, S., Raninen, J., Rehm, M. X., Scafato, E., Shield, K. D., Trapencieris, M., and Gmel, G. (2015). Prevalence of and potential influencing factors for alcohol dependence in Europe. *European addiction research*, 21(1):6–18.

[Rorden and Brett, 2000] Rorden, C. and Brett, M. (2000). Stereotaxic display of brain lesions. *Behavioural neurology*, 12(4):191–200.

[Rosvall and Bergstrom, 2008] Rosvall, M. and Bergstrom, C. T. (2008). Maps of random walks on complex networks reveal community structure. *Proceedings of the National Academy of Sciences*, 105(4):1118–1123.

[Roth et al., 2007] Roth, Y., Amir, A., Levkovitz, Y., and Zangen, A. (2007). Three-dimensional distribution of the electric field induced in the brain by transcranial magnetic stimulation using figure-8 and deep h-coils. *Journal of Clinical Neurophysiology*, 24(1):31–38.

[Roth et al., 2002] Roth, Y., Zangen, A., and Hallett, M. (2002). A coil design for transcranial magnetic stimulation of deep brain regions. *Journal of Clinical Neurophysiology*, 19(4):361–370.

[Rubinov and Sporns, 2010] Rubinov, M. and Sporns, O. (2010). Complex network measures of brain connectivity: uses and interpretations. *Neuroimage*, 52(3):1059–1069.

[Rubinov and Sporns, 2011] Rubinov, M. and Sporns, O. (2011). Weight-conserving characterization of complex functional brain networks. *Neuroimage*, 56(4):2068–2079.

[Saad et al., 2012] Saad, Z. S., Gotts, S. J., Murphy, K., Chen, G., Jo, H. J., Martin, A., and Cox, R. W. (2012). Trouble at rest: how correlation patterns and group differences become distorted after global signal regression. *Brain connectivity*, 2:25–32.

[Salimi-Khorshidi et al., 2014] Salimi-Khorshidi, G., Douaud, G., Beckmann, C. F., Glasser, M. F., Griffanti, L., and Smith, S. M. (2014). Automatic denoising of functional mri data: combining independent component analysis and hierarchical fusion of classifiers. *Neuroimage*, 90:449–468.

[Santarnecchi et al., 2014] Santarnecchi, E., Galli, G., Polizzotto, N. R., Rossi, A., and Rossi, S. (2014). Efficiency of weak brain connections support general cognitive functioning. *Human Brain Mapping*, 35(9):4566–4582.

[Satterthwaite et al., 2013] Satterthwaite, T. D., Elliott, M. A., Gerraty, R. T., Ruparel, K., Loughead, J., Calkins, M. E., Eickhoff, S. B., Hakonarson, H., Gur, R. C., Gur, R. E., et al. (2013). An improved framework for confound regression and filtering for control of motion artifact in the preprocessing of resting-state functional connectivity data. *Neuroimage*, 64:240–256.

[Satterthwaite et al., 2012] Satterthwaite, T. D., Wolf, D. H., Loughead, J., Ruparel, K., Elliott, M. A., Hakonarson, H., Gur, R. C., and Gur, R. E. (2012). Impact of in-scanner head motion on multiple measures of functional connectivity: relevance for studies of neurodevelopment in youth. *Neuroimage*, 60(1):623–632.

[Schlesinger et al., 2017] Schlesinger, K. J., Turner, B. O., Grafton, S. T., Miller, M. B., and Carlson, J. M. (2017). Improving resolution of dynamic communities in human brain networks through targeted node removal. *PLOS ONE*, 12(12).

[Schwarz and McGonigle, 2011] Schwarz, A. J. and McGonigle, J. (2011). Negative edges and soft thresholding in complex network analysis of resting state functional connectivity data. *NeuroImage*, 55(3):1132–1146.

[Scuppa et al., 2019] Scuppa, G., Tambalo, S., Pfarr, S., Sommer, W. H., and Bifone, A. (2019). Aberrant insular cortex connectivity in abstinent alcohol-dependent rats is reversed by dopamine d3 receptor blockade. *Addiction biology*.

[Seeley et al., 2007] Seeley, W. W., Menon, V., Schatzberg, A. F., Keller, J., Glover, G. H., Kenna, H., Reiss, A. L., and Greicius, M. D. (2007). Dissociable intrinsic connectivity networks for salience processing and executive control. *Journal of Neuroscience*, 27(9):2349–2356.

[Senatorov et al., 2014] Senatorov, V. V., Damadzic, R., Mann, C. L., Schwandt, M. L., George, D. T., Hommer, D. W., Heilig, M., and Momenan, R. (2014). Reduced anterior insula, enlarged amygdala in alcoholism and associated depleted von economo neurons. *Brain*, 138(1):69–79.

[Shcherbinin et al., 2015] Shcherbinin, S., Doyle, O., Zelaya, F. O., De Simoni, S., Mehta, M. A., and Schwarz, A. J. (2015). Modulatory effects of ketamine, risperidone and lamotrigine on resting brain perfusion in healthy human subjects. *Psychopharmacology*, 232(21-22):4191–4204.

[Siegel et al., 2014] Siegel, J. S., Power, J. D., Dubis, J. W., Vogel, A. C., Church, J. A., Schlaggar, B. L., and Petersen, S. E. (2014). Statistical improvements in functional magnetic resonance imaging analyses produced by censoring high-motion data points. *Human brain mapping*, 35(5):1981–1996.

[Simon, 1962] Simon, H. A. (1962). The architecture of complexity. *Proceedings of the American Philosophical Society*, 106(6):467–482.

[Simpson et al., 2011] Simpson, S. L., Hayasaka, S., and Laurienti, P. J. (2011). Exponential random graph modeling for complex brain networks. *PloS one*, 6(5):e20039.

[Simpson et al., 2012] Simpson, S. L., Moussa, M. N., and Laurienti, P. J. (2012). An exponential random graph modeling approach to creating group-based representative whole-brain connectivity networks. *Neuroimage*, 60(2):1117–1126.

[Sinke et al., 2016] Sinke, M. R., Dijkhuizen, R. M., Caimo, A., Stam, C. J., and Otte, W. M. (2016). Bayesian exponential random graph modeling of whole-brain structural networks across lifespan. *Neuroimage*, 135:79–91.

[Sjoerds et al., 2015] Sjoerds, Z., Stufflebeam, S. M., Veltman, D. J., Van den Brink, W., Penninx, B. W. J. H., and Douw, L. (2015). Loss of brain graph network efficiency in alcohol dependence. *Addiction Biology*, 22:523–534.

[Spagnolo and Goldman, 2016] Spagnolo, P. A. and Goldman, D. (2016). Neuromodulation interventions for addictive disorders: challenges, promise, and roadmap for future research. *Brain*, 140(5):1183–1203.

[Sporns, 2018] Sporns, O. (2018). Graph theory methods: applications in brain networks. *Dialogues in Clinical Neuroscience*, 20(2):111.

[Sporns and Betzel, 2016] Sporns, O. and Betzel, R. F. (2016). Modular brain networks. *Annual review of psychology*, 67:613–640.

[Sporns et al., 2004] Sporns, O., Chialvo, D. R., Kaiser, M., and Hilgetag, C. C. (2004). Organization, development and function of complex brain networks. *Trends in cognitive sciences*, 8(9):418–425.

[Sporns et al., 2007] Sporns, O., Honey, C. J., and Kötter, R. (2007). Identification and classification of hubs in brain networks. *PloS one*, 2(10):e1049.

[Sporns et al., 2005] Sporns, O., Tononi, G., and Kötter, R. (2005). The human connectome: A structural description of the human brain. *PLoS Comput. Biol.*, 1(4):0245–0251.

[Squartini and Garlaschelli, 2017] Squartini, T. and Garlaschelli, D. (2017). *Maximum-Entropy Networks: Pattern Detection, Network Reconstruction and Graph Combinatorics*. Springer International Publishing.

[Stone et al., 2012] Stone, J. M., Dietrich, C., Edden, R., Mehta, M. A., De Simoni, S., Reed, L. J., Krystal, J. H., Nutt, D., and Barker, G. J. (2012). Ketamine effects on brain gaba and glutamate levels with 1h-mrs: relationship to ketamine-induced psychopathology. *Molecular psychiatry*, 17(7):664.

[Strafella et al., 2001] Strafella, A. P., Paus, T., Barrett, J., and Dagher, A. (2001). Repetitive transcranial magnetic stimulation of the human prefrontal cortex induces dopamine release in the caudate nucleus. *Journal of Neuroscience*, 21(15):RC157–RC157.

[Strafella et al., 2003] Strafella, A. P., Paus, T., Fraraccio, M., and Dagher, A. (2003). Striatal dopamine release induced by repetitive transcranial magnetic stimulation of the human motor cortex. *Brain*, 126(12):2609–2615.

[Sullivan et al., 2013] Sullivan, E. V., Müller-Oehring, E. M., Pitel, A.-L., Chanraud, S., Shankaranarayanan, A., Alsop, D. C., Rohlfing, T., and Pfefferbaum, A. (2013). A Selective Insular Perfusion Deficit Contributes to Compromised Salience Network Connectivity in Recovering Alcoholic Men. *Biological Psychiatry*, 74(7):547–555.

[Tewarie et al., 2015] Tewarie, P., van Dellen, E., Hillebrand, A., and Stam, C. J. (2015). The minimum spanning tree: an unbiased method for brain network analysis. *Neuroimage*, 104:177–188.

[Trevizol et al., 2016] Trevizol, A. P., Shiozawa, P., Cook, I. A., Sato, I. A., Kaku, C. B., Guimarães, F. B., Sachdev, P., Sarkhel, S., and Cordeiro, Q. (2016). Transcranial magnetic stimulation for obsessive-compulsive disorder: an updated systematic review and meta-analysis. *The journal of ECT*, 32(4):262–266.

[van den Heuvel et al., 2017a] van den Heuvel, M., de Lange, S., Zalesky, A., Seguin, C., Yeo, T., and Schmidt, R. (2017a). Proportional thresholding in resting-state fMRI functional connectivity networks and consequences for patient-control connectome studies: Issues and recommendations. *NeuroImage*, 152:437–449.

[van den Heuvel et al., 2017b] van den Heuvel, M. P., de Lange, S. C., Zalesky, A., Seguin, C., Yeo, B. T., and Schmidt, R. (2017b). Proportional thresholding in resting-state fmri functional connectivity networks and consequences for patient-control connectome studies: Issues and recommendations. *Neuroimage*, 152:437–449.

[van den Heuvel and Hulshoff Pol, 2010] van den Heuvel, M. P. and Hulshoff Pol, H. E. (2010). Exploring the brain network: a review on resting-state fMRI functional connectivity. *Eur. Neuropsychopharmacol.*, 20(8):519–534.

[Van Dijk et al., 2012] Van Dijk, K. R., Sabuncu, M. R., and Buckner, R. L. (2012). The influence of head motion on intrinsic functional connectivity mri. *Neuroimage*, 59(1):431–438.

[van Eijk et al., 2013] van Eijk, J., Demirakca, T., Frischknecht, U., Hermann, D., Mann, K., and Ende, G. (2013). Rapid partial regeneration of brain volume

during the first 14 days of abstinence from alcohol. *Alcoholism: Clinical and Experimental Research*, 37(1):67–74.

[van Holst et al., 2012] van Holst, R. J., de Ruiter, M. B., van den Brink, W., Veltman, D. J., and Goudriaan, A. E. (2012). A voxel-based morphometry study comparing problem gamblers, alcohol abusers, and healthy controls. *Drug and alcohol dependence*, 124(1-2):142–148.

[van Wijk et al., 2010] van Wijk, B. C. M., Stam, C. J., and Daffertshofer, A. (2010). Comparing Brain Networks of Different Size and Connectivity Density Using Graph Theory. *PLoS ONE*, 5(10).

[Verdejo-Garcia et al., 2012] Verdejo-Garcia, A., Clark, L., and Dunn, B. D. (2012). The role of interoception in addiction: a critical review. *Neuroscience & Biobehavioral Reviews*, 36(8):1857–1869.

[Vergara et al., 2017] Vergara, V. M., Liu, J., Claus, E. D., Hutchison, K., and Calhoun, V. (2017). Alterations of resting state functional network connectivity in the brain of nicotine and alcohol users. *Neuroimage*, 151:45–54.

[Villafuerte et al., 2012] Villafuerte, S., Heitzeg, M. M., Foley, S., Yau, W. W., Majczenko, K., Zubieta, J.-K., Zucker, R. A., and Burmeister, M. (2012). Impulsiveness and insula activation during reward anticipation are associated with genetic variants in gabra2 in a family sample enriched for alcoholism. *Molecular psychiatry*, 17(5):511.

[Volkow and Morales, 2015] Volkow, N. and Morales, M. (2015). The brain on drugs: from reward to addiction. *Cell*, 162(4):712–725.

[Volkow and Fowler, 2000] Volkow, N. D. and Fowler, J. S. (2000). Addiction, a disease of compulsion and drive: involvement of the orbitofrontal cortex. *Cerebral cortex*, 10(3):318–325.

[Volkow et al., 2002] Volkow, N. D., Fowler, J. S., Wang, G.-J., and Goldstein, R. Z. (2002). Role of dopamine, the frontal cortex and memory circuits in drug addiction: insight from imaging studies. *Neurobiology of learning and memory*, 78(3):610–624.

[Volkow et al., 2016] Volkow, N. D., Koob, G. F., and Mclellan, A. T. (2016). Neurobiologic Advances from the Brain Disease Model of Addiction. *N Engl J Med*, 374:363–71.

[Volkow et al., 2013] Volkow, N. D., Wang, G.-J., Tomasi, D., and Baler, R. D. (2013). Unbalanced neuronal circuits in addiction. *Current Opinion in Neurobiology*, 23(4):639–648.

[Vollstädt-Klein et al., 2012] Vollstädt-Klein, S., Loeber, S., Richter, A., Kirsch, M., Bach, P., von der Goltz, C., Hermann, D., Mann, K., and Kiefer, F. (2012). Validating incentive salience with functional magnetic resonance imaging: association between mesolimbic cue reactivity and attentional bias in alcohol-dependent patients. *Addiction biology*, 17(4):807–816.

[Wang et al., 2018] Wang, Y., Chen, J., Zhao, Y., Nie, H., and Liu, C. (2018). Disrupted brain network efficiency and decreased functional connectivity in multisensory modality regions in male patients with alcohol use disorder. *Frontiers in human neuroscience*, 12:513.

[Wang et al., 2015] Wang, Z., Suh, J., Li, Z., Li, Y., Franklin, T., O'Brien, C., and Childress, A. R. (2015). A hyper-connected but less efficient small-world network in the substance-dependent brain. *Drug and Alcohol Dependence*, 152:102–108.

[Watts and Strogatz, 1998] Watts, D. J. and Strogatz, S. H. (1998). Collective dynamics of 'small-world'networks. *nature*, 393(6684):440.

[Weiland et al., 2014] Weiland, B. J., Sabbineni, A., Calhoun, V. D., Welsh, R. C., Bryan, A. D., Jung, R. E., Mayer, A. R., and Hutchison, K. E. (2014). Reduced left executive control network functional connectivity is associated with alcohol use disorders. *Alcoholism: Clinical and Experimental Research*, 38(9):2445–2453.

[Wilde, 2013] Wilde, M. M. (2013). *Quantum information theory*. Cambridge University Press.

[World Health Organization (WHO), 1990] World Health Organization (WHO) (1990). Composite International Diagnostic Interview. Technical report.

[World Health Organization (WHO), 2018] World Health Organization (WHO) (2018). Global Status Report on alcohol and health 2018. Technical report.

[Wrase et al., 2008] Wrase, J., Makris, N., Braus, D. F., Mann, K., Smolka, M. N., Kennedy, D. N., Caviness, V. S., Hodge, S. M., Tang, L., Albaugh, M., et al. (2008). Amygdala volume associated with alcohol abuse relapse and craving. *American Journal of Psychiatry*, 165(9):1179–1184.

[Xia et al., 2013] Xia, M., Wang, J., and He, Y. (2013). BrainNet Viewer: a network visualization tool for human brain connectomics. *PLoS ONE*, 8(7):e68910.

[Xiao et al., 2013] Xiao, L., Bechara, A., Gong, Q., Huang, X., Li, X., Xue, G., Wong, S., Lu, Z.-L., Palmer, P., Wei, Y., et al. (2013). Abnormal affective decision making revealed in adolescent binge drinkers using a functional magnetic resonance imaging study. *Psychology of Addictive Behaviors*, 27(2):443.

[Yang et al., 2016a] Yang, X., Tian, F., Zhang, H., Zeng, J., Chen, T., Wang, S., Jia, Z., and Gong, Q. (2016a). Cortical and subcortical gray matter shrinkage in alcohol-use disorders: a voxel-based meta-analysis. *Neuroscience & Biobehavioral Reviews*, 66:92–103.

[Yang et al., 2016b] Yang, Z., Algesheimer, R., and Tessone, C. J. (2016b). A comparative analysis of community detection algorithms on artificial networks. *Scientific reports*, 6:30750.

[Yu et al., 2012] Yu, Q., Plis, S. M., Erhardt, E. B., Allen, E. a., Sui, J., Kiehl, K. a., Pearlson, G., and Calhoun, V. D. (2012). Modular Organization of Functional Network Connectivity in Healthy Controls and Patients with Schizophrenia during the Resting State. *Front. Syst. Neurosci.*, 5(January):1–16.

[Yu et al., 2011] Yu, Q., Sui, J., Rachakonda, S., He, H., Gruner, W., Pearlson, G., Kiehl, K. A., and Calhoun, V. D. (2011). Altered topological properties of functional network connectivity in schizophrenia during resting state: A small-world brain network study. *PLoS One*, 6(9).

[Zalesky et al., 2010a] Zalesky, A., Fornito, A., and Bullmore, E. T. (2010a). Network-based statistic: identifying differences in brain networks. *Neuroimage*, 53(4):1197–1207.

[Zalesky et al., 2016] Zalesky, A., Fornito, A., Cocchi, L., Gollo, L. L., van den Heuvel, M. P., and Breakspear, M. (2016). Connectome sensitivity or specificity: which is more important? *NeuroImage*, 142:407–420.

[Zalesky et al., 2010b] Zalesky, A., Fornito, A., Harding, I. H., Cocchi, L., Yücel, M., Pantelis, C., and Bullmore, E. T. (2010b). Whole-brain anatomical networks: does the choice of nodes matter? *Neuroimage*, 50(3):970–983.

[Zhu et al., 2018] Zhu, J., Zhao, W., Zhang, C., Wang, H., Cheng, W., Li, Z., Qian, Y., Li, X., and Yu, Y. (2018). Disrupted topological organization of the motor execution network in alcohol dependence. *Psychiatry Research: Neuroimaging*, 280:1–8.

[Zhu et al., 2015] Zhu, X., Cortes, C. R., Mathur, K., Tomasi, D., and Momenan, R. (2015). Model-free functional connectivity and impulsivity correlates of alcohol dependence: a resting-state study. *Addiction Biology*, 22(1):206–217.

[Zorlu et al., 2017] Zorlu, N., Çapraz, N., Oztekin, E., Bagci, B., Di Biase, M. A., Zalesky, A., Gelal, F., Bora, E., Durmaz, E., Beşiroğlu, L., and Sarıçiçek, A. (2017). Rich club and reward network connectivity as endophenotypes for alcohol dependence: a diffusion tensor imaging study. *Addiction Biology*.